In singulo study of the transcription elongation by *Mycobacterium tuberculosis* RNA polymerase and its inhibition by Aroyl-Aryl-Phenylalaninamide, Streptolydigin, and Pseudouridimycin

by

Omar Carlos Herrera Asmat

A dissertation submitted in partial satisfaction of the

requirements for the degree of

Doctor of Philosophy

in

Molecular and Cell Biology

in the

Graduate Division

of the

University of California, Berkeley

Committee in charge:

Professor Carlos Bustamante, Chair

Professor Oskar Hallatschek

Professor Andreas Martin

Professor Jeffery Cox

Fall 2022

In singulo study of the transcription elongation by *Mycobacterium tuberculosis* RNA polymerase and its inhibition by Aroyl-Aryl-Phenylalaninamide, Streptolydigin, and Pseudouridimycin

Omar Carlos Herrera Asmat

Abstract

In singulo study of the transcription elongation by *Mycobacterium tuberculosis* RNA polymerase and its inhibition by Aroyl-Aryl-Phenylalaninamide, Streptolydigin, and Pseudouridimycin

by

Omar Carlos Herrera Asmat

Doctor of Philosophy in Molecular and Cell Biology

University of California, Berkeley

Professor Carlos Bustamante, Chair

Tuberculosis (TB) is an airborne disease that kills 1.5 million people and affects ~ 9 million worldwide. Its etiological agent, *Mycobacterium tuberculosis* (Mtb), persists in a third of the general population. There is also an emergent problem of drug and multidrug resistance in Mtb that creates the need for novel drugs. In the treatment against TB, one target of antibiotics is the prokaryotic RNA polymerase (RNAP), an essential multitask enzyme that catalyzes RNA synthesis during transcription. Rifampicin, the first-line antibiotic anti-TB, binds and inhibits the MtbRNAP.

Consequently, combatting TB requires a better understanding of the primary mechanism of transcription by MtbRNAP. In fact, during Mtb transcription, unique and essential factors might affect the MtbRNAP dynamics and regulate its activity. That regulation plays a significant role in the adaptation and pathogenesis of the parasite. Therefore, understanding how these factors and new antibiotics modulate together the MtbRNAP activity will contribute valid information to address TB. To this end, we use a single-molecule approach based on high-resolution optical tweezers to study transcription elongation by MtbRNAP in the context of its DNA elements, transcriptional factors, and antibiotics.

I dedicate this work to my parents, Rosa Teresa and Victor Manuel, and my siblings, Victor Hugo, and Rosa Bell.

Table of contents

List of Figures

Acknowledgments

Before presenting my findings, I want to express my deep gratitude to Professor Carlos Bustamante, who has been my advisor and support throughout my Ph.D. studies and research and has exhibited patience, excitement, passion, and a wealth of knowledge. The assistance he gave me with my thesis was priceless. During my time as a Ph.D. candidate, my advisor was an excellent guide and teacher.

I also want to thank the three professors on my thesis committee, Andreas Martin, Oskar Hallatschek, and Jeffery Cox, for providing insightful criticism, asking excellent questions, and understanding when I needed to postpone my committee meeting during sensitive family circumstances. Thanks to my committee's hard work, I broadened my horizons and enriched my perspective.

My sincere thanks also go to principal investigator Richard Ebright for kindly offering the MtbRNAP inhibitors PUM, STL, and AAP and disposition to discuss results, as well as associate Professor Juan Del Valle for providing inhibitor deshydro-PUM.

During my time in the laboratory, I had the pleasure of working with the graduate student Alex Tong and with post-doc Wenxia Lin. Alex helped me with and provided MATLAB tools for repeat analysis, dwell-time distribution, and pause-chance histograms. Wenxia shared data on *E coli* polymerase with antibiotic PUM using one shunt and assisted me with the TIRF assays. I got assisting help from undergrad students Dalton Amador with DNA template preparation, Nae Jeong Kim with a biotinylation screen and fishing troubleshooting, Jiayi Elaine Liu, and Vivian Hoang Tran with collecting single-molecule traces of *M. tuberculosis* polymerase with Streptolydigin and *E. coli* polymerase in passive mode. In addition, I want to thank post-doc Shannon Yan for her technical support in fixing the time-share instrument's radio-frequency board and installing a new laser in October 2022, post-doc Liang Meng Wee for support in the protocol of the oxygen-scavenger system and enzyme sortase, graduate student Cristhian Cañari for kindly offering the Cy3-peptide for sortase reaction and fluorescent measurements. I cannot express how grateful I am to everyone in the Bustamante lab who participated during group meetings to refine my ideas and make them more concrete. Members from other labs helped me too. I thank joint post-doc Erik Jonsson for the advice on valve positioners control, graduate student Erika M. López-Alfonzo for training in the stop-flow instrument, and visiting professor Francisco Monroy for learning the physical information perspective of optical tweezers.

Ultimately, I want to thank my parents, Rosa and Victor, and my siblings, Victor Hugo and Rosa Bell, from the bottom of my heart. Even though I was far from home, they were close to me; I would never be able to achieve my goals.

Chapter 1. Introduction to *in-singulo* elongation and inhibition of *Mycobacterium tuberculosis* RNA polymerase

Prokaryotic transcription shares the same primary stages as eukaryotic: initiation, starting with the DNA promoter recognition; elongation, for the active processive extending of the nascent RNA; and termination, to stop transcription and fall off from the template [1]. The bacteria RNA polymerase (RNAP) is a multimeric conserve protein of a core of subunits $\alpha_2\beta\beta'\omega$, the catalytic unit of transcription, and the holoenzyme form of subunits $\alpha_2\beta\beta'\omega\sigma$, for the specific promoter initiation. While studies *in bulk* done in *Mycobacteria* and *E. coli* RNA polymerases confirmed the conservation of the central architecture of tuberculosis enzyme [2–6], exist specific inter-subunit interactions[7] and novel structural motif[8,9], as well as transcription factors that can modulate its activity differently [10], of which in *M. tuberculosis* (Mtb) there are many unique[11]. Indeed, the initiation transcription bubble collapses without the stabilization by factors, contrary to the elongating bubble (~12bp of DNA and ~9bp of RNA/ DNA register), according to functional assays[12,13]. In addition, the modulation of transcription can comprise the action of roadblocks affecting the enzyme processivity during elongation. Lee and Borukhov listed the roadblocks interrupting the elongation process, including specific DNA sequences, DNA topology, lesions in transcribed DNA templates, RNA secondary structures, DNA-binding proteins, DNA replication, and repair machinery, ribosomes, other transcription complexes, and RNAP-binding transcription factors[1]. Despite this broad range of modulation or regulation possibilities, our work focuses mainly on the RNAP *per se* and a few essential factors.

Nucleotide additional cycle

In the elongation complex, the RNA synthesis takes place one nucleotide at a time, sequentially and repeatedly, a process called the nucleotide addition cycle (NAC). Kang *et al.* describe the NAC sub-steps[14]. The first step is the nucleic-acid translocation from the pre- to post-translocated states. These are of particular interest because the thermal movement of polymerase ratchets between those positions or states, being rectified by the binding of the incoming rNTP, eventually incorporated in the nascent RNA chain[15,16]. Here, the RNA/ DNA register makes space for the rNTP binding site and aligns the next template DNA base for base pairing. The ways to recognize between pre-and post-translocation are vast, from Exo-nucleobase footprinting[17], fluorescent nitrogen base analog-based translocation assay[18], endo, and exonucleolytic cleavages, and pyrophosphorolysis kinetics[19]. The next step is rNTP binding, characterized by folding the RNAP active site-proximal trigger loop (TL) motif into the trigger helices (TH), and where

the chemistry step occurs, a catalysis SN2 (nucleophilic attack) for the formation of the covalent bond. The following step is the TH unfolding and the pyrophosphate release, where, simultaneously, there is a translocation step to prepare the active site for the next NAC. Therefore, the effective elongation rate (k_{el}) is the inverse of the average time it takes a pause-free NAC[20].

RNA polymerase as a catalytic circuit network

Based on structural and computational data and functional assays, the RNAP comprises a network of alternative circuits of conformational change couplings between catalytic elements and allosteric motifs during the NAC[21–28]. Evidence from molecular dynamics simulations and mutagenesis experiments point to the bridge helix (BH) as a molecular switch where the N- and C-terminals hinges, and kinks connect different catalytic components. In this manner, in the active center, the primary coupling between the BH C-terminal and the highly flexible TL acts on various RNA polymerase activities, including rNTP loading, RNA chemistry, forward translocation, backtracking, and pausing signals recognition in termination[16,21,29]. The closed-folded conformer of the TL selects the correct rNTPs binding at the i+1 site to ensure transcription fidelity [16,29,30] indirectly stimulates catalysis. After phosphodiester bond formation and pyrophosphate release, the open-unfolded TL conformer moves away from the catalytic site and the incorporated rNMP[29,30].

On the other hand, other circuits connect the β link domain, β fork domain, and F-loop to residues tyrosine, phenylalanine, and isoleucine (YFI) at BH N-terminal, respectively. These circuits might be necessary for regulating catalysis, elongation, termination, and translocation[31].

Since RNAP inhibitors potentially disrupt any of these circuits, carefully evaluating their effects among prokaryotic polymerases would display species-specific circuit contributions reflecting the non-conservation of the allosteric motifs[32].

Transcriptional pauses

The pauses are the non-catalytically recognized RNAP states, off-pathway in competition and branching off from any NAC sub-steps. There are different classifications of pauses, according to Janissen *et al* [33]. Some are the product of factor regulation and sequence-dependent events. In contrast, others respond randomly to the polymerase conformation changes[34]. In addition, there are ubiquitous elemental pause states [35] of the short lifetime of ~ 1 sec. These elemental pauses originate other pauses through lifetime modulation, e.g., RNA hairpin-stabilized pauses are rare long-live pauses regulated by the structure upstream of the nascent RNA. Furthermore, the long live pauses, usually associated with backtrack events, are divided into the ones that recover by either intrinsic cleavages or assisted cleavages by Gre factors or those that recover by diffusive mechanisms.

Different parameters help describe the pausing kinetics, e.g., pause frequency, pause density, pause strength, pause probability, and the rates of pause escape and entry. The pause escape rate (k_{-p}) measures the pause lifetime (pause duration), while the pause density o frequency is the number of pauses per nucleotide and measures the rate of pause entry (k_p). The pause efficiency or pause probability (P_{total}) measures the kinetic competition of the elongation rate *versus* the pause entry rate (k_p/ k_p+k_{el}). In addition, the

pause strength counts as the product of the pause efficiency and pauses escape (P_p*k_{-p}). Other research uses the pause frequency to refer to the number of pauses per unit of time[36].

Single-molecule study of transcription elongation

Why use single-molecule (SM) techniques to study transcription? Ensemble or *in* bulk experiments average polymerase behavior. SM studies showed that each RNAP is heterogeneous in activity[35,37,38]. In addition, SM detects transient transcriptional events, such as small pauses[39] and factor binding, and dynamic events, such as RNA folding[40] and backtracking events[41–44].

RNA polymerase as a molecular motor

Research showed that RNA polymerase behaves as a macromolecular motor because it converts the chemical energy from the hydrolysis and condensation of rNTPs in mechanical movement[45–47]. Since in transcription elongation, the polymerase extends the RNA in successive steps of NAC (multiple turnovers) before detachment from the DNA template, it behaves as a kinetically non-Cleland enzyme with processivity, an intrinsic property of molecular motors[48]. In addition, the transcription trajectory that results from averaging the RNA polymerase movement on the DNA template has directionally[46]. The RNAP is a more complex chemical motor because it has, in addition to several different movements, catalytic activity under regulation[49].

Transcription elongation as a drugs target

Although the rifampicin-resistant mechanism in Mtb makes transcription initiation a critical topic[50–52], here we focused on the transcription elongation for the following reasons: (i) targeting initiation does not avoid transcription elongation[53], (ii) emerging RIF-resistant and compensatory mutants evade transcription initiation[54–58], (ii) multiple ways of regulation of initiation[59], mostly promoter-dependent, and under different environmental conditions[60–62], converge in practice to only one way of elongation, (iii) interruption or arresting of elongation by inhibitors has a more significant impact in RNA production than in initiation since the abortive initiation process is part of the transcription process, (iv) there are fewer RNAP molecules enrolled in elongation phase compare to the initiation, which represents a target more sucesstible[63].

Regulation and inhibition of MtbRNAP elongation

Regulators can modulate the activity of the prokaryotic RNAP by accessing the secondary channel and affecting BH and TL. The BH and the TL preferentially adopt a particular conformational state upon binding.[64,65] In MtbRNAP, the essential and constitutive factor, MtbGreA, might alter the BH structure, which leads reduction of pauses duration and abortive initiation events[66]. Similarly, other unique Mtb factors that inhibit and suppress pauses in RNAP, such as Rv3788 and Rv0639[69,70], respectively, can also affect the BH conformation.

Antibiotics also modulate the MtbRNAP activity. According to Lee and Borukhov[1], the small molecule inhibitors that target the prokaryotic RNAP divide into three groups. The first group is inhibitors that disrupt the interaction of RNAP—DNA/RNA/rNTPs, such as

Rifampicin (RIF) and Pseudouridimycin (PUM). The second group is inhibitors constraining the RNAP active mobile elements during NAC, e.g., CBR, Streptolydigin (STL), and Aroyl-Aryl-Phenylalaninamides (AAP). The third group is inhibitors that disrupt the RNAP- σ^{70} interactions, e.g., the pharmacophore GKL003. In this manner, we are interested in studying AAP, STL, and PUM in this work.

STL, a tetrameric-acid antibiotic effective against EcoRNAP, inhibits the initiation and elongation states by binding BH and TL of the RNAP. Even though STL exhibits a non-target-based resistance for Mtb[67], because of an effective efflux that quickly pumps it from the cell interior, this drug can be used in vitro to investigate the catalytic cycle of the MtbRNAP[67]. On the other hand, PUM, a nucleoside analog, inhibits bacterial RNAPs by competing for rUTP incorporation in the active site [68]. Expected is that PUM inactivates the polymerase by increasing the pausing; however, we have little knowledge of MtbRNAP recovery via backtracking events. Another antibiotic, N(α)-Aroyl-N-Aryl-Phenylalaninamides (AAP), inhibits specifically the MtbRNAP by binding three amino acids at the N-terminus of BH[8]. However, whether AAP or STL affects the activity or the pause phases of MtbRNAP when binding to the catalytic domains is unknown.

Chapter 2. The pleomorphic dynamic of recovery from inhibition of transcription elongation by *M. tuberculosis* RNA polymerase.

Abstract

The *Mycobacterium tuberculosis* RNA polymerase (MtbRNAP) is a valid drug target to combat tuberculosis (TB). Required is, consequently, a better understanding of its basic mechanism of transcription and drug inhibition. We did the first biophysical characterization of MtbRNAP elongation and inhibition by Aroyl-Aryl-Phenylalaninamide (AAP), Streptolydigin (STL), and Pseudouridimycin (PUM). We found that MtbRNAP transcribes half as fast as EcoRNAP with comparable processivity. Using the force-velocity relationship, MtbRNAP is robust as EcoRNAP. In addition, utilizing the *molecular ruler* technique, MtbRNAP pauses inefficiently on the Eco elementary sequences because of weak recognition.

Regarding the antibiotic's effect, we observed that AAP affects the global velocity of MtbRNAP, namely pause and pause-free periods. Upon AAP inhibition, MtbRNAP elongation can adopt two exchangeable states of reduced global velocities: *slow* and *super-slow*. In the slow state, there is mainly an increased probability of pausing, while in the super slow state, there is a decrease in the effective elongation rate (inverse of the average time of pause-free NAC). Additionally, the *molecular fate* of MtbRNAP paused by STL is determined by the recovery from depth backtracks via endonucleolysis rather than by a spontaneous diffusive mechanism. On the other hand, PUM modifies the pausing of RNAP at elementary pause by increasing the pause density (number of pauses per unit length transcribed) in regions upstream of the elementary pause site, while it can also induce *switch*es of global velocity. MtbRNAP switches its global velocity more frequently than EcoRNAP (~12-16% *versus* ~1- 4%), suggesting a difference in the coordination between conserved catalytic elements and non-conserved allosteric motifs among these enzymes. Future research should address conformational changes in the RNAP that explain those states.

Introduction

Tuberculosis is an infectious illness with the morbidity of a third of the world's population and the second-highest cause of death from a single infectious agent, *Mycobacterium tuberculosis* (Mtb)[69]. The problematic incidence of TB multi-drug resistance (MDR) also includes resistance to rifampicin (RIF), the first-line anti-TB medication. This drug targets the bacterial RNA polymerase (RNAP) to prevent nascent RNA growth beyond three nucleotides (nt)[8,70,71]. Since more than 70 percent of Rif-resistance mutations occur on *M. tuberculosis* RNAP (MtbRNAP)[54,55,72–78], it is crucial to understand how this enzyme operates. Similarly, it is necessary to research anti-TB drugs with novel binding sites that avoid cross-reactivity, such as N(α)-aroyl-N-aryl-phenylalaninamides (AAP)[79,80], streptolydigin (SLT)[64,67,81] and pseudouridimycin (PUM)[82–84]. While significant progress has been made in the structural determination of their mechanism of action[64,68,85], we currently lack careful functional characterization of these drugs on the enzyme[28].

In the last three decades, single-molecule transcription studies on *E. coli* and yeast RNAP (EcoRNAP and Pol II, respectively)[86] revealed that the RNAP elongation displays periods of processive nucleotide addition interspersed by variously lasting pauses (*active and pause phases*, respectively)[87–89]. Pausing events play critical roles in regulating transcription and coordinating it with other processes that occur co-transcriptionally, such as translation[90,91], splicing[92,93], and DNA repair[94,95]. Single-molecule studies can measure fast pausing dynamics, reveal and characterize backtracking in real-time, and get distributions of events rather than just average parameters.

Furthermore, single-molecule (SM) mechanical manipulation studies of *E.* coli and yeast RNA polymerases provided crucial information about the enzyme's mechanical robustness[46,96,97] and performance, demonstrating that there are variations in motor operation among polymerase molecules (*static dispersion*) or within a polymerase (*dynamic dispersion*)[37]. Due to its higher temporal-spatial resolution[98], SM methods also allowed the direct observation of transient events like short regulatory pauses[39,99], which are thought to play an essential role in RNA folding[40], dynamics events like backtracking [39,42–44], or even the single-base stepping of the molecule during its transcription cycle[100,101]. Likewise, these methods have been used to detect the functional effects of the interactions of the polymerase with DNA elements like promoters[102] or transcription factors.

The biophysical studies of transcription by MtbRNAP focused mainly on the conformational changes and specific interactions between the polymerase, its unique factors, and non-canonical DNA promoter sequences in forming the stable active open complex competent to initiate RNA polymerization[50,51]. Nearly all efforts were on elucidating the structure of initiation complexes[103] and their derivatives with antibiotics to prevent that transition. However, it has been found that RIF-resistant RNAP mutants evade the initiation phase and competitively perform RNA elongation[54,58,73,76,77,104,105]. Thus, these studies have paid little attention to the dynamics of inhibition by drugs targeting the transcribing MtbRNAP and poorly understood the *molecular fate* of the enzyme following its association with the antibiotic. Therefore, in this work, we used SM techniques because of the advantages over traditional *bulk* assays to track in real-time MtbRNAP elongation to determine whether the drug terminates transcription (chain

terminator)[106], competes for substates (competitive inhibitor)[107] or modulates the polymerase activity (allosteric inhibitor). Additionally, we could evaluate the drug's sequence-dependent effect employing different DNA templates, and we derived the apparent drug residence time or, equivalently, the dissociation rate of the drug from the active polymerase[108].

The aims are to characterize the dynamics and kinetics *in singulo* of MtbRNAP elongation and the mechanism by which the antibiotics AAP, STL, and PUM inhibit its activity by using high-resolution optical tweezers (HROT)

Results

Mechanochemistry of *M. tuberculosis* RNAP

We studied *in-singulo* and, with high-temporal resolution accuracy, the transcription elongation by MtbRNAP using force-spectroscopy (Figure 1a). We employed different optical-tweezers setups such as assisting, opposing, or passive modes to measure the polymerase performance at mesophilic temperature (22° C) and under other biochemical conditions. Some measurements compared MtbRNAP and EcoRNAP since the latter is the most studied polymerase *in-singulo*.

It is generally accepted that MtbRNAP transcribes slower than its Eco counterpart[109,110]. Nevertheless, whether that is due to the molecular motor *per se,* or its molecular modulation is unknown. To address this point, we collected elongation data from Eco and Mtb RNAPs under assisting force (Figure 1b)[109]. As previously found in EcoRNAP, Mtb transcriptional trace also comprises two interspersed phases: pauses and pause-free periods. Then, we low-pass filtered multiple traces to extract the phase rates and represent them as probability distributions. We found that MtbRNAP transcribes processively and half as fast as EcoRNAP. Above 50% of the enzymes tested can transcribe almost three kilobases of the DNA template without the transcription factor's help. The enzyme also displays lower dynamic than static dispersion (Figure 1c). To further characterize the dynamics of the enzyme, we obtained the rates and distributions of MtbRNAP alternative transcriptional modes by fitting the complementary cumulative distribution function (CCDF) of the enzyme dwells extracted from the single-molecule traces with a base-pair staircase algorithm to multi-exponential analysis. In our model, the averaged effective elongation rate (k_{el}) is above four nucleotides per second, the average pause escape of elementary and short pauses (k_{-p}) between four and one-half nucleotides per second, and the slower rates correspond to long pauses or backtracking events.

Next, we determined the MtbRNAP mechanical robustness by detecting changes in the effective elongation rate with opposing loading force in passive mode. We found that this polymerase is mechanically robust; its effective elongation rate (k_{el}) was insensitive to the increase in the opposing force until it dropped when it reached an *operational stall force* (F_{stall}), as described before for EcoRNAP [96]. According to previous studies, the F_{stall} results from force-induced backtracking of the enzyme over the template. This process used by the enzyme is part of its error-editing capability[44]. Indeed, above 70 % of the operationally stalled MtbRNAPs were in the *backtracked state,* and the average stall force ($\langle F_{stall} \rangle$) was 19.3 ± 1.2 pN.

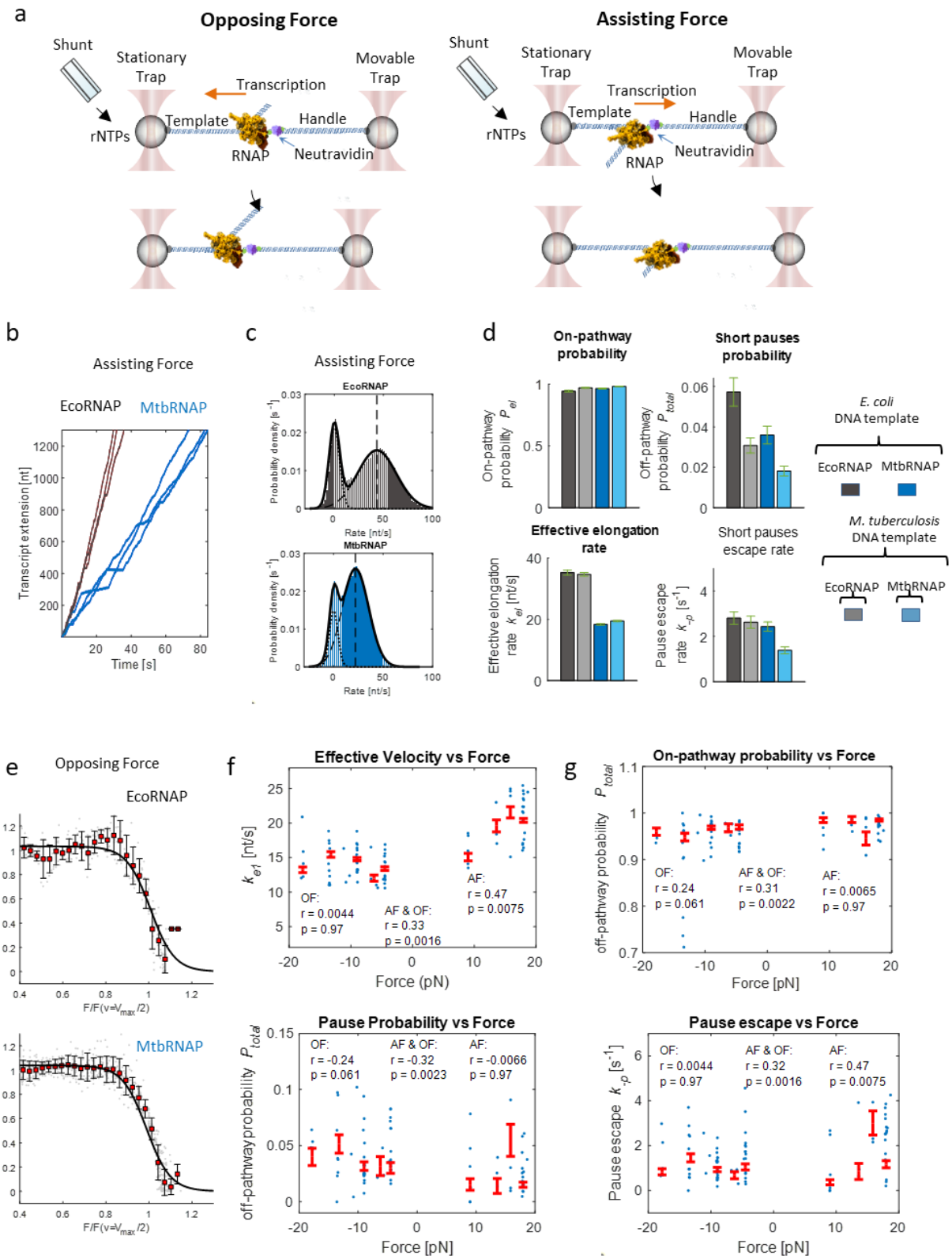
a
Opposing Force
Shunt
Stationary Trap
Movable Trap
Transcription
rNTPs
Template
Handle
RNAP
Neutravidin
Assisting Force
b
Assisting Force
EcoRNAP
MtbRNAP
Transcript extension [nt]
Time [s]
c
Assisting Force
EcoRNAP
MtbRNAP
Probability density [s⁻¹]
Rate [nt/s]
d
On-pathway probability
Short pauses probability
On-pathway probability P_{el}
Off-pathway probability P_{total}
E. coli DNA template
EcoRNAP
MtbRNAP
M. tuberculosis DNA template
Effective elongation rate
Short pauses escape rate
Effective elongation rate k_{el} [nt/s]
Pause escape rate k_{-p} [s⁻¹]
e
Opposing Force
EcoRNAP
MtbRNAP
v/V_max
F/F(v=V_max/2)
f
Effective Velocity vs Force
k_{el} [nt/s]
OF: r = 0.0044 p = 0.97
AF & OF: r = 0.33 p = 0,0016
AF: r = 0.47 p = 0.0075
Force (pN)
Pause Probability vs Force
off-pathway probability P_{total}
OF: r = -0.24 p = 0.061
AF & OF: r = -0.32 p = 0.0023
AF: r = -0.0066 p = 0.97
Force [pN]
g
On-pathway probability vs Force
off-pathway probability P_{total}
OF: r = 0.24 p = 0.061
AF & OF: r = 0.31 p = 0.0022
AF: r = 0.0065 p = 0.97
Force [pN]
Pause escape vs Force
Pause escape k_{-p} [s⁻¹]
OF: r = 0.0044 p = 0.97
AF & OF: r = 0.32 p = 0.0016
AF: r = 0.47 p = 0.0075
Force [pN]

Figure 1. Single-molecule transcription elongation by *M. tuberculosis* RNA polymerase under high-resolution optical tweezers (HROT).

a. Optical tweezers (OT) setups isolate the RNAP from the laser beam through a DNA handle. On the left, the trapping force opposes the RNAP movement or the opposing force (OF), which may be constant or passive. In passive mode, the trap's position keeps fixed, and the bead-bead distance increases the tension. In contrast, the instrument reduces the trap's distance in the constant mode to maintain the force invariant. On the right, under constant assisting force (AF), the trapping force is in the direction of the polymerase movement; consequently, the trap's distance increases. In addition, to restart the transcription activity, we open a shunt to add rNTPs to the experimental region.
b. *In-singulo* reconstitution of MtbRNAP elongation showed that this enzyme transcribes more than a kilobase of DNA template without the assistance of any factors. The position versus time graph compares single transcriptional trajectories between Eco and MtbRNA polymerases (The black and blue traces, respectively). The activities collected at 18 pN constant AF, 22° C and saturating rNTPs correspond to the transcription of the DNA template derived from Mtb genes rpoB and rpoC.
c. MtbRNAP transcribes slower than EcoRNAP. Characteristics traces of both enzymes, in dark gray, EcoRNAP, and blue, MtbRNAP. We applied Savitzky-Golay tools to filter the traces and obtained the bimodal rate distribution histograms (degree = 1; span = 101 s, window time = 1 s). The non-zero center gaussian distribution corresponds to the pause, while the other distribution is the pause-free velocity (PFV). The MtbRNAP mean PFV is half as the EcoRNAP one.
d. MtbRNAP is mechanically robust as EcoRNAP. Top, force-velocity relationship analysis of MtbRNAP (Arrhenius-like fit with parameter A = 1.9e-08 ± 2.6e-08, V_0 = 7.0 ± 0.6 nt/s, and δ = 14 ± 1 nt) shows insensitive polymerase velocity to force changes until the stall force (F_{stall}). Bottom, F_{stall} distribution, with < F_{stall} > = 19.3 ± 1.2 pN. Likewise, at the bottom, the force-velocity relationship analysis of EcoRNAP (Arrhenius-like fit with parameter A = 2.3e-08 ± 2.7e-08, V_0 = 7.2 ± 1.1 nt/s, and δ = 13 ± 1 nt) shows comparative values, its < F_{stall} > = 17.1 ± 1.1 pN.
e. The geometry of the force applied moderately affects MtbRNAP's effective elongation rate (k_{el}) and pause escape rate (k_p). We extracted the kinetics and probability parameters using a bi-exponential fit of the dwell-time distribution (time window = 5 / 1 kHz).
f. The geometry of the force applied does not significantly affect the *Mtb*RNAP's pause probability (P_{total}) or on-pathway or elongation probability (P_{el}). We extracted the kinetics and probability parameters using a bi-exponential fit of the dwell-time distribution (time window = 5 / 1 kHz).
g. The pause escape rate (k_p) of MtbRNAP is more sensitive to the DNA sequence than EcoRNAP. The transcription of Eco and Mtb DNA templates revealed that MtbRNAP not only pauses less frequently than EcoRNAP but also pauses for a longer duration in its high GC content DNA template.

Accordingly, treating the RNAP as a molecular motor, we used an Arrhenius-like formula to analyze the Force-Velocity relationship, $V(F) = \frac{V_0(1+A)}{1 + A \exp\left(\frac{F\delta}{k_b T}\right)}$, where V_0 is the velocity at zero force, δ is the distance to the transition state between competent and incompetent polymerases, and A is a dimensionless constant that determines the degree to which either mechanical or biochemical events limit the enzymatic cycle at vanishing load[111]. Thus, we obtained an unphysical distance of δ = 14 ± 1 nt and the dimensionless parameter A = 1.9e-08 << 1, indicating that MtbRNAP became stalled by attaining a

mechanically induced *backtracked state*. (Figure 1d). Moreover, tracking the kinetics rates and distribution of active and paused states of MtbRNAP by using the constant-force mode of the OT instrument[112,113] showed that the effective elongation rate (k_{el}) and the pause escape rate (k_{-p}) respond moderately to assisting force mode, [Pearson correlation coefficient (r) equal to 0.47] (Figure 1e). However, the probability of the effective elongation rate (P_{el}) and pauses (P_{total}) was insensitive to force (Figure 1f). However, we observed that the pause escape rate (k_{-p}) by MtbRNAP is sensitive to the origin of the DNA template, reduced by transcribing the Mtb DNA template (Figure 1f). In chapter 4, we evaluated the modulation of MtbRNAP by Mtb regulators under assisting and opposing forces and found no correlation between pause exit rate (k_{-p}) and pause probability (P_{total}), indicating that the pausing involves transitions to an off-pathway state and that this feature is well-conserved among prokaryotic polymerases.

Our results show that it is possible to use force-spectroscopy to characterize the dynamics of transcription by MtbRNAP to study its modulation by antibiotics.

MtbRNAP weakly recognizes the Eco elementary pause sequences

According to *in vivo* and *bulk* investigations, the prokaryotes and eukaryotes share several consensus transcriptional pause sequences (nascent RNA $_{Y-1G+1}$ and the non-template DNA $_{G-11}$) of differing strengths[114]. Previously, our research team monitored the EcoRNAP transcription dynamics crossing the elemental pauses *a*, *b*, *c*, *d,* and '*his'* by placing these pauses as eight tandem repeats using HROT (Figure 2a)[39]. This approach made it possible to use the resulting pauses of the enzyme to align the molecular transcription traces from different enzymes (Eco *molecular ruler*). With high-precision trace alignment, the researchers determined the probability of the different pauses, discovered that the polymerase slowed down before pause entry, and could follow transcription in real-time with single base-pair resolution. Here, we used the same DNA template to characterize the dynamics of the TB enzyme.

We found that the pausing pattern in the residence time histogram (RTH) of MtbRNAP is very different from that of EcoRNAP (Figure 2b). The reason is not due to the occurrence of random pauses by MtbRNAP; instead, it is due to non-existent or inefficient pause recognition by the mycobacterium enzyme, as we discovered that this polymerase barely produced the bands corresponding to pauses *a* and *b* and did not recognize the sequence '*his'* in *bulk* transcription experiments (Supplementary Figure 12a).

Significantly, we found that MtbRNAP recognizes the pause c (Figure 2c). Accordingly, we inserted this pause sequence in an Mtb *rpoB* gene region to create a new molecular ruler that could perform a detailed characterization of the enzyme. We tested this ruler *in singulo* and found that even at saturating concentrations of nucleotides, MtbRNAP recognizes this pause and produces a reproducible Residence Time Histogram (RTH) (Figure 2d) and permits a characterization of the force dependence of the pause duration in addition to its pause strength.

We utilize this tool later to evaluate if the antibiotic's mechanism comprises sequence-dependent effects.

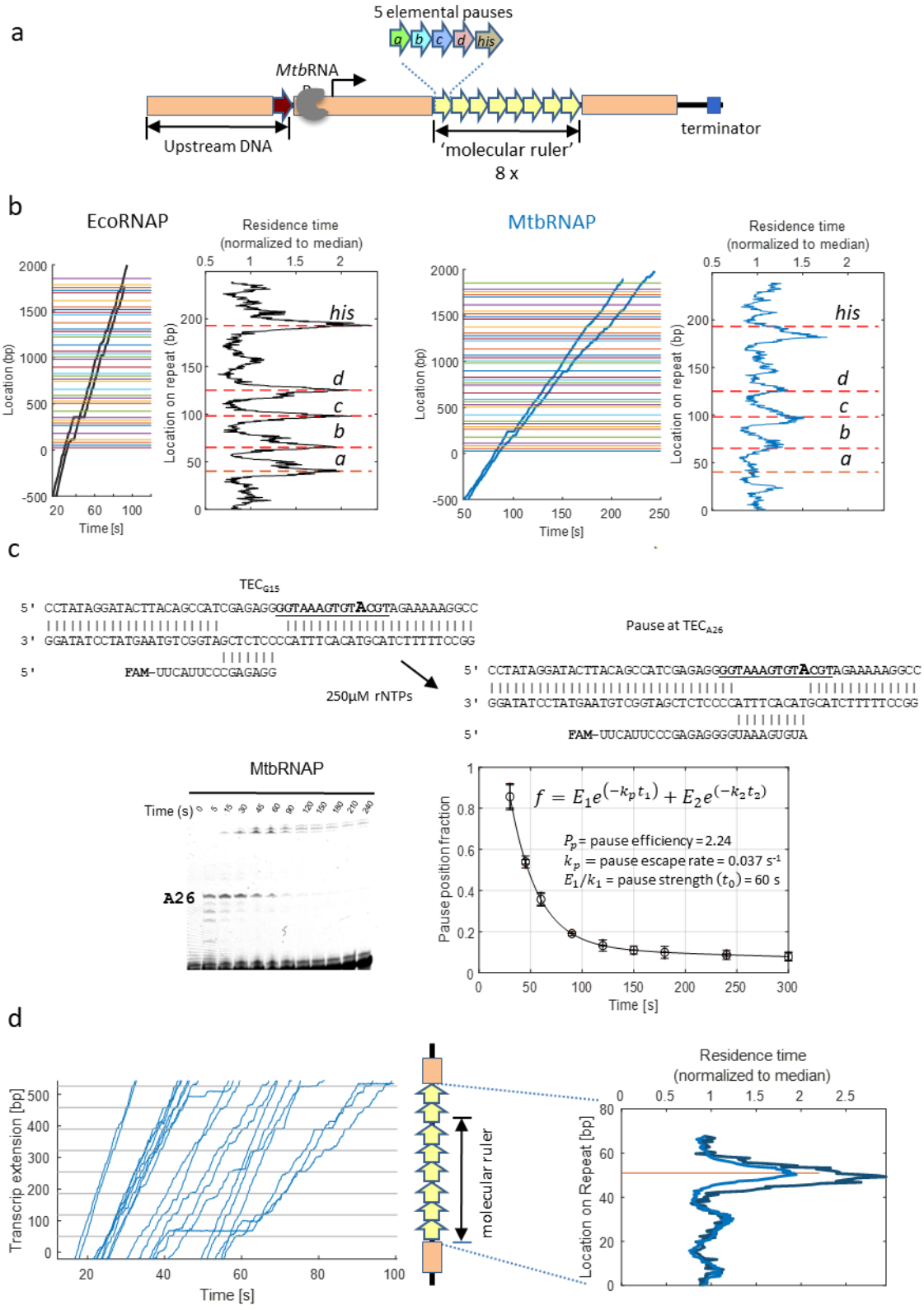
a
5 elemental pauses
a b c d his
MtbRNA
Upstream DNA
'molecular ruler'
8 x
terminator
b
EcoRNAP
Residence time
(normalized to median)
Location (bp)
Time [s]
Location on repeat (bp)
his
d
c
b
a
MtbRNAP
c
TEC G15
5' CCTATAGGATACTTACAGCCATCGAGAGGGGTAAAGTGTACGTAGAAAAAGGCC
3' GGATATCCTATGAATGTCGGTAGCTCTCCCCATTTCACATGCATCTTTTTCCGG
5' FAM-UUCAUUCCCGAGAGG
250μM rNTPs
Pause at TEC A26
5' CCTATAGGATACTTACAGCCATCGAGAGGGGTAAAGTGTACGTAGAAAAAGGCC
3' GGATATCCTATGAATGTCGGTAGCTCTCCCCATTTCACATGCATCTTTTTCCGG
5' FAM-UUCAUUCCCGAGAGGGGUAAAGUGUA
MtbRNAP
Time (s)
A26
Pause position fraction
$f = E_1 e^{(-k_p t_1)} + E_2 e^{(-k_2 t_2)}$
P_p = pause efficiency = 2.24
k_p = pause escape rate = 0.037 s^{-1}
E_1/k_1 = pause strength (t_0) = 60 s
d
Transcrip extension [bp]
molecular ruler
Residence time
(normalized to median)
Location on Repeat [bp]

Figure 2. Sequence dependence pausing by MtbRNAP.

a. The representation shows the *molecular ruler* employed to study EcoRNAP pauses. The DNA template consists of 8 repeats of five *Eco* elementary pauses *a*, *b*, *c*, *d*, and '*his*' arranged in tandem. This method also helps determine the location of the polymerase on the template and measure the pause strength.
b. MtbRNAP does not recognize or pause as effectively as EcoRNAP the Eco elementary pauses sequences. Residence time histograms (RTHs) of EcoRNAP and MtbRNAP display distinctive patterns of pause strength (peak height) and location. On the left side of each RTHs are representative alignments of RNA polymerase traces. The multicolor horizontal lines point to the pause's locations. MtbRNAP weakly recognizes pause sites a, b, and d and does not recognize the Eco '*his*' pause, barely detecting the pause's peak. We collected the transcription activities using a cocktail of rNTPs[39] (1 mM rUTP, 1 mM rGTP, 0.5 mM rATP, and 0.25 mM rCTP) at 15-20 pN, for EcoRNAP and 18 pN, for MtbRNAP.
c. MtbRNAP efficiently recognizes sequence derived from Eco elemental pause c. At the top is an artificial transcription bubble scheme with a 5' FAM labeled RNA used for bulk elongation assay. The stalled ternary elongation complex at position G15 (TEC_{G15}) resumes RNA polymerization activity upon adding 250 µM rNTPs. At the bottom is a UREA PAGE gel that shows the clearance of a pause site at TEG_{A26} with a half-life($t_{1/2}$) of ~ 27 s (inverse of the pause escape 1/ k_1). The fitted graph on the right depicts the *Mtb*RNAP paused state lifetime, and the extracted parameters indicate that this is kinetically equivalent to the elemental paused state of the *Eco*RNAP[114].
d. The Mtb molecular ruler enables the analysis of sequence dependence pausing by MtbRNAP *in-singulo*. Like the Eco molecular ruler, the alignment of traces on the left results from the transcription of a template of eight repeats but with one pause sequence. The histogram on the right indicates a prominent peak of the residence time of MtbRNAP. We collected the single MtbRNAPs transcriptions at saturating rNTPs concentration (1 mM) and 18 pN.

AAP inhibits MtbRNAP elongation by switching it into two slow, active, and exchangeable states.

Next, we investigated how the allosteric drug Nα-aroyl-N-aryl-Phenylalaninamide (AAP) selectively inhibits the MtbRNAP transcription. The counterpart of AAP, CBR pyrazole, is a small molecule that inhibits the EcoRNAP transcription initiation and elongation[115]. These antibiotics disrupt the coordination between the bridge helix (BH) and the trigger loop (TL) by binding to a species-specific hydrophobic pocket at the interface between the BH and the beta subunit (β), which is located far from the catalytic site[8,116,117]. According to the structural analysis of the drug-polymerase complex, the distortion of the BH suggests that the inhibitor will enhance pausing while decreasing catalysis. In addition, real-time fluorescent measurements of the kinetics of formation of the post-translocated state *in bulk*[28] indicate that the inhibition results from tilting the equilibrium towards an inactive state relative to the active state. Nevertheless, the resulting model does not distinguish between an inactive state and a slowly transcribing enzyme or between an inactive, paused, backtracked, or stalled polymerase. An advantage of our optical tweezers approach is that, upon injection of the antibiotic, we can directly monitor changes in the dynamics of a single polymerase in elongation and, therefore, interconversion events of these modes or states caused by the antibiotic in real-time, thereby revealing the nature of the AAP-mediated inhibition.

Thus, we performed the SM assay with saturating nucleotides concentration and AAP nanomolar amount (35-560 nM) of an optimized version of the DAAP-1[80], IX-216a (Figure 3a), of increased affinity for MtbRNAP BH-β hydrophobic pocket. Consequently, we found that IX-216a slows down the MtbRNAP global velocity, which includes the pause and pause-free periods (Figure 3b). The resulting single-molecule traces reveal that in the presence of AAP, MtbRNAP elongation contains two discrete regions of *fast* and *slo*w global velocities. These regions are due to the spontaneous conversion of the enzyme to a slow transcribing mode. In addition, in these events or *transcription switching*, the enzyme can maintain RNA synthesis at the expense of increasing its *dynamic dispersion* (Figure 3c). Although a significant fraction of the slow elongating polymerases ultimately detaches from the DNA template (Figure 3d), the observation of switching events of recovery of the regular global velocity in up to 41% of affected polymerases indicates that the action of AAP is reversible, and not related to a terminal process such as a photodamage event. Accordingly, AAP is not a strict chain terminator.

Moreover, this inhibition is highly selective for the *Mycobacterium* enzyme since IX-216a did not produce any change in the elongating phase of EcoRNAP (Figure 3e). We performed buffer exchange experiments (Figure 3f) to determine whether IX-216a had a higher affinity for the ternary elongation stalled complex (TEC) during the SM starvation phase of the enzymes and before the addition of the nucleotides. We found that the resume of the enzyme activity decreased significantly when the addition of the antibiotics was in the starvation phase compared to after the addition of nucleotides. This result indicates that AAP has more affinity for the TEC without nucleotides. In agreement with this finding, we observed only inhibition of transcription elongation when the enzyme was pre-incubated with the antibiotic before adding NTPs using a *bulk* transcription assay (data not shown).

We found that the elongating MtbRNAP in the slow regions could coexist in three different states, *fast*, *slow,* or *super-slow* (Figure 4a). To characterize them in detail, we extracted the dwells from various fast and slow regions obtained in the presence of AAP and the activities without this drug as a control (Figure 4b). Our examination of the Dwell Time Distribution (DTD) of the fast regions with IX-216a revealed that they are the drug-*unbound states* of the polymerase, as they are indistinguishable from control transcription elongation (Figure 4c). However, we cannot rule out that the unbound state interacts transiently with the inhibitor below the temporal resolution of our technique. Correspondingly, the slow regions are the *bound states* of MtbRNAP. In addition, the analysis of DTDs of different slow regions allowed us to make two crucial findings: IX-216a shifts the distribution of polymerase states towards the paused one and can also convert the active MtbRNAP state into any of two active slow and super-slow states above-mentioned (Figure 4c). Both states have reduced velocities to different extents. In the slow state, the most notable change is an increase in the probability of short and long-lived pauses, whereas, in the super-slow state, the most striking difference is a halving of the effective elongation rate.

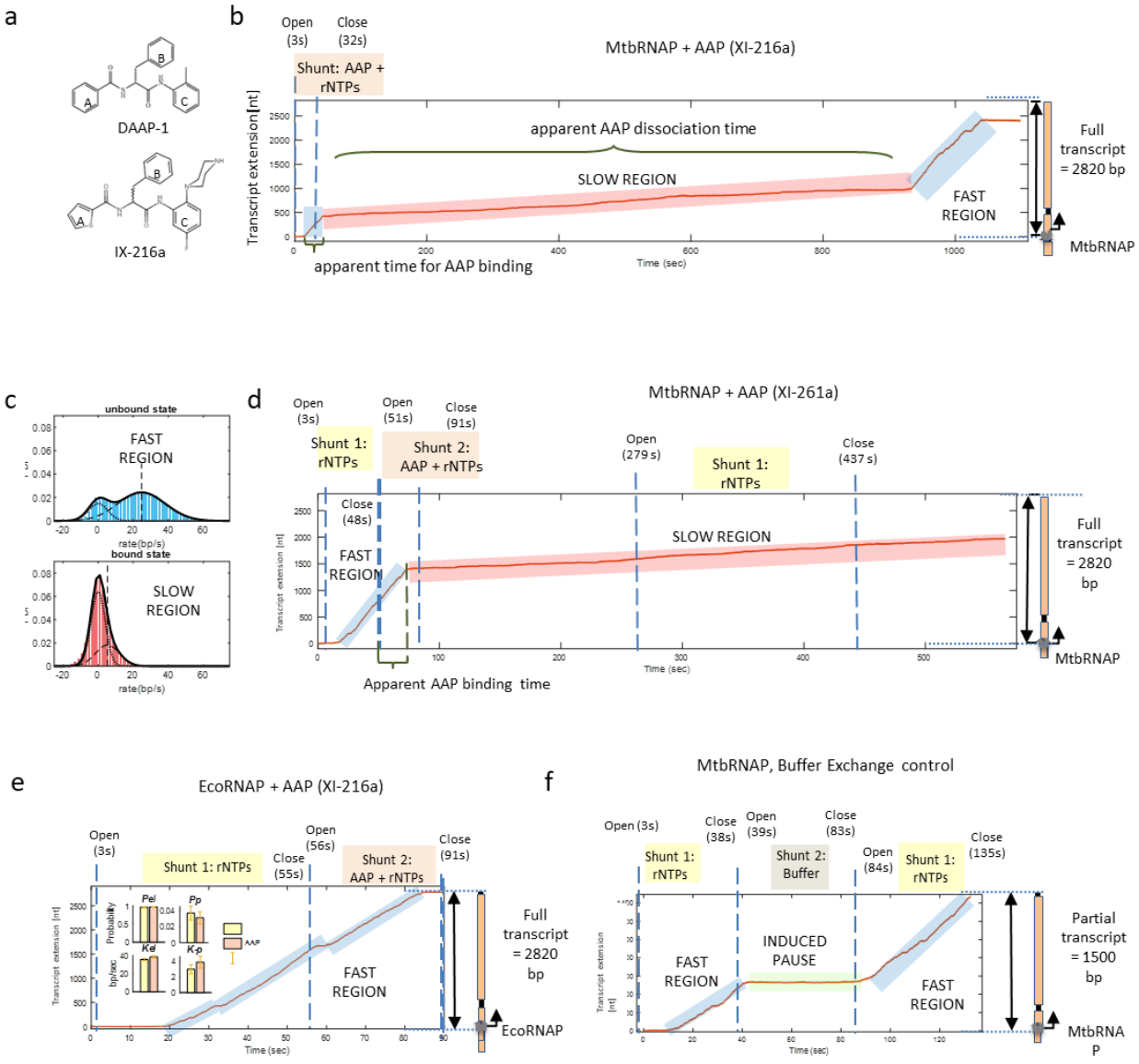

Figure 3. AAP specifically slowdowns the MtbRNAP

a. Molecular representation of the Nα-aroyl-N-aryl-Phenylalaninamide (AAP) shows the modification of rings A and C to increase affinity for the MtbRNAP. DAAP-1 is one of the first discovered AAP, and IX-216a is the optimized drug.

b. IX-216a switches the MtbRNAP global velocity rather than pausing or halting it. The distance versus time graph of an 18 pN AF single MtbRNAP transcription in the presence of AAP and saturating nucleotides (280 nM IX-216a and 1 mM rNTPs) depicts fast and slow regions of global velocity. At the beginning of the trace, following the injection of nucleotides and the antibiotic via the shunt (highlighted box on the top), the stalled polymerase resumed activity at a standard average velocity (~ 20 nt/s). Then, it eventually lowers its velocity due to AAP binding. Depending on the evaluated condition, ~ 41 % of polymerases can recover their initial velocity. The change in global velocity represents switches events. We noticed that the apparent association time (t_a) for AAP binding corresponds to the time between the shunt

opening and the switch's appearance. On the other hand, the apparent AAP dissociation time encompassed the slow region's lifetime.

c. IX-216a can reduce MtbRNAP velocity by half. Histograms show rates of probability distribution corresponding to the fast and slow regions. The PFV distribution from the slow region nearly overlaps the distribution of the pauses.
d. AAP remains engaged in MtbRNAP elongation. Using shunts to do buffer exchange in the slow region to wash the antibiotic out did not restore polymerase velocity immediately. At the end of the trace, the polymerase might detach from the DNA template as tether break events or stall. The detachment and stalling events could occur in up to 45% and 13% of polymerases, respectively. We experimented with assisting force by opening the second shunt to supplement AAP right before the arrival of the MtbRNAP on the ruler sequence.
e. IX-216a does not alter single EcoRNAP activity. Two-shunts experiment shows that 280 nM IX-216a does not switch or alter a single EcoRNAP activity. The inset shows a bar plot comparing AAP's effect on distribution and rates of the active and paused states of the polymerase compared to the control (transcription buffer). We found no effect on rates or distribution of EcoRNAP caused by AAP.
f. The control experiment of buffer exchange shows RNAP responds instantly to the buffer condition. Upon the remotion of the nucleotides, the *Mtb*RNAP, in active elongation, immediately enters an extended pause state that lasts until injecting back the nucleotides.

Knowing that the RNAP is a processive motor that binds the DNA template and takes successive catalytic steps before detaching[48], we evaluated AAP's effect on the *Mycobacterium* enzyme's processivity. We found that IX-216a reduces the processivity of the elongating MtbRNAP, and the super-slow state is the least processive (Figure 4d). However, the lifetime distributions of both slow and super-slow states are almost identical (Figure 5a). Once in any of those states, interconversion events occurred in up to 18% of the enzymes, suggesting that the unbound, slow, and super-slow states belong to an off-pathway triangle kinetic scheme (Figure 5b, c). Our results indicate that most transitions are independent of the MtbRNAP translocation states (pre-translocated *versus* post-translocated) since their transition probabilities change little under assisting or opposing force modes (Figure 5b, c). Likewise, the number of *switches* per trace seems independent of the translocation state of MtbRNAP (Figure 5d).

Although the AAP effect on MtbRNAP elongation still allows forward movement, albeit slowly, the drug's effect may be the change in the enzyme's affinity for the nucleotides. If that were the case, reducing the amount of nucleotides would significantly alter the distribution of the slow or super-slow states, contrary to what would be expected in the unbound state. Therefore, we reason that measuring transcription activities at low concentrations of nucleotides would help evaluate any effect on the states' probabilities. Since the unbound state's effective elongation rate (k_{el}) is significantly reduced at low nucleotide concentrations, we only observed super-slow states from switching events. Consequently, we observed no significant change in the DTDs among states (Figure 5e). Thus, we did not find evidence that AAP allosterically affects the polymerase affinity for the nucleotides.

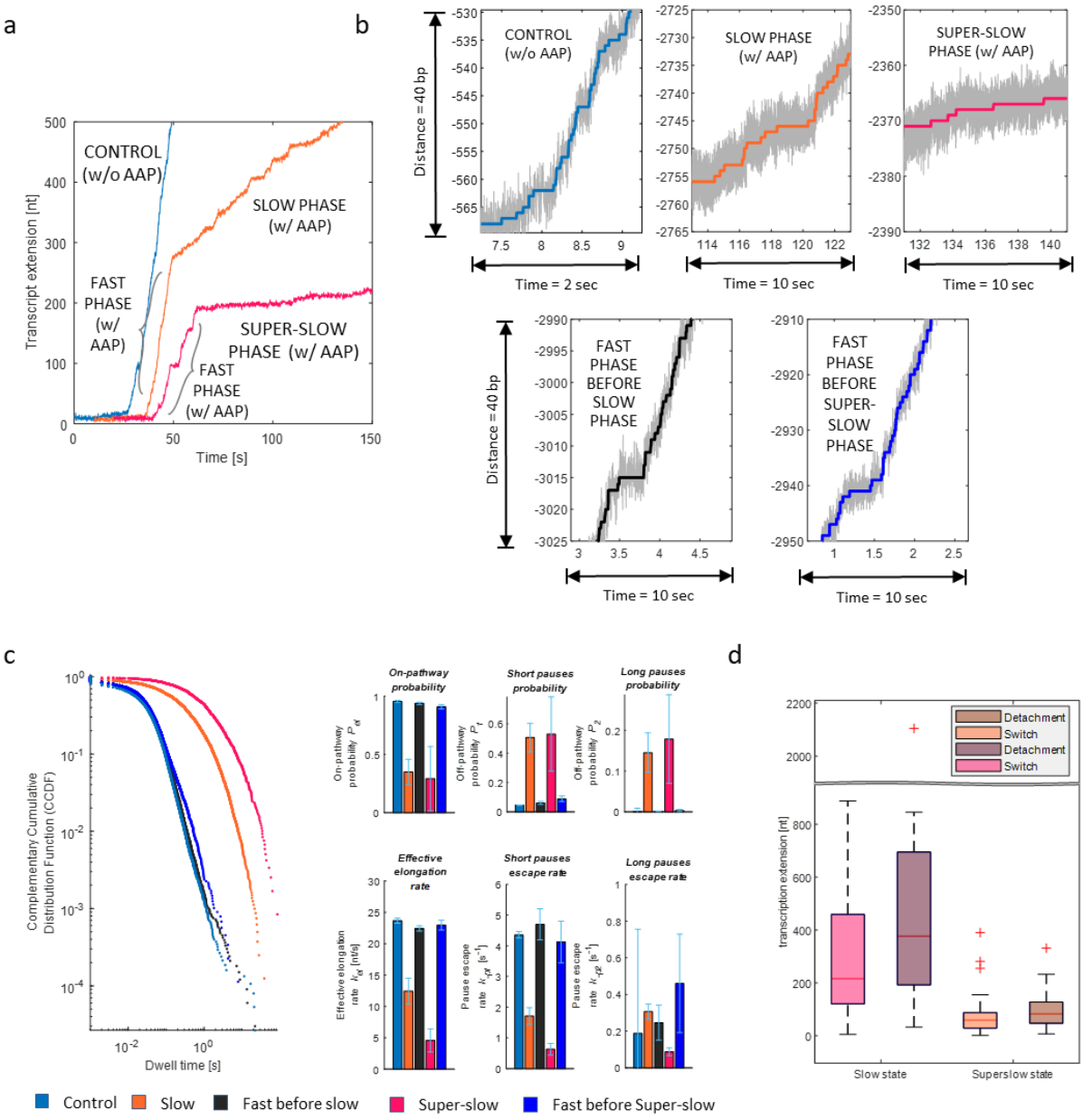

Figure 4. IX-216a (AAP) switches MtbRNAP into two different slow elongating states.

a. IX-216a produces two states of the active MtbRNAP: one slow state (orange curve) and one super-slow state (pink curve). The graph includes a trace obtained in the absence of IX-216a (blue curve) as a control to show the moment the switch takes place from the fast regions. We collected the many activities at 18 pN AF, 1 mM rNTPs, and IX-216a in the range of 35- 560 nM range.

b. The slow and super-slow states contain bursts and pauses. Graphs of base-pair staircase fitting of the control trace and the super-slow and slow regions depicting the dwells in the same scale of bursts and pauses of these different polymerase states.

c. The fast region in the presence of IX-216a is the unbound state. (Left) Analysis of the complementary cumulative distribution functions (CCDF) of the dwells of the control trace without Ix-216a and the fast regions in the presence of IX-216a showed that they are identical. (Right) IX-216a affects the slow and super-slow states differently by tilting the equilibrium from active toward paused states and decreasing the effective elongation rates. The bars plots represent the kinetics parameters extracted from the complementary cumulative distribution function $\mathrm{CCDF} = \sum_{i=1}^{n} a_i e^{-k_i t}$ Where a_i = probability of the state and k_i = kinetic rate. The slow state mainly has increased pausing, and the super-slow state has reduced the effective elongation rate. In addition, as mentioned above, the fast regions share similar rates and distribution values as those without IX-216a.
d. The super-slow state is less processive than the slow state. The bar plots show the final progression of the elongating MtbRNAP in those states under different force geometry. Neither assisting nor opposing modes change the intrinsic tendency of the processivity of those states.

Traditional biochemistry uses the concepts of half-maximal inhibitory concentration (IC_{50}) and apparent dissociation constant (K_D) indistinguishably when studying small-molecule inhibitors of RNA polymerase. Calculating the K_D of these drugs is challenging because it requires measuring the association and dissociation kinetics rates (k_{on} and k_{off}) in non-equilibrium conditions. In addition, there is no available technique to measure these kinetic rate values for small drugs binding an elongating RNA polymerase. Since we have access to the AAP's apparent association and dissociation (or residence) times for the elongating MtbRNAP during the *switching* events, we derived the apparent IX-216a k_{on} and k_{off} from their respective lifetime distributions. Thus, we found that the low K_D of AAP for the elongating MtbRNAP is due to its very slow k_{off} (Figure 5f), which is the ideal residence time for drug inhibitors[118], because as high as the residence time is, so the drug's potency is. In addition, we support the model of one molecule of AAP affecting the polymerases by the following reasons: (i) varying the AAP concentration did not affect the DTD, and (ii) washing the antibiotic out of the affected polymerase did not immediately switch back the global velocity.

Later, we questioned whether the AAP effect is sequence-dependent. Using the Mtb *molecular ruler*, we measured the effect of AAP on pausing while crossing the tandem repeat. We found that when the enzyme was in slow states while crossing the repeats, its ability to recognize the elemental pause sequence *c* increased. This increased pause recognition is to be expected if the paused state is off the main pathway and, therefore, its visiting is in kinetic competition with the on-pathway transcription. Strictly speaking, the enzyme always detaches from the template when crossing the repeat in its *super-slow state* (Figure 6a, b). Anecdotally, we can report that no enzyme was seen to cross the whole repeat while in the *super-slow state* crossing the whole repeat and that few backtrack events precede the DNA detachment (Figure 6a). In the RTH, we can observe many polymerases pause (in the pause *c* location) before slowing down, but the detachment position on the ruler is not located in the pause site. In addition, IX-216a increases the enzyme's pause density, manifesting in the appearance of new RTH peaks (Figure 6a, b, c). Global analysis of the processive part of the slow and super-slow states transcribing a different DNA template revealed that the pauses of MtbRNAPs in the presence of the antibiotic are off-pathway because their dwell-time distributions did not change when the enzyme was subjected to assisting or opposing force.

.

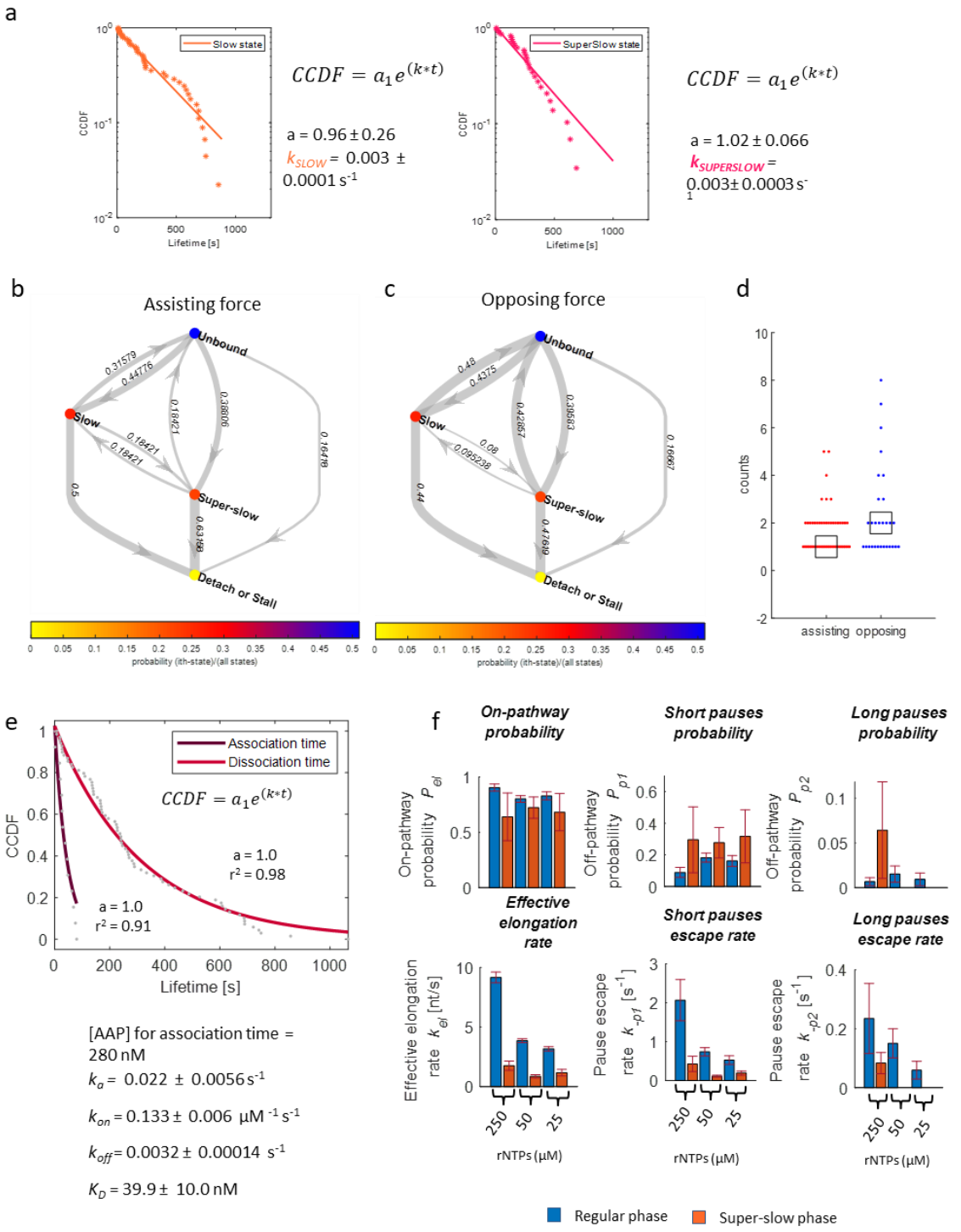

Figure 5. The slow and super-slow states can interconvert with each other

a. Lifetimes of the slow and super-slow states are comparable. We excluded tether-breaks events and only accepted the switches that proceed to the regular active polymerase or any slowing states.

b. Transition probabilities under AF show significant events of tether breaks from the slow and super-slow states. In addition, there are more chances to revert to the regular velocity of the active polymerase from the slow state.
c. Transition probabilities under OF show higher chances of recovering and stalling from the super-slow and slow states, respectively.
d. The direction of the tension does not bias the number of switches, indicating that translocation might not originate the phenomenon.
e. The reduction of nucleotide concentration in the presence of AAP affects neither the distribution nor the kinetic rates. That suggests that AAP does not affect the MtbRNAP affinity for the nucleotides
f. The lifetime distribution of the apparent microscopic association and dissociation shows that the residence time or k_{off} of AAP for the elongating polymerase is slow.

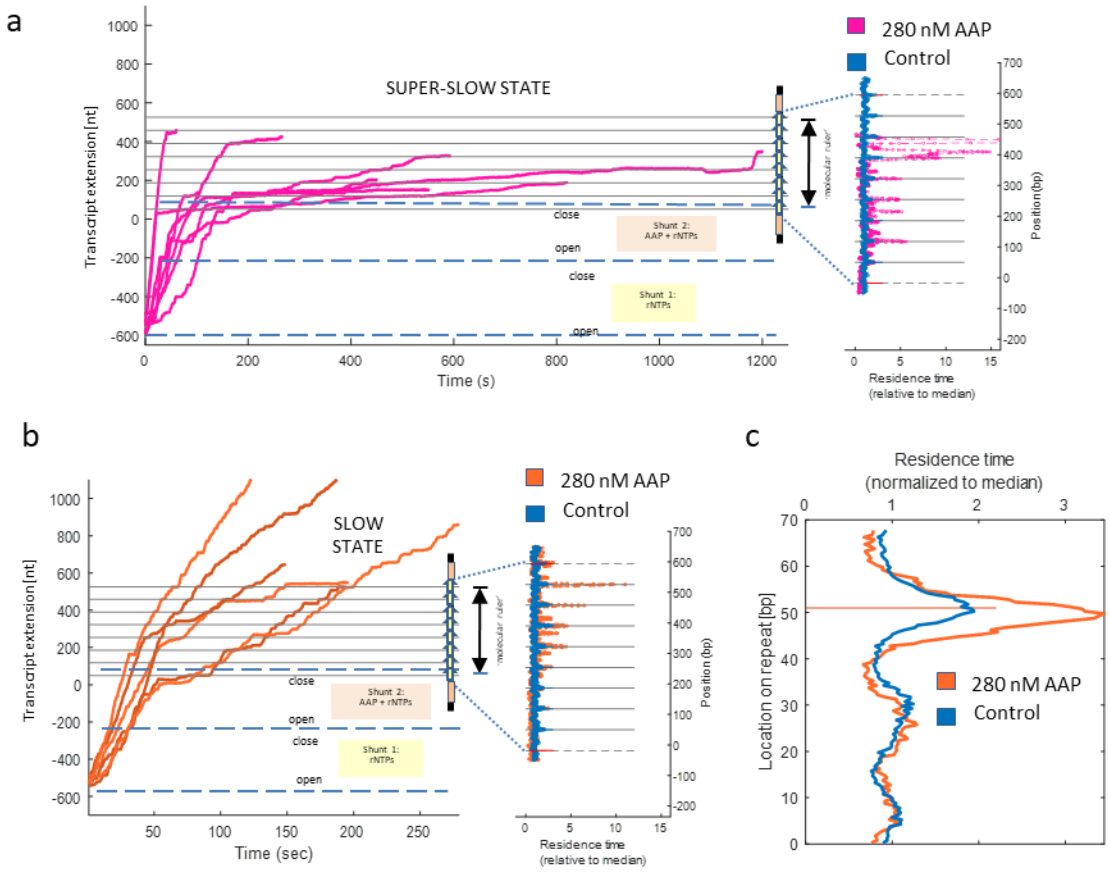

Figure 6. The super-slow state decreases processivity while crossing the pause repeat.
a. The super-slow state detaches from the DNA template while crossing the pause repeat sequence. The graph shows the alignment of the traces and the region before the polymerases fall off. On the right is the corresponding non-averaged RTH, showing each pause residence peak. The super-slow state did not go over the whole ruler and broke before the end.
b. The study of the dynamic of crossing the pause repeat by the slow state shows that the AAP effect is sequence-dependent. AAP increases the residence time on pause c.

c. The average residence time histogram (RTH) of the MtbRNAP slow state crossing the pause *c* repeat shows that AAP also increases the pause density of the polymerase because of the broader peak upstream at the elemental pause site.

Streptolydigin affects MtbRNAP to make long-live pauses associated with backtrack events.

Streptolydigin (STL), an antibiotic composed of tetrameric acid, streptolol, and sugar moieties, inhibits the initiation, elongation, and pyrophosphorolysis of the bacterial RNA polymerase[119,120]. Previous research showed that STL enters the secondary channel (SC), binds, and disrupts the BH-TL interface, straightening the BH and distorting the TL to change the equilibrium between pre- and post-translocated states[64,121]. As a result, STL prevents the polymerase active site from isomerizing from an inactive to an active conformation without affecting forward translocation, nucleotide loading, or catalysis. The STL mechanism depends upon the previous polymerase state, stabilizing catalytically inactive substrate-bound transcription intermediates. The unknown is, however, what occurs after this stabilization. Our understanding of the *molecular fate* of the inhibited RNA polymerase is limited.

For this reason, we studied the dynamics of the recovery of RNAP from the natural post-translocation bias imposed by STL[28,64,121], thought to occur stochastically along the DNA template. Further, due to the controversies surrounding the description of STL action on sequence-dependence events, we employed our *molecular ruler* approach to evaluate the effect of this drug on pausing. Likewise, using optical tweezers, we avoid biases observed in *bulk* single-turnover assays that hinder RNAP's ability to carry out its regular functionality. In addition, we utilized the elongation of MtbRNAP, which is more sensitive to STL than EcoRNAP due to the 792D residue in the BH, which interacts strongly with the acetamide group of STL[28,121].

Thus, under assisting force, micromolar concentrations of STL inhibited the elongation of MtbRNAP by inducing sporadic pauses of varying lengths that recover via backtracking (Figure 7a). Knowing that STL occupies the EcoRNAP in the pre-and post-translocation states[64] and verifying that such is also the case for MtbRNAP[18,64] (Figure 7b), a detailed analysis of the dynamic of two-step mechanism of backtrack would provide insights into when the STL is released. Therefore, we surmise that during the pre-backtrack time and before backtracking, STL remains bound to the polymerase in the post- or pre-translocated states (Figure 7c, d). As the polymerase moves from the pre-translocated state to the backtracked state, STL may dissociate from it. On average, the depth backtrack events were 7 ± 1 nt (Figure 7e), higher than backtrack events in EcoRNAP rescued by cognate transcription factor GreA. Indeed, MtbRNAP was able to correct it without any factor help. Additionally, we found that the region of backtrack recovery contains dynamic steps that exceed our spatial-resolution detection limit; as a result, we employed the highest temporal resolution of our instrument to study this period. Thus, the data accurately follows a single exponential decay (Figure 7d), corresponding to RNA cleavages rather than the power law distribution ~ $t^{-3/2}$ of diffusive backtrack[42], in agreement with the recent observation of deep backtrack in different polymerases[33].

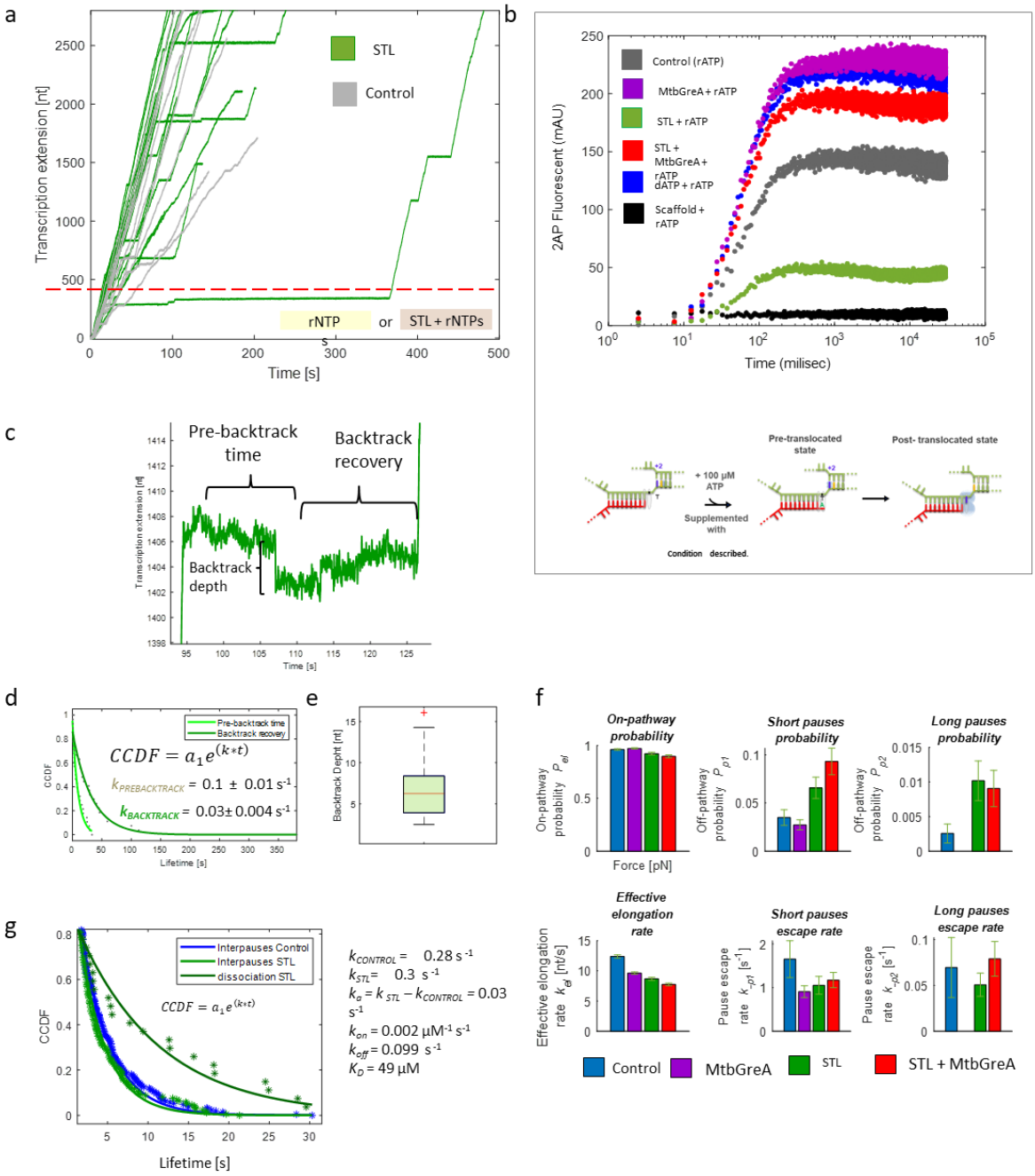

Figure 7. Inhibition by STL induces MtbRNAP depth backtracks to recover endonucleolytically.

a. SLT induces long pauses on the MtbRNAP. Even though the traces in green (with 15-45 µM STL) pauses, they transcribe almost the whole DNA template as the control (gray traces). The traces correspond to assisting force mode at saturating nucleotide concentration.

b. Nitrogen analog-based fluorescent translocation measurements show that STL stabilizes the post-translocated state of MtbRNAP (green dots). We used the 2-Aminopurine (λex/ λem = 330 / 375 nm) introduced in the transcription bubble *i+2* position to show an increase of fluorescent by ~ 20 % of the polymerase incorporating one nucleotide (PPI-free rATP-extended MtbTEC). Compared to the control with MtbGreA, STL also induces the pre-

translocated states. STL did not induce backward movement from the post-translocated state, unlike tagetitoxin, as in previous work with EcoRNAP[28].

c. The trace schematically represents the regions of pre-backtrack time, depth backtrack, and recovery time during STL inhibition of MtbRNAP.
d. The backtrack lifetime follows a single exponential decay from recovery from paused induced by STL on the MtbRNAP.
e. The MtbRNAP backtrack depth induced by STL inhibition is greater than the diffusive mechanism.
f. DTD of MtbRNAP from 5 pN constant opposing force data suggests that MtbGreA increases the pause exit rate (k_{-p}) of extended pauses caused by STL. This finding means that the mechanism of backtrack recovery is likely endonucleolytic dependent. The plot bars represent different conditions, including the control (buffer with 1 % glycerol and 1 % methanol), 15 µM STL, 0.5µ M MtbGreA, or 15 µM STL plus 0.5 µM MtbGreA. According to these results, MtbGreA assists the MtbRNAP in the cleavage of the 3' end of the protruding RNA. At the same time, it blocks the secondary channel, affecting the binding of incoming NTPs, which reduces the effective elongation rate, as we observe.
g. The dissociation constant (K_D) of STL derives from the apparent association (k_a) and association (k_{off}) kinetics rates. We obtained k_{off} from the lifetime distribution of the pre-backtrack time at assisting force and k_a, from the difference in inter-pause times kinetics rate in the presence (k_{SLT}) and absence ($k_{CONTROL}$) of STL at opposing forces. The k_{on} is obtained by dividing k_a over the used concentration of STL (15 µM). Finally, we calculated the K_D by dividing the k_{off} over the k_{on}. The result indicates that k_{off} of STL is higher than AAP.

The half-life time of MtbRNAP in the backtracked states before resuming activity is ~ 32.3 +- 3.8 s. These long-backtracked pauses likely recover via intrinsic endonucleolysis by MtbRNAP. To address this hypothesis, we used MtbGreA, known to assist the excision of the protruding 3'end of the RNA resulting from the backtrack states [122]. Accordingly, we predict this would lead to a shortening in pausing. Thus, we collected data on MtbRNAP elongation on opposing forces in the presence of MtbGreA and STL and evaluated the kinetic parameters. We found that MtbGreA reduces the pause duration (increase in pause escape k_{-p}), otherwise increased by STL (Figure 7f).

It is challenging to distinguish the events of binding and release of STL from MtbRNAP experimentally. To address this issue, we derived the microscopic binding and unbinding rate constants from the time the MtbRNAP is in the paused phase under the assumption that this fraction is proportional to the apparent time STL remains bound to the polymerase[123]. Therefore, using the pre-backtrack time distribution determined from micromolar concentrations of STL, we calculated STL k_{off} to be 0.099 ± 0.012 sec^{-1}, which is faster than the corresponding constant for AAP and explains why the higher concentration of STL is required to be effective *in vitro*. To determine STL k_{on}, we used opposing force data because pause duration is prolonged (> 1 s) and facilitates obtaining the apparent association rates (k_a). We derived the k_a from the difference in lifetime distributions of inter-pause periods in the presence and absence of STL. Dividing the k_a by the drug concentration renders a k_{on} equal to 0.02 ± 0.009. Thus, the apparent STL K_D for the elongating MtbRNAP was ~ 49 µM (Figure 7g).

Later, we evaluated the possibility of the STL mechanism being sequence dependent. Suppose STL does not increase the pause density. In that case, its mechanism depends on stabilizing a previously inactive state of the MtbRNAP. Suppose STL reduces the RNA polymerase residence time. Then, STL might affect the post-translocated state over the

pre-translocated state associated with an increase in pausing[18,124,125]. Using the Mtb molecular ruler, we observed that STL only increases the residence time of MtbRNAP crossing the elemental pause sequence (Figure 8a, b). These results suggest that the STL mechanism stabilized the pre-translocated state and depends on a pre-formed catalytically inactive polymerase state. If STL affected the post-translocated state more, it would increase the chance to resume and escape from pause *c*, which we did not observe.

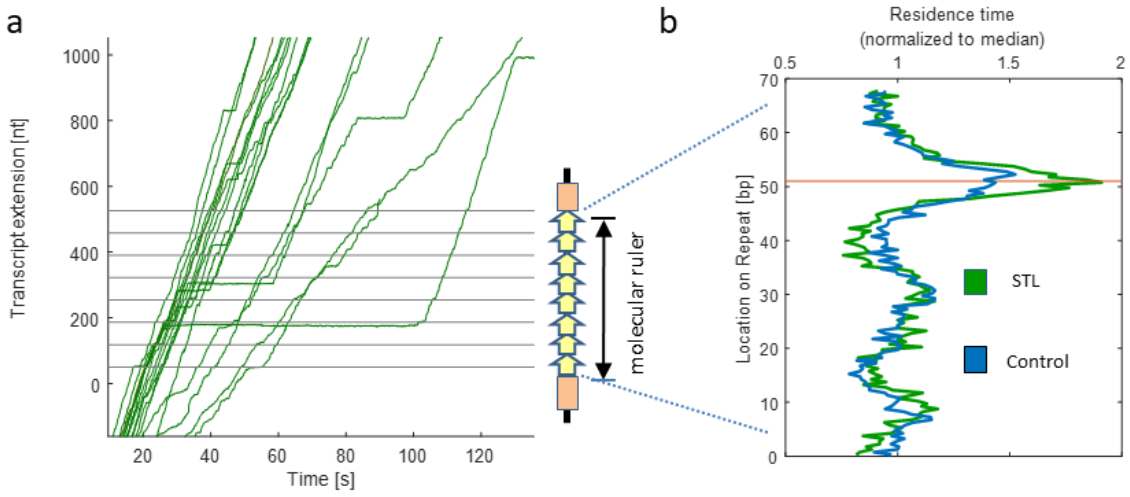

Figure 8. STL increases the residence time of MtbRNAP crossing elemental pause c

a. Alignment of traces of MtbRNAP of an assisting force in the presence of 15-45 µM STL shows that STL does not impede the enzyme from crossing the repeat section. In other words, STL is not a string chain terminator.
b. RTH shows that STL increases the pause strength at the elemental pause pausing but does not increase the pause density. This observation suggests that STL's effect depends on the initial inactive state of MtbRNAP.

Pseudouridimycin increases the pause density in EcoRNAP and switches the active state of MtbRNAP into two slow active states.

Pseudouridimycin (PUM), the first competitive nucleotide addition inhibitor (NAI) discovered against bacterial RNA polymerase, hinders rUTP occupancy at the NTP addition site (A). PUM interacts specifically with RNAP essential residues and the preceding RNA 3'-nucleotide. PUM inhibits gram-positive and gram-negative bacteria polymerases as opposed to human or viral polymerases. Although elongation *bulk* tests demonstrate that PUM pauses the EcoRNAP one nucleotide before rUTP incorporation positions, we do not fully comprehend the kinetics of this inhibition and how the enzyme dynamically recovers. To understand these phenomena, we first analyzed the effect of PUM on the EcoRNAP pausing probability and density, followed by analyzing the difference in pause recovery with MtbRNAP.

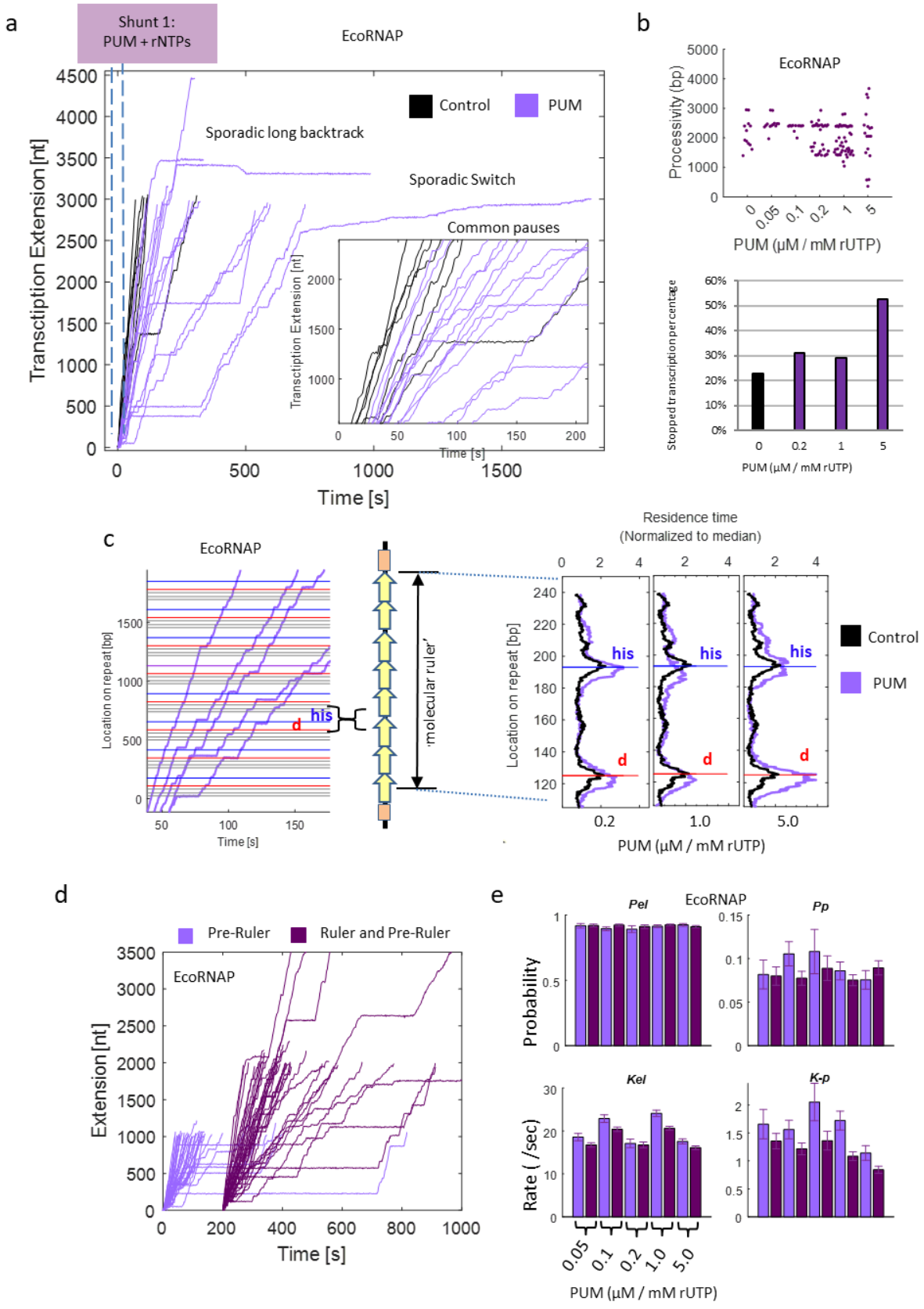
a
Shunt 1:
PUM + rNTPs
EcoRNAP
Control
PUM
Sporadic long backtrack
Sporadic Switch
Common pauses
Transcription Extension [nt]
Time [s]
b
EcoRNAP
Processivity (bp)
PUM (µM / mM rUTP)
Stopped transcription percentage
c
EcoRNAP
Location on repeat [bp]
his
d
'molecular ruler'
Residence time
(Normalized to median)
Control
PUM
d
Pre-Ruler
Ruler and Pre-Ruler
EcoRNAP
Extension [nt]
Time [s]
e
EcoRNAP
Pel
Pp
Kel
K-p
Probability
Rate (/sec)
PUM (µM / mM rUTP)

Figure 9. PUM increases the pause density of EcoRNAP crossing the elemental pauses

a. PUM inhibits the EcoRNAP transcription by inducing pauses that recover without backtracking. SM traces at AF of EcoRNAP collecting at 1 µM PUM, and 1 mM rNTPs show pauses created by the antibiotic. In addition, the plot displays a sporadic long backtrack and switch event observed once for all concentration tests of PUM.
b. PUM does not share the properties of a strict chain terminator. The plot on the top shows the end of the transcription elongation by EcoRNAP at different concentrations of PUM under assisting forces. On the bottom, the bar plot shows the percentage of polymerases that did not reach the end termination region.
c. PUM increases the pause density of EcoRNAP crossing the elemental pauses. The three graphs show the residence time histograms of EcoRNAP obtained with PUM (in purple) compared to those without it (in black). Represented are in the RTHs, the peaks for pause sequence *d* and *his*, as increase the antibiotic concentration, their residence time increases. However, at higher concentrations of PUM, the EcoRNAP does not efficiently recognize the pause sequence, likely affecting the RNA folding formation of the hairpin pause.
d. The slowing kinetics of EcoRNAP caused by PUM is not sequence-dependent. The graphs show two groups of a section of traces corresponding to the Pre-ruler (pre-repeat) and the ruler and post-ruler, respectively.
e. The bar pot at the side shows no differences in the kinetics rate or distribution of those sections among different antibiotic concentrations.

Addin PUM *in trans* caused EcoRNAP to make long, and medium pauses evenly distributed across the DNA template (Figure 9a). In addition, the increment of the PUM/rUTP molar ratio from 1e-3 to 5e-3 reduced the productive transcription from 9% to 28%, respectively, including irreversible stalling or tether breaking (Figure 9b). Since the IC_{50} of PUM is ~ 100nM (personal communication with Ph.D. Richard Ebright), and at 50 times the IC50, more than half of polymerases transcribe the template beyond 2.5kb, reaching the termination region, it appears that PUM does not share the characteristics of a strict chain terminator. Also, in the pauses caused by PUM, EcoRNAP recovers without backtracking events (inscribed graph of Figure 9a).

In addition, we investigate if PUM could cause these pauses by a sequence-dependent mechanism. To understand that further, we tested how increasing the PUM/rUTP ratio from 2e-4 to 1e-3 affects the polymerase residence time while crossing the Eco elemental pauses sequence repeats. After the m*olecular ruler* alignment of the traces, the RTHs revealed that PUM strengthened pause *b* and *his* residence peak*s* by increasing their height and broadening their upstream regions, which correspond to competitive inhibition rUTP incorporation positions (Figure 9c). However, working at a higher PUM/rUTP ratio (5e-3) weakened the *'his'* pause strength, presumably by altering the kinetics of the hairpin RNA folding. Along with this observation, PUM also increases the polymerase pause density since a new broad peak in the RTH appeared downstream of *his* pause peak.

Later, we tested if PUM affects the velocity of EcoRNAP for the following reasons: First, regardless of the PUM/rUTP molar ratios studied, in the pause repeat region, there was a noticeable decrease in the global enzyme velocity likely due to the previously observed effect of pause entry[39], and second, in few traces the velocity switch to a slow mode. For the first case, we compared the DTDs of the transcription sections before traversing the repeat region (pre-ruler) with those crossing and downstream the pause

repeat. Then, we found that PUM does not change the effective elongation velocity (k_{el}) of EcoRNAP crossing the pause repeat (Figure 9d).

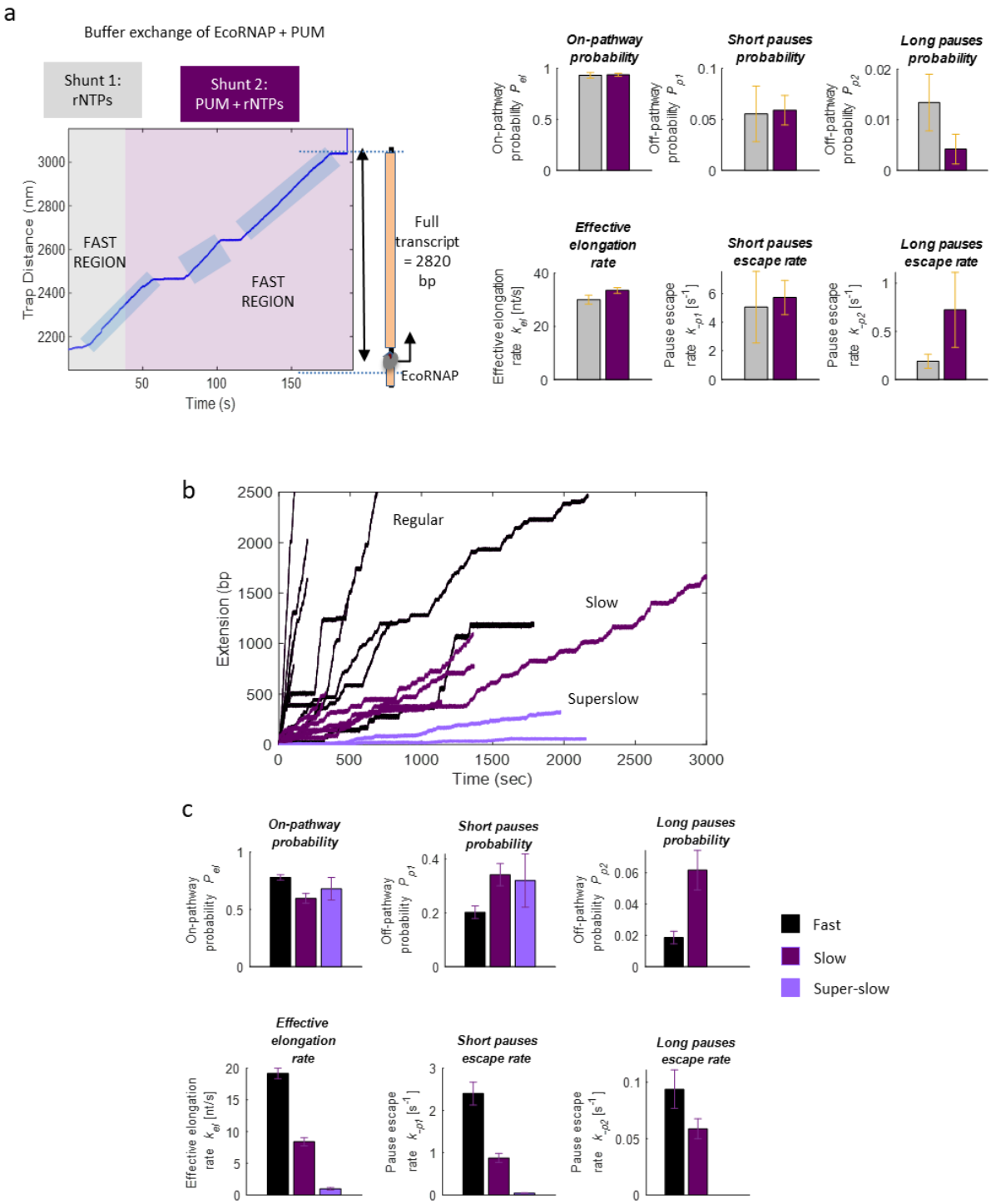

Figure 10. PUM induces EcoRNAP to convert to slow transcribing mode infrequently.

a. Adding PUM on already resumed and elongating EcoRNAP does not show instantaneous switch events or changes in velocity. At the left is a graph displaying an *in-singulo* EcoRNAP transcribing the Mtb DNA template. Upon opening the second shunt to proportionate the antibiotic, the polymerase instantly enters a long pause that resumes without backtracking. The resuming activity section is that section for comparison with the transcription section before adding PUM. On the right, the bar plot shows that the effective elongation rate of those sections is comparable. Therefore, we conclude that PUM does not induce instantaneous switches in EcoRNAP as seen in MtbRNAP with AAP
b. The plot represents the few slowing elongating EcoRNAP traces observed in the presence of PUM (1-4% of treated enzymes) resembling the slow, and super-slow states found with AAP.
c. The bar plot shows a significant reduction in the effective elongation rate (k_{el}) and an increase in pause probability for the EcoRNAP slow and super-slow state induced by PUM.

Furthermore, we conducted buffer exchange experiments of PUM for Eco enzymes transcribing other DNA templates, searching for an instantaneous change in velocity. Likewise, we did not find any significant instantaneous change in velocity passing from PUM-free elongation to a condition with this antibiotic (Figure 10a). In the second case, we only observed 6 switching events out of 150 enzymes treated, 4 for slow and 2 for super-slow, 4% and 1% total, respectively (Figure 10b). Our DTD analysis indicates these states resemble the AAP ones, except for having lower velocity and low pausing probability (Figure 10c). Our experiments suggest that PUM does not instantly reduces the EcoRNAP velocity; nevertheless, this occurs in sporadic stochastic situations.

Next, we studied the dynamics of MtbRNAP elongation inhibition by PUM. Since a novel derivative of PUM, deshydroxy-PUM or FE04 (Figure 11a), showed higher stability to hydrolysis in an aqueous solution at room temperature, we included it in our analysis. Thus, the *in-singulo* elongation data reveals that MtbRNAP molecules, upon the injection of the drug, often pause without losing their ability to escape; however, the enzyme in ~ 28% of cases entry to a *transcribing state* with slow or slower global velocities from which it seldom reverts or switch (Figure 11b). These states contain regions of a lower signal-noise ratio due to an oscillating mode of forward and backward jumps, convoluted in distinct extended pauses, sporadic backtracking events, and a few slow bursts (Figure 11c). These jumps were in the range of 20-10 bp. A thorough analysis of the DTD, including low-noise regions of these slow transcribing polymerases caused by PUM, confirmed that they share features with the *slow* and *super-slow* states caused by AAP (Figure 11d and e). Indeed, the probability of finding the MtbRNAP in the *active state* with PUM is slightly higher than with AAP (0.6-0.4 *versus* 0.4-0.2 *slow* and *super-slow states*, respectively).

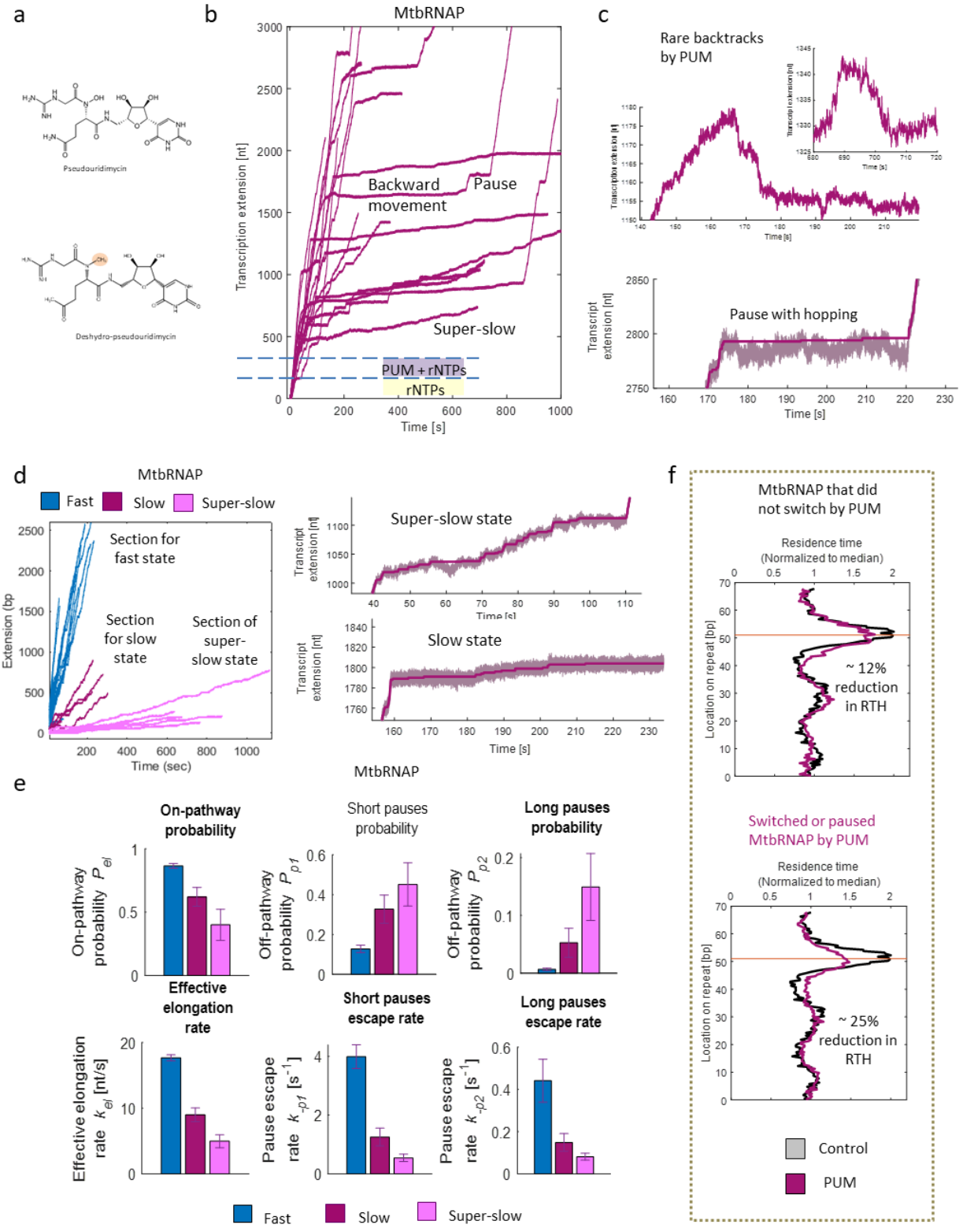
a
Pseudouridimycin
Deshydro-pseudouridimycin
b
MtbRNAP
Transcription extension [nt]
Time [s]
Backward movement
Pause
Super-slow
PUM + rNTPs
rNTPs
c
Rare backtracks by PUM
Transcript extension [nt]
Time [s]
Pause with hopping
d
MtbRNAP
Fast
Slow
Super-slow
Extension (bp
Time (sec)
Section for fast state
Section for slow state
Section of super-slow state
Super-slow state
Slow state
Transcript extension [nt]
Time [s]
e
MtbRNAP
On-pathway probability
Short pauses probability
Long pauses probability
On-pathway probability P_{el}
Off-pathway probability P_{p1}
Off-pathway probability P_{p2}
Effective elongation rate
Short pauses escape rate
Long pauses escape rate
Effective elongation rate k_{el} [nt/s]
Pause escape rate k_{-p1} [s^{-1}]
Pause escape rate k_{-p2} [s^{-1}]
Fast
Slow
Super-slow
f
MtbRNAP that did not switch by PUM
Residence time (Normalized to median)
Location on repeat [bp]
~ 12% reduction in RTH
Switched or paused MtbRNAP by PUM
~ 25% reduction in RTH
Control
PUM

Figure 11. PUM switches the active MtbRNAP into slow active states

a. Previous work showed that substituting the hydroxyl group for a methyl group in the hydroxamate bound of pseudouridimycin (PUM) stabilizes it from side chain hydrolysis[84]. The draw represents the structure of PUM and deshydro-PUM.
d. Single-molecule MtbRNAP transcription traces in the presence of 5 μM PUM show that, at the difference to EcoRNAP, MtbRNAP frequently switches to slow transcribing states. A system of two shunts injects the nucleotides alone first, following the nucleotides with the drug to collect the activity inhibition.
e. In detail, the PUM's inhibiting effect on the MtbRNAP shows lower signal-noise ratio trajectories. These trajectories have oscillating jumps and hopping easily visible with the enzyme in an apparent paused state. In addition, there are very few traces with rare backward movements. The traces with the backward movement do not fit well with the stepping staircase algorithm to extract the dwell time distribution.
f. The plot on the left compares trace sections containing the fast, slow, and super-slow states of MtbRNAP caused by PUM. The plots on the right show the staircase fitting of these MtbRNAP slow and super-slow states.
g. PUM switches the active MtbRNAP state into two slow active states. We only extracted the dwells from the reproducible sub-sections and calculated the Dwell-time Distribution (DTD) parameters. The DTDs bar plot shows the states have reduced velocity and increased pausing, like those affected by AAP.
h. PUM weakens MtbRNAP recognition of the elemental pause c. The RTH reduces independent of the effect on velocity. In other words, even enzymes that do not switch velocities have reduced pause efficiency at consensus sequence c. We speculated that PUM did alter the pause recognition by creating neighboring pauses.

We hypothesized that PUM inhibition is sequence-dependent, given that PUM did not affect the global velocity of MtbRNAP transcription on a *U-less* DNA template *in bulk*. Thus, to determine the effect of PUM on the polymerase pausing, we employed the Mtb molecular ruler previously developed for AAP. The RTH analysis revealed that PUM affected the ability of the RNAP to recognize the pause *c* even if the RNAP did not switch (Figure 11f). On the other hand, the enzymes that switched their global velocity in the presence of PUM reduced their residence time by 12 %, independent of where the switch event occurred -inside or outside the repeat sequence (~ 11% and ~ 13% of traces, respectively).

Discussion and Conclusion

MtbRNAP is a mechanically stable enzyme with differential modulation pause consensus requirements

Bulk studies of *Mycobacteria* and Eco RNA polymerases showed significant differences at the modulation level[4–7,10,13,57,122,126–129] and conservation in the translocation activity. Our data suggest that the previously slow overall transcription rate found in Mtb compared to Eco[109] might also result from the molecular motor *per se* and factors modulation. Since this overall rate is a convolution of phases of activity and pausing events, usually differently regulated[98,130,131], we carefully compared the differences between the Mtb and Eco RNAPs. For example, depending on the experimental conditions, the *in singulo* and *in vivo* approaches on EcoRNAP have found significant heterogeneity in transcriptional velocity among individual[132,133133] or trailing polymerases[90,134] rangings broadly between 3-40 nt/sec[37,39,88,89,135–137], or 62-25 nt/sec[134,138], respectively. Therefore, we aimed to describe the dynamics of the elongational stage for MtbRNAP to provide information relevant to future drug design.

The s*tall force* of an RNAP is the maximum force against which the enzyme can transcribe[139]. Compared to data on EcoRNAP of another group of researchers[87], our passive mode experiments with MtbRNAP show that this enzyme performs as a highly processive enzyme and reaches a comparable opposing loading force[87]. As in its Eco counterpart, the rate of transcription of the MtbRNAP is largely insensitive to the application of an opposing force until, eventually, the enzyme slows down. This result indicates that the movement or translocation steps are not rate-limiting under the conditions of our experiments. In addition, it is noteworthy that in previous studies, the α subunit was the part grabbed in the EcoRNAP experiments, unlike the experiments performed here with MtbRNAP in which the enzyme is grabbed from the β’ subunit. This difference raises the possibility that the assay geometry could affect the observed activity of the MtbRNAP. However, for better comparison, we performed experiments on EcoRNAP attached by its β' subunit, like the MtbRNAP setup, and found comparable results.

In EcoRNAP and other polymerases, the effective rate of elongation and the time before recovery from the pause state are sensitive to the direction of the force applied, unlike the pause probability or pause efficiency[39,41,89,112]. A similar result is observed with the application of force on MtbRNAP, supporting the idea that the pausing mechanism involves the visitation of non-catalytical states off-the-main elongation pathway and that it is well-conserved among polymerases.

RNA polymerase is sensitive to the sequence it transcribes, exhibiting elemental paused states incapable of loading the rNTP, whose lifetime modulation is multipartite comprising backtracking, nascent RNA folding, and transcription regulator binding[14,140]. The significant differences in global pausing among Eco and Mtb RNAPs indicate specific interactions formed with DNA elements. However, based on our molecular ruler and *bulk* results, MtbRNAP weakly recognized the Eco elementary pause sequences. These findings suggest that Eco and Mtb polymerases have identical consensus pause sequences. The pause variation in sequence *his* is due to sequence dependency at the upstream hairpin, which changes the pause lifetime. Furthermore, we cannot rule out the

possibility that DNA structure, such as G-quadruplex, alters polymerase pausing. Future studies would investigate the interaction between GQs and transcriptional pause in Mtb *in vivo*.

Two distinct modes of inhibition of MtbRNAP elongation by AAP

Structural and mutagenesis[23,117] studies support the model of a network of cycling circuits connecting catalytic elements in the RNA polymerase [23,25,26,141,142], such as the BH's N- and C- terminals. Paradoxically, drugs exhibiting an allosteric effect that bind nearby regions in a catalytic site and share the same crystal conformer have pleomorphic functional outcomes on the polymerase. For example, Salinamide (Sal), STL, CBR, and AAP stabilize the same BH straight conformation[8,64,116,143], but have different inhibitory effects. The actual conformer associated with the inhibitory effect may be thermodynamically unstable and may not have been observed structurally yet[117].

According to the model of disruption of BH-TL coupling[28], binding the hydrophobic pocket at the interface of the BH-β subunit by AAP destabilizes the TL folding (open state) to slow down catalysis and alters BH bending to increase translocation and enhance pause probability, as we observed for STL, increased in pause duration. However, our finding that AAP does not entirely terminate the nucleotide incorporation and that the polymerase continues all the time transcribing with the interspersed pause and pause-free periods hints at the existence of an additional transcription circuit connecting the RNAP catalytic site that, apart from the BH[27] and TL[28,115], might be species-specific, i.e., the β'F loop[32,117].

AAP converts the fast-elongating MtbRNAP state into two slow-elongating states with a high probability of pausing. It is unknown what conformational changes in the MtbRNAP explain the slow and the super-slow states. Since only one stable binding state appears in the published crystal structure of AAP-MtbRNAP, we cannot attribute that to different binding modes of the ligand drug, but we cannot rule out either. For example, with the cognate drug CBR, there are alternative binding conformations and two different functional effects. We do not know what specific features in the conformers explain the effects described. The inability to resolve structure conformations changes still limits us from understanding these effects.

The distortion of the catalytic elements by AAP may contribute to the increased pause efficiency at certain template positions that could turn to non-progressive transcription[28], as we observed in the super-slow state that detaches from the template. If that sequence-dependent effect results from the altered coordination of the BH with other elements is unknown[26,28].

Furthermore, in other preliminary data, we tested the inhibitory effect of AAP and STL in the presence of MtbGreA. To see the recovery pathway, we injected MtbGreA into an already drug-affected polymerase, either slowly transcribing or pausing due to backtracking. We found that MtbGreA does rescue the polymerase from the AAP effect, suggesting that the AAP does not affect the TL and may affect more polymerase sites to cause these conformational changes.

In conclusion, we observed the effects of the binding and unbinding events of the antibiotic and the two ways of inhibition of the elongation: the slow state, characterized primarily by altered pausing, and the super-slow state, which displays a reduced velocity instead. Moreover, we spontaneously observed the enzyme's interconversion between

the two modes of inhibition. We also used the frequency of switching and the lasting of each mode to estimate the k_{off} of AAP, which is found to be small for MtbRNAP, which makes it possible to separate the two functional modes during active transcription temporally. Finally, we find that the application of force affects little some transition probabilities.

Future research should address whether the switches' events are sequence-dependent and if the polymerase velocity before a switch influences the transition *velocity.*

STL biases the backtracking states of MtbRNAP during recovery of inhibition

Traditional assays using artificial transcription bubbles mimicking the backtracked state found that STL inhibits nucleolytic activity. However, our SM results showed that STL induces MtbRNAP transitions to backtrack states of high depth that can still recover. Previous artificial bubbles used whose structure was confirmed as backtrack states not necessarily correlate with the nucleolytic activity[144], we proposed that STL slow down the intrinsic RNA endonucleolysis in agreement with the observation of the long pre-backtracking time that lasts tens of seconds. On the other hand, our fluorescent *bulk* assays showed STL biasing or shifting the equilibrium of post/pre-translocated states. We interpret the steady-state fluorescent signal as a polymerase population in a post-translocation state bound to an STL molecule of high residence time along with another population in the pre-translocated state that may or may not have the STL bound, depending on the stability of the complex. We made this assumption because, in practice, the 2-aminopurine fluorescence assay showed the percentage of post-translocation, and the pre-translocated stated is thought to happen. To reconcile these results with the SMs, we proposed the existence of a non-stable pre-translocation state, able to start the backtrack movement. In addition, this pre-translocated state is also a transitory state towards that backtracked state.

The observation that the backtrack state's recovery lifetime does not follow the diffusive backtrack mechanism suggests that STL bias the backtrack states of the MtbRNAP toward deep backtrack. In addition, we proved using MtbGreA that STL that the long backtrack pauses recover via assisted endonucleolysis. Furthermore, we observed that STL increases the residence time of MtbRNAP crossing the elemental pause sequence but not the pause density. These results suggest that the STL binding events that turn to RNAP inhibition directly depend on the probability of finding the polymerase in catalytically inactive states. Further research will try to observe in real-time this proposed pre-translocated intermediate state.

Pseudouridimycin inhibition reveals differences in shifting preference between EcoRNAP and MtbRNAP

Our results demonstrate that PUM increases the polymerase pause density based on its known competition mechanism for rUTP incorporation[82]. Our experiment also suggests that EcoRNAP pausing near the upstream of a hairpin-pause sequence might alter the kinetics of the RNA folding formation. Consequently, that might interfere with the modulation of the residence time at the elemental pause *his.* Likewise, we observed a

significant fraction of the population of MtbRNAP and EcoRNAP (not shown) affected in recognizing the consensus pause *c* without impairing processivity, effective rate velocity, or pausing probability. Future experiments tracking RNA folding in real-time, such as force spectroscopy, might also help reveal the inhibiting role of PUM at the level of transcription termination.

We anticipated that the effect of PUM on the MtbRNAP elongation depends directly on the polymerase's active state. According to our findings, the frequency of MtbRNAP's switch events induced by PUM is significantly higher than that of EcoRNAP. Despite the conservation in the drug-binding site among the prokaryotic polymerases, perhaps other structural or functional motifs -that coordinate differently with the catalytic region- would play a role in the mechanism of switch[32,145]. In addition, the ability to retain certain conformational constraints as a memory mechanism by the elongating polymerase that allows it to escape the inhibitory state needs attention.

Supplementary Figure of Chapter 2

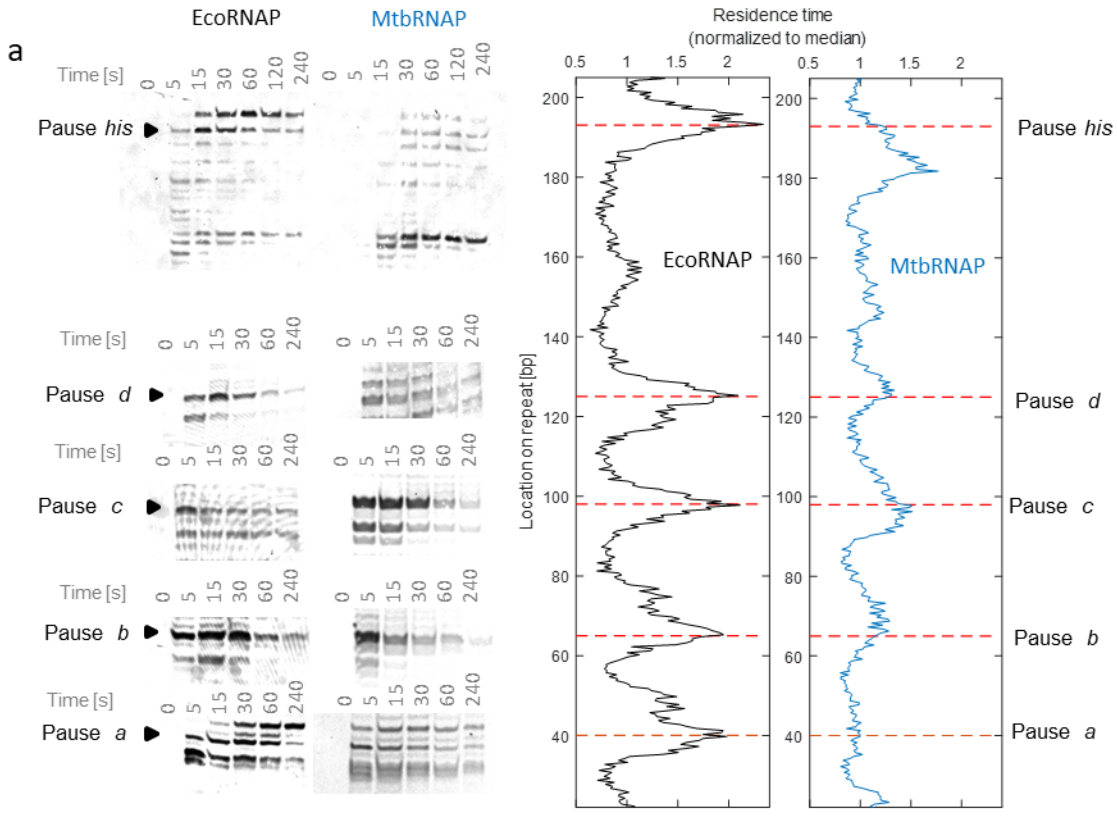

Figure 12. MtbRNAP pauses inefficiently on Eco elementary pauses

a. The comparison of transcription gel bands (left) with the residence time histograms obtained with high-resolution optical tweezers (right) shows that MtbRNAP pause inefficiently.

Chapter 3. Global interferences between MtbCarD and MtbGreA during MtbRNAP transcription

Abstract

Tuberculosis (TB) is one of the top twenty causes of death worldwide. In anti-TB treatment, the *Mycobacterium tuberculosis* RNA polymerase (MtbRNAP) is one of the pharmacologically validated targets. Many recent structural and functional studies have characterized the modulation of transcription initiation of MtbRNAP by the essential factor MtbCarD. However, whether CarD modulates the elongation phase and the dynamics of that modulation have remained unknown. This chapter describes the use of high-resolution optical tweezers to observe that MtbCarD interfered with the transcription elongation cycle by increasing the enzymes' pausing probability. However, we found that the presence of MtbGreA, another essential transcription factor, eliminated the MtbCarD effect. In addition, we investigated the possibility that the MtbGreA interferes with MtbCarD at the level of promoter clearance using smFRET. Our preliminary results suggest that global interference between MtbCarD and MtbGreA might be allosteric binding to the MtbRNAP. Future research should focus on revealing the possibility of that scenario *in* vivo in TB and clarify the role of transcription factor interference in Mtb*.*

.

Introduction

After the Covid-19 pandemic, Tuberculosis (TB) is the second cause of death worldwide from a single infectious agent, *Mycobacterium tuberculosis* (Mtb). Moreover, the worldwide trend is toward increasing the mortality rate[69]. The lack of TB surveillance in developing countries and the high cost of treatment favored the emergence of the appearance of multi-drug resistance strains of the pathogen[69]. Above half of the clinical mutations displaying resistance to rifampicin (RIF) are in the Mtb RNA polymerase *(*MtbRNAP). This enzyme plays an essential gene expression role, allowing the *Mycobacterium* to adapt against host defense[146]. Indeed, Mtb transcription regulation orchestrates the operation of many novel factors and unique DNA elements[51,146–148]. Studying Mtb transcription *in vivo* is challenging because of the specialized biosafety level and the slow growth rate of the *Mycobacterium*[146].

Systems to reconstitute Mtb transcription *in vitro* helped mimic different cell conditions[149]. Much research studied the initiation phase[51,150,151], but there is less knowledge of Mtb elongation. Specifically, there is a great deal of interest in characterizing the activity of Mtb transcription factors since it is known that Mtb does not have the same repertoire of factors as other microorganisms and (many of them are absent in other organisms) or are known to perform different functions[126,148,152]. Thus, these factors could represent an important new target to combat RIF-resistant mutants and have become the new pharmacological targets in anti-TB treatments[153].

Two highly-expressed essential factors, MtbCarD and MtbGreA, are global regulators for mycobacterial pathogenesis[122,149,154–163], and the organism's survival under different stresses, including antibiotic stress[156]. MtbCarD, along with *RbpA* and sigma factors, stabilizes the transcription initiation complex (IC)[154,155,157,164], assists in DNA promoter melting, and slows down promoter escape[165,166]. Since it has been reported that there is no MtbCarD occupancy in the elongation phase[63], we questioned what drives a stable IC to proceed to the elongation phase without the factor. In addition, the current perspective on MtbGreA function, of participating in rescue elongation of the ternary complex from backtracked states[122], has been renewed because, in Mtb*,* it abundantly occupies the promoter region. In addition, it has been shown that MtbGreA enhances promoter clearance[161]. Therefore, since both proteins- MtbCarD and MtbGreA- associate with the promoter region, and only MtbGreA persists in elongation after MtbCarD releases in promoter clearance, we decided to investigate the possible transcriptional interference between these Mtb transcription factors.

Consequently, we used high-resolution optical tweezers (HROT) to identify potential transient modulatory effects of MtbRNAP elongation by factors in real-time and single-molecule FRET (smFRET) to monitor possible dynamic interactions between the factors in the MtbRNAP initiation complex. This study attempts to reconstitute the MtbRNAP activity in the context of its relevant factors, which play a crucial role during transcription modulation *in vivo*.

Results

MtbGreA abolishes the MtbCarD modulation of pausing by MtbRNAP *in singulo*

During its stress response, *Mycobacterium* displays higher concentrations of MtbCarD and MtbGreA*.* We wonder how these conditions affect Mtb transcription elongation. To determine if MtbCarD increases pause duration or pause density, we evaluated the elongation by MtbRNAP in the presence of these two factors using assisting force (AF) and opposing force (OF) modes (Figure 1a and Figure 13a). Accordingly, the addition of MtbCarD *in trans* increased the pause density or the pause entry[167] (pauses per 100 bp) of MtbRNAP transcribing rpoB-rpoC genes. (Figure 13b). In contrast to *in* vivo observations, this result suggests that MtbCarD could create pauses and have a role in the elongation phase. On the other hand, we found that MtbGreA reduces the density of pauses otherwise increased by MtbCarD (Figure 13c). Another possibility is that MtbCarD extends small pauses previously undetectable by our algorithm. However, the latter is unlikely since we did not observe any increase in pause duration or decrease in the pause escape rate (k_{-p}) (Figure 13d). Moreover, we inspected the dwell time distributions (DTDs) of active and paused polymerase states to search for changes and found that MtbCarD and MtbGreA neither affected the rates nor the probabilities of MtbRNAP. (Figure 13d).

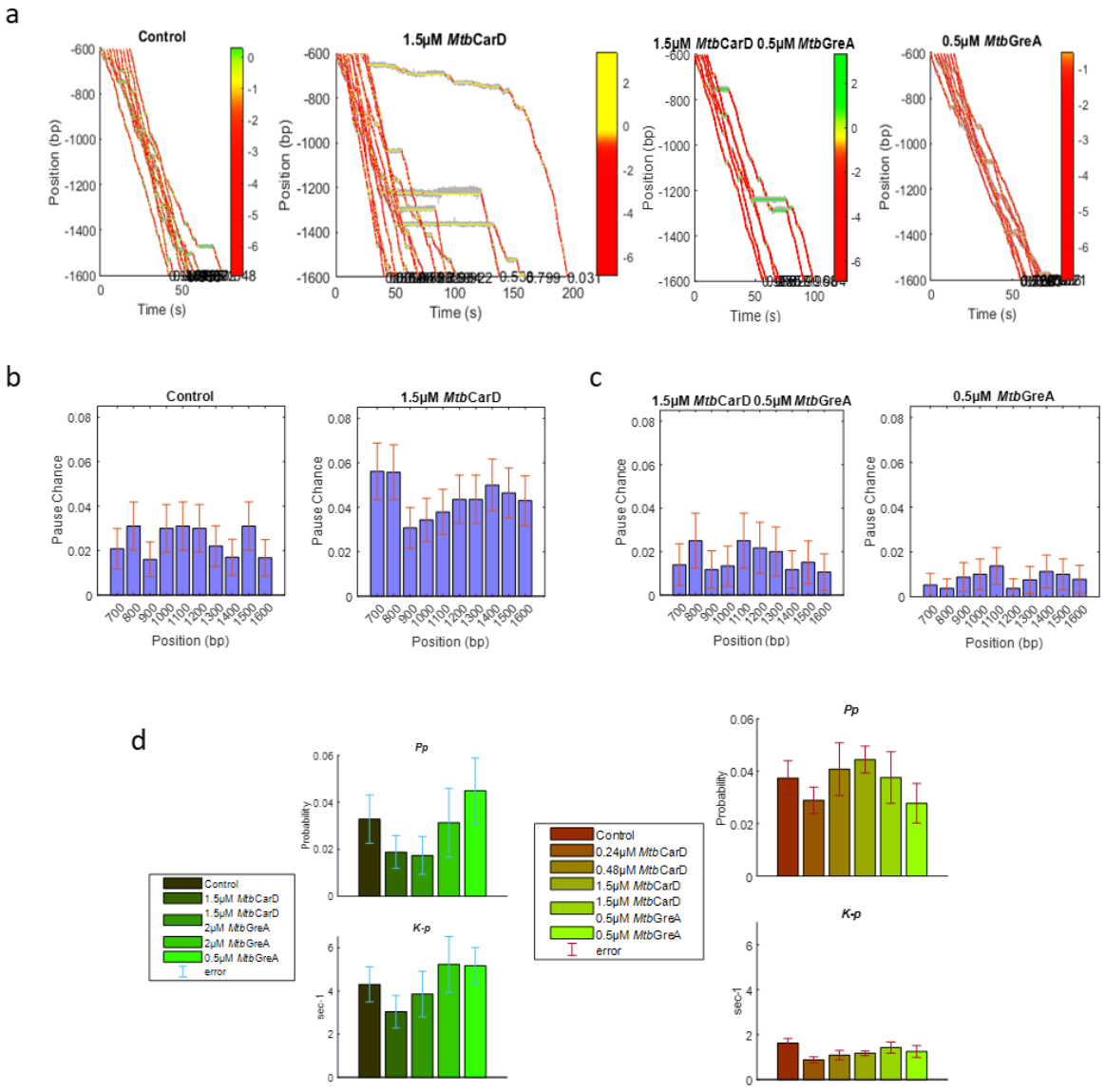

Figure 13. MtbGreA abolishes the MtbCarD effect on MtbRNAP pausing.

a. Reconstitution of *in-singulo* MtbRNAP elongation in the presence of MtbCarD and MtbGreA shows transcription interference. Graphs are transcriptional traces obtained at 5 pN constant OF; they have a colored pattern of recognition of pauses. The red color represents the higher probability of finding a pause-free velocity, while the green-yellow pauses. The y-axis indicates the regions in the DNA template used for analysis, from around 600 bp to 1600 bp, to make a fair comparison between conditions.

b. MtbCarD increases the pause density of the MtbRNAP elongation under opposing force (OF). The bar plots are the pause chance of event pauses per 100 bp of transcription under 5 pN constant OF and 1 mM rNTPs. The legends describe the concentration used of MtbCarD. MtbCarD.

c. MtbGreA reduces MtbRNAP pause density in the presence of MtbCarD. Under similar conditions of A, in the presence of both proteins, MtbCarD and MtbGreA, the polymerase pausing on the DNA template did not change. The legends show the concentration used for

each factor. We derived the distributions and rates from a biexponential fitting of the DTD as a CCDF (Figure 4D).

d. MtbCarD and MtbGreA affect neither the MtbRNAP pause escape rate (k_{-p}) nor pause strength probability (P_p). The bars plot on the left is a condition at ~18 pN constant AF, and on the right, at 5pN constant Opposing Force. No significant difference exists in the distribution or kinetic rates among the protein concentrations or force geometries. The force geometry only affected the pause duration, related to pausing escape[112], and there was no correlation between k_{-p} and P_p, indicating that the mechanism of pauses as an off-pathway is well-conserved in MtbRNAP.

These findings show that the MtbCarD effect is force-dependent (Figure 13d). We rule out that MtbCarD intervenes in backtracking pausing since the average time that it takes an RNA polymerase to recover from the pauses induced by MtbCarD was ~1.1 sec, lower than the average lifetime for backtrack recovery[42,44]; although there were long pauses, they were too sporadic to do solid statistical analysis. Suppose MtbCarD interacts with the Mtb ternary elongation complex (MtbTEC). In that case, that interaction must be transient, as it can be poorly retained by pulldown assay (Figure 15a of Supplementary) and does not appear co-eluted with the MtbTECs under size-exclusion chromatography (SEC) (Figure 15b of Supplementary). Some retention of MtbCarD might be due to DNA-binding activity[149] in agreement with our observation of non-specific interactions of fluorescent-labeled MtbCarD with λ DNA using an optical tweezers instrument with single-molecule fluorescence detection capability (Figure 15d, e of Supplementary).

Therefore, our findings suggest that the physical interaction of MtbCarD and the MtbRNAP, if it occurs, must be unstable and transient but enough to increase pausing and, on the other hand, affected by MtbGreA. Because there is no physical interaction between *Mtb*CarD and MtbGreA in SAXS assays (data not shown)**,** the interference might likely occur through the polymerase. Thus, we needed a way to study a transient interaction between these three components, MtbGreA, MtbCarD, and MtbRNAP. For that reason, we decided to use smFRET to detect potential interaction between these factors on the MtbRNAP.

A preliminary smFRET study suggests dynamic interactions between Mtb factors on the initiation complex

We used the spatial resolution of 3-8 nm of smFRET[168] to detect possible physical interactions between MtbGreA and MtbCarD bound on the MtbRNAP. We made a simple model of MtbGreA bound on the secondary channel of the polymerase in complex with MtbCarD (CarD-MtbRNAP-GreA). We used the available conformer of the open initiation complex (IC) of CarD-MtbRNAP (PDB 6EDT) and aligned it to a homology model of MtbGreA (SWISS-model, PDB template 6RI7). We expected ~75.5 Å between Cy5 and Cy3 dyes placed on mutated residues E30C and T26C of MtbCarD and MtbGreA, respectively (Figure 14a). The assay consists of first immobilizing on a surface the pre-assembled IC of Cy5-CarD-MtbRNAP to do TIRF, followed by flowing Cy3-MtbGreA to do FRET. Figure 14B depicts the dynamic interaction between Cy3-MtbGreA and Cy5-MtbCarD bound on the MtbRNAP in representative smFRET trajectories before the Cy5 fluorescence intensity decreased to zero. Cy5 quenching or Cy5-MtbCarD release are the two possible causes of the increase in Cy5-Cy3 distance above 100 Å. We rule out Cy5 quenching because in the absence of MtbGreA, in most of the traces of Cy5-CarD-

MtbRNAP, Cy5 fluorescent intensity went down to zero from one preceding state instead of two states that only occurs in the presence of MtbGreA (Figure 14b). These preliminary results suggest an association between MtbCarD release from MtbRNAP and the preceding dynamic interaction caused by MtbGreA.

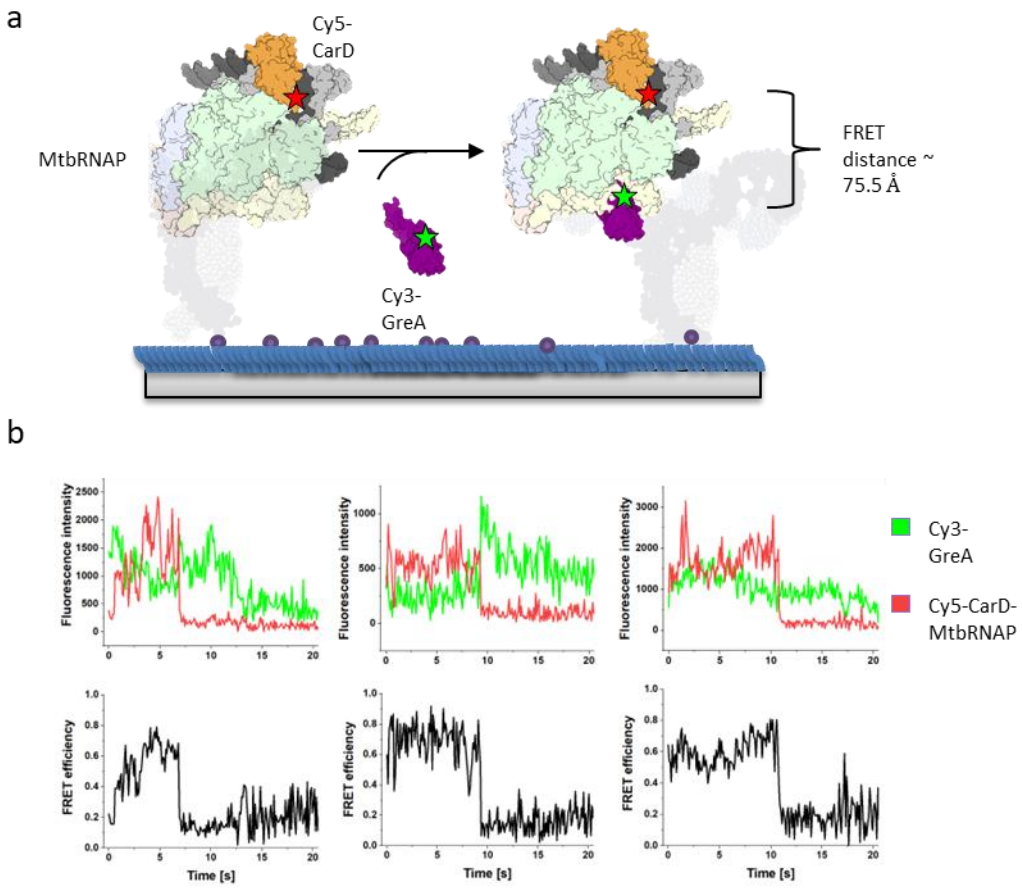

Figure 14. Dynamic interaction between Cy3-MtbGreA and Cy5-MtbCarD bound on the MtbRNAP

a. MtbCarD and MtbGreA colocalization on the surface-fixed MtbRNAP by TIRF spectroscopy. TIRF surface setup and dye geometry. We deposit on the surface pre-form initiation complex of Cy5-CarD-MtbRNAP to do TIRF and the flow Cy3-MtbGreA to detect FRET. We labeled with Cy5-MtbCarD at E30C and with Cy3 Glu30 T26C. The expected FRET distance is ~ 75.5 Å using a model derived from PDBs 6EDT and a homology model of MtbGreA (SWISS-model, PDB template 6RI7).
b. Single-molecule traces of colocalization by TIRF of Cy5-MtbCarD and Cy3-MtbGreA on the MtbRNAP. Before Cy5 fluorescence intensity went down to zero, we observed that dynamic trajectories happen between the two dyes in one step, while a few traces have two different preceding states.

Discussion and Conclusion

Global interference between MtbGreA and MtbCarD during MtbRNAP transcription

Studies with chromatin immunoprecipitation sequencing (ChIP-Seq) done in *Mycobacterium* found CarD interacting near the gene promoters[63]; however, we found that it is enough to add MtbGreA to abolish the effect of MtbCarD in elongation. This result may reconcile the SM with ChIP-seq data and suggest an interference between elongation and initiation factors. MtbGreA does not physically interact with MtbCarD; thereby, the interference might be through MtbRNAP.

MtbCarD free in solution delays the global transcription *in bulk* (Figure 16a, b of Supplementary). That effect might result from slowing the promoter clearance or direct interaction with the elongation complex[10]. In addition, MtbCarD can bind the DNA via its C-domain and the polymerase β subunit through its N-domain and increase avidity by forming high-order oligomeric states [156]. It is possible that MtbCarD that binds the DNA might encounter and pause the MtbRNAP, while MtbGreA binds the RNAP through the secondary channel to change its conformation and rescue or prevent the pause.

We propose a model of interferences between these two Mtb factors that might be global, transient, and allosteric. They are global because they occur independently of the transcription phase. They would be transient because the average pause duration by MtbCarD is around one sec. They would be allosteric because the proteins do not physically interact with each other, and it operates through the binding on opposite sides of RNAP. Further research will allow improvement on this initial model.

Supplementary Figures of Chapter 3

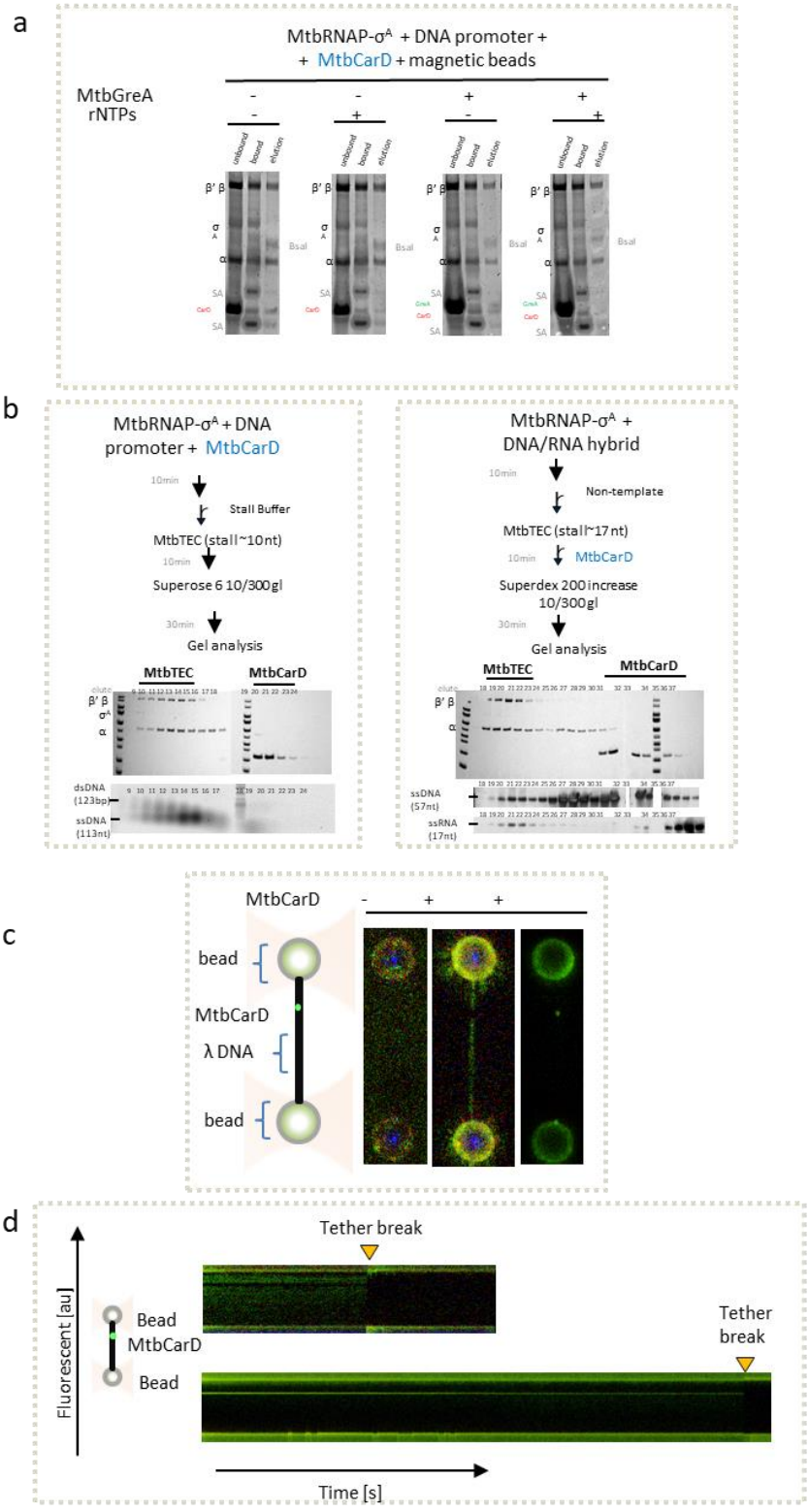

Figure 15. MtbCarD binds weakly artificial MtbTECs, and non-specifically the λ DNA

a. Mild washing conditions on a pulldown assay show low retention of MtbCarD with MtbTECs. MtbCarD elutes from the pulldown dsDNA template of the elongating MtbRNAP and MtbGreA. Upon adding rNTPs, MtbCarD releases from the MtbRNAP, possibly during the promoter escape. The addition of MtbGreA favors that release. The assay uses a biotinylated DNA template of ~ 200 bp and a resin of magnetic streptavidin beads. The symbol represents the following proteins: SA, streptavidin from the resin, and BsaI, the restriction enzyme used to elute the DNA. In the gel, the proteins in the unbound lanes correspond to the flow-through, the bound lanes, the non-specific protein from the pellet, and elution, the specific interaction.
b. Using size-exclusion chromatography (SEC), MtbCarD does not co-elute with the elongation complexes of Mtb prepared either from promoter initiation (work-flow on the left) or artificial bubble (work-flow on the right). Before the SEC run, we pre-incubated the factor with TEC.
c. MtbCarD interacts non-specifically with the λ DNA. From 100 to 500 nM, Cy3-MtbCarD decorated a stretched 16 µm λ-DNA. We detected little spots and faint fluorescent regions along the 16 Kb genomic DNA of binding events using an optical tweezers instrument combined with fluorescent confocal microscopy.
d. Two representative kymograph traces show the Mtb remains bound on the λ DNA for a few minutes. This interaction can persist inclusive with DNA stretched above 15 pN.

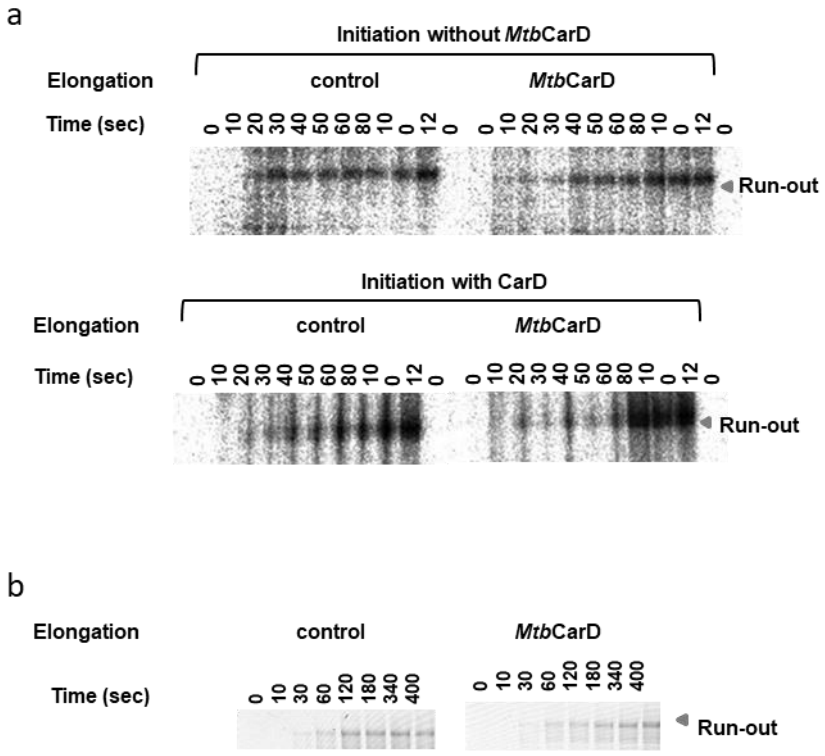

Figure 16. *Mtb*CarD free in solution delays *Mtb* global transcription

a. Promoter-initiated MtbRNAP transcription shows that MtbCarD slows down RNA product synthesis. These results show the action of MtbCarD in the elongation phase independently of being initiated (bottom gel) or not (top gel) with the same factor.

b. Likewise, MtbTECs from artificial bubble formation shows that free MtbCarD delays its global velocity. After washing the TEC, elongation resumes by adding 100 µM rNTPs (gel of the left side) or 100 µM rNTPs + 1.5 µM MtbCarD (gel of the right side). We stopped the reaction accordingly with the time course specified on the gels.

Chapter 4. Final Conclusions

At standard conditions, MtbRNAP transcribes half as fast as EcoRNAP. As a bacterial polymerase, MtbRNAP processively elongates the RNA thousands of bases without elongation factors. In addition, it is as mechanically robust as EcoRNAP; its operational thermodynamic stalling force is 19 pN. The pause density, duration level, strength, and efficiency of Mtb polymerase global pausing differ from Eco. Indeed, MtbRNAP pauses inefficiently on the Eco elemental pause sequences, not because its consensus pause sequence is different but because the upstream regions' requirement to regulate pause lifetime is different.

Aroyl-Aryl-Phenylalanimide (AAP) affects MtbRNAP by converting it into two exchangeable slow-elongating enzymes. Polymerase continues to transcribe with interspersed pauses and velocity regions. In the slow state, there is mainly an increase in the pause probability; in the super-slow state, there is a decrease in the effective elongation rate. Moreover, the slow state is more processive than the super-slow state. Although AAP is not a chain terminator, the super-slow state lost processivity while crossing the Mtb molecular ruler. Our findings also show that AAP's apparent k_{off} is very slow, providing a low K_D in the order of decades of nanomolar. This characteristic makes it a good candidate for treatment.

On the other hand, Streptolydigin (STL) is not a chain terminator for MtbRNAP. It favors the pre- and post-translocated states of MtbRNAP. The paused MtbRNAP state caused by this antibiotic recovered by deep backtracking associated with intrinsic RNA endonucleolysis rather than a diffusive mechanism.

Related to Pseudouridimycin (PUM) effect, it does not behave as a strict chain terminator. By increasing the number of pauses in the location upstream of the elementary pause site, PUM can reduce the occurrence of the elementary paused state of Eco and Mtb polymerases. The PUM-induced MtbRNAP slowed states are typically a set of noisy extended pauses, high jumps of 10–20 bp, hopping, and backward motions. In addition, PUM switches both Eco and Mtb RNAPs. However, the MtbRNAP switching rate is significantly higher than the EcoRNAP switching rate (28% *versus* 4%), indicating functional and structural variations in the coordination between conserved and non-conserved catalytic active elements among these enzymes.

MtbGreA decreased the elongating MtbRNAP pause density, otherwise increased by MtbCarD, which explains the low MtbCarD occupancy *in vivo* during the elongation phase[63]. In addition, on the initiation complex, MtbGreA binding affects MtbCarD release. This interference must be allosteric through the polymerase, global along the transcription stages, and brief (less than a second).

Possible caveats

The current limitation of our *in-singulo* reconstitution of Mtb transcription is that it does not resemble the crowding conditions of the cell interior because high viscosity alters the trapping properties of optical tweezers. Likewise, contrary to prokaryotic nucleoids, the DNA template has a low degree of compactness. In addition, our assays do not consider

that during the melting and movement of the transcriptional bubble, the torsional constraints imposed by the DNA may affect polymerase performance. Indeed, in vivo, the machinery of helicases might play a role in controlling the DNA torsion created by the MtbRNAP[128].

Why do some organisms have fast and slow polymerases? Some research tried to answer it at the level of cell growth rate. However, there is no evidence of the transcription rates coupled to the cellular growth rates besides correlation analysis[110,169]. Other researchers proposed that it results from the polymerase adaptation to the GC content of the DNA template displaying different processivity[170]. In addition, the remarkable similarity of RNAP structures within the genus of Mycobacteria, on the other hand, cannot account for the variations in intra-species transcription and growth rates[151,171,172]. Regulating the processes that control cellular growth demands the collaboration of structural, functional, system, and evolutionary research to provide a solution to this topic.

While gathering data, we improved the efficiency of the formation of transcription complexes and the resume of activity using artificial templates and scaffolds. We questioned whether the structure of the stalled complex resembled the native structure or whether the restart of activity distorted our observations.

Enzymatic activity heterogeneity observations by our research group and others still fall under open questions[35,37,173]. Thus, the activities may be due to transcription switching during random pauses, indicating that the integrity of the enzyme remains unaffected [33]. However, on the other side, constant exposure to high radiation levels results in slow and noisy enzymatic trajectories[39]. In general, we are unsure if it could be the outcome of RNA polymerases with variable stoichiometry caused by lacking factors or subunits or of photodamaged effect. More research is necessary to shed further light on these ambiguities,

Future Aims

To understand the variation in the lifetime of the backtracked, paused, halted, and arrested polymerase states and the implications for Mycobacteria transcription regulation, it is necessary to determine the molecular structure of the elemental pause state of MtbRNAP in comparison to EcoRNAP.

Important insights regarding the RNAP circuit network and the impact of regulators can be learned using cysteine crosslinking (CPX) on the conformational states of RNA polymerase's catalytic components[65]. Future studies may take a dynamic approach to this problem, monitoring recognized crosslinked states in real time to ascertain the coordination and mechanism of the RNAP transcriptional circuits.

Bibliography

1. Lee, J. & Borukhov, S. Bacterial RNA Polymerase-DNA Interaction—The Driving Force of Gene Expression and the Target for Drug Action. *Front Mol Biosci* **3**, 73 (2016).
2. Banerjee, R., Rudra, P., Prajapati, R. K., Sengupta, S. & Mukhopadhyay, J. Optimization of recombinant Mycobacterium tuberculosis RNA polymerase expression and purification. doi:10.1016/j.tube.2014.03.008.
3. Jacques, J. F., Rodrigue, S., Brzezinski, R. & Gaudreau, L. A recombinant Mycobacterium tuberculosis in vitro transcription system. *FEMS Microbiol Lett* **255**, 140–147 (2006).
4. Czyz, A., Mooney, R. A., Iaconi, A. & Landick, R. Mycobacterial RNA Polymerase Requires a U-Tract at Intrinsic Terminators and Is Aided by NusG at Suboptimal Terminators. *mBio* **5**, (2014).
5. Hu, Y., Morichaud, Z., Chen, S., Leonetti, J. P. & Brodolin, K. Mycobacterium tuberculosis RbpA protein is a new type of transcriptional activator that stabilizes the σA-containing RNA polymerase holoenzyme. *Nucleic Acids Res* **40**, 6547 (2012).
6. China, A. & Nagaraja, V. Purification of RNA polymerase from mycobacteria for optimized promoter-polymerase interactions. *Protein Expr Purif* **69**, 235–242 (2010).
7. Mao, C. *et al.* Association of ω with the C-Terminal Region of the β′ Subunit Is Essential for Assembly of RNA Polymerase in Mycobacterium tuberculosis. *J Bacteriol* **200**, (2018).
8. Lin, W. *et al.* Structural basis of Mycobacterium tuberculosis transcription and transcription inhibition. *Mol Cell* **66**, 169 (2017).
9. Hubin, E. A. *et al.* Structure and function of the mycobacterial transcription initiation complex with the essential regulator RbpA. *Elife* **6**, e22520 (2017).
10. Jensen, D., Manzano, A. R., Rammohan, J., Stallings, C. L. & Galburt, E. A. CarD and RbpA modify the kinetics of initial transcription and slow promoter escape of the Mycobacterium tuberculosis RNA polymerase. *Nucleic Acids Res* **47**, 6685 (2019).
11. Hatfull, G. F. & Jacobs, W. R. *Molecular genetics of mycobacteria*. (ASM Press, 2000).
12. Sidorenkov, I., Komissarova, N. & Kashlev, M. Crucial role of the RNA:DNA hybrid in the processivity of transcription. *Mol Cell* **2**, 55–64 (1998).
13. Herrera-Asmat, O. *et al.* Production and characterization of a highly pure RNA polymerase holoenzyme from Mycobacterium tuberculosis. *Protein Expr Purif* **134**, 1–10 (2017).
14. Kang, J. Y., Mishanina, T. v., Landick, R. & Darst, S. A. Mechanisms of transcriptional pausing in bacteria. *J Mol Biol* **431**, 4007 (2019).
15. Hodges, C., Bintu, L., Lubkowska, L., Kashlev, M. & Bustamante, C. Nucleosomal fluctuations govern the transcription dynamics of RNA polymerase II. *Science (1979)* **325**, 626–628 (2009).

16. Bar-Nahum, G. *et al.* A ratchet mechanism of transcription elongation and its control. *Cell* **120**, 183–193 (2005).
17. Nedialkov, Y. A. & Burton, Z. F. Translocation and fidelity of Escherichia coli RNA polymerase. *Transcription* **4**, 136 (2013).
18. Malinen, A. M. *et al.* Active site opening and closure control translocation of multisubunit RNA polymerase. *Nucleic Acids Res* **40**, 7442 (2012).
19. Hein, P. P., Palangat, M. & Landick, R. RNA Transcript 3′-Proximal Sequence Affects Translocation Bias of RNA Polymerase. *Biochemistry* **50**, 7002 (2011).
20. Janissen, R., Eslami-Mossallam, B., Artsimovitch, I., Depken, M. & Dekker, N. H. High-throughput single-molecule experiments reveal heterogeneity, state switching, and three interconnected pause states in transcription. *Cell Rep* **39**, 110749 (2022).
21. Borukhov, S. & Nudler, E. RNA polymerase: the vehicle of transcription. (2008) doi:10.1016/j.tim.2007.12.006.
22. Garriga, D., Ferrer-Orta, C., Querol-Audí, J., Oliva, B. & Verdaguer, N. Role of Motif B Loop in Allosteric Regulation of RNA-Dependent RNA Polymerization Activity. *J Mol Biol* **425**, 2279–2287 (2013).
23. Wang, Z. F., Fu, Y. ben, Wang, P. Y. & Xie, P. Dynamics of bridge helix bending in RNA polymerase II. *Proteins: Structure, Function, and Bioinformatics* **85**, 614–629 (2017).
24. Weinzierl, R. O. J. Nanomechanical constraints acting on the catalytic site of cellular RNA polymerases. *Biochem Soc Trans* **38**, 428–432 (2010).
25. Zhang, N. *et al.* Mutations in RNA Polymerase Bridge Helix and Switch Regions Affect Active-Site Networks and Transcript-Assisted Hydrolysis. *J Mol Biol* **427**, 3516 (2015).
26. Nedialkov, Y. A. *et al.* The RNA polymerase bridge helix YFI motif in catalysis, fidelity and translocation. *Biochim Biophys Acta* **1829**, 187 (2013).
27. Weinzierl, R. O. J. The nucleotide addition cycle of RNA polymerase is controlled by two molecular hinges in the Bridge Helix domain. *BMC Biol* **8**, 134 (2010).
28. Malinen, A. M. *et al.* CBR antimicrobials alter coupling between the bridge helix and the β subunit in RNA polymerase. *Nat Commun* **5**, 3408 (2014).
29. Vassylyev, D. G., Vassylyeva, M. N., Perederina, A., Tahirov, T. H. & Artsimovitch, I. Structural basis for transcription elongation by bacterial RNA polymerase. *Nature* **448**, 157–162 (2007).
30. Wang, D., Bushnell, D. A., Westover, K. D., Kaplan, C. D. & Kornberg, R. D. Structural Basis of Transcription: Role of the Trigger Loop in Substrate Specificity and Catalysis. *Cell* **127**, 941–954 (2006).
31. Nedialkov, Y. A. *et al.* The RNA polymerase bridge helix YFI motif in catalysis, fidelity and translocation. *Biochim Biophys Acta Gene Regul Mech* **1829**, 187–198 (2013).
32. Miropolskaya, N., Artsimovitch, I., Klimašauskas, S., Nikiforov, V. & Kulbachinskiy, A. Allosteric control of catalysis by the F loop of RNA polymerase. *Proc Natl Acad Sci U S A* **106**, 18942 (2009).

33. Janissen, R., Eslami-Mossallam, B., Artsimovitch, I., Depken, M. & Dekker, N. H. High-throughput single-molecule experiments reveal heterogeneity, state switching, and three interconnected pause states in transcription. *CellReports* **39**, 110749 (2022).
34. Kang, J. Y., Mishanina, T. v., Landick, R. & Darst, S. A. Mechanisms of transcriptional pausing in bacteria. *J Mol Biol* **431**, 4007 (2019).
35. Neuman, K. C., Abbondanzieri, E. A., Landick, R., Gelles, J. & Block, S. M. Ubiquitous Transcriptional Pausing Is Independent of RNA Polymerase Backtracking. *Cell* **115**, 437–447 (2003).
36. Neuman, K. C. & Nagy, A. Single-molecule force spectroscopy: optical tweezers, magnetic tweezers and atomic force microscopy. *Nat Methods* **5**, 491 (2008).
37. Davenport, R. J., Wuite, G. J., Landick, R. & Bustamante, C. Single-molecule study of transcriptional pausing and arrest by E. coli RNA polymerase. *Science* **287**, 2497–500 (2000).
38. Tolić-Nørrelykke, S. F., Engh, A. M., Landick, R. & Gelles, J. Diversity in the Rates of Transcript Elongation by Single RNA Polymerase Molecules. *Journal of Biological Chemistry* **279**, 3292–3299 (2004).
39. Gabizon, R., Lee, A., Vahedian-Movahed, H., Ebright, R. H. & Bustamante, C. J. Pause sequences facilitate entry into long-lived paused states by reducing RNA polymerase transcription rates. *Nat Commun* **9**, 1–10 (2018).
40. Fukuda, S. *et al.* The Biogenesis of SRP RNA Is Modulated by an RNA Folding Intermediate Attained during Transcription. *Mol Cell* **77**, 241-250.e8 (2020).
41. Neuman, K. C., Abbondanzieri, E. A., Landick, R., Gelles, J. & Block, S. M. Ubiquitous transcriptional pausing is independent of RNA polymerase backtracking. *Cell* **115**, 437–47 (2003).
42. Lisica, A. *et al.* Mechanisms of backtrack recovery by RNA polymerases I and II. *Proc Natl Acad Sci U S A* **113**, 2946–51 (2016).
43. Shaevitz, J. W., Abbondanzieri, E. A., Landick, R. & Block, S. M. Backtracking by single RNA polymerase molecules observed at near-base-pair resolution. *Nature* **426**, 684–687 (2003).
44. Galburt, E. A. *et al.* Backtracking determines the force sensitivity of RNAP II in a factor-dependent manner. *Nature* **446**, 820–823 (2007).
45. Larson, M. H., Greenleaf, W. J., Landick, R. & Block, S. M. Applied Force Reveals Mechanistic and Energetic Details of Transcription Termination. *Cell* **132**, 971–982 (2008).
46. Yin, H. *et al.* Transcription Against an Applied Force. *Science (1979)* **270**, 1653–1657 (1995).
47. Wang, M. D. *et al.* Force and velocity measured for single molecules of RNA polymerase. *Science* **282**, 902–907 (1998).
48. Higuchi, H. & Endow, S. A. Directionality and processivity of molecular motors. *Curr Opin Cell Biol* **14**, 50–57 (2002).
49. Gelles, J. & Landick, R. RNA Polymerase as a Molecular Motor. *Cell* **93**, 13–16 (1998).

50. Chen, J., Boyaci, H. & Campbell, E. A. Diverse and Unified Mechanisms of Transcription Initiation in Bacteria. *Nat Rev Microbiol* **19**, 95 (2021).
51. Boyaci, H., Saecker, R. M. & Campbell, E. A. Transcription initiation in mycobacteria: a biophysical perspective. *Transcription* **11**, 53 (2020).
52. Campbell, E. A. *et al. Structural Mechanism for Rifampicin Inhibition of Bacterial RNA Polymerase Mutations conferring Rif resistance (Rif R) map almost exclusively to the rpoB gene (encoding the RNAP subunit) in every organism tested, including E. coli netic analyses have provided molecular details of amino*. *Cell* vol. 104 (2001).
53. Wilmańska, D., Czyz, M., Studzian, K., Piestrzeniewicz, M. K. & Gniazdowski, M. Effects of anticancer drugs on transcription in vitro. *Zeitschrift fur Naturforschung - Section C Journal of Biosciences* **56**, 886–891 (2001).
54. Brandis, G., Wrande, M., Liljas, L. & Hughes, D. Fitness-compensatory mutations in rifampicin-resistant RNA polymerase. *Mol Microbiol* **85**, 142–151 (2012).
55. Wu, W. *et al.* Transcriptional Approach for Decoding the Mechanism of rpoC Compensatory Mutations for the Fitness Cost in Rifampicin-Resistant Mycobacterium tuberculosis. *Front Microbiol* **9**, (2018).
56. Brandis, G., Pietsch, F., Alemayehu, R. & Hughes, D. Comprehensive phenotypic characterization of rifampicin resistance mutations in Salmonella provides insight into the evolution of resistance in Mycobacterium tuberculosis. *Journal of Antimicrobial Chemotherapy* **70**, 680–685 (2015).
57. Gill, S. K. & Garcia, G. A. Rifamycin inhibition of WT and Rif-resistant Mycobacterium tuberculosis and Escherichia coli RNA polymerases in vitro. *Tuberculosis* **91**, 361–369 (2011).
58. Stefan, M. A., Ugur, F. S. & Garcia, G. A. Source of the Fitness Defect in Rifamycin-Resistant Mycobacterium tuberculosis RNA Polymerase and the Mechanism of Compensation by Mutations in the β′ Subunit. *Antimicrob Agents Chemother* **62**, (2018).
59. Zhu, D. X., Garner, A. L., Galburt, E. A. & Stallings, C. L. CarD contributes to diverse gene expression outcomes throughout the genome of Mycobacterium tuberculosis. *Proc Natl Acad Sci U S A* **116**, 13573–13581 (2019).
60. Sharma, S. *et al.* Transcriptome analysis of mycobacteria in sputum samples of pulmonary tuberculosis patients. *PLoS One* **12**, (2017).
61. Aguilar-Ayala, D. A. *et al.* The transcriptome of Mycobacterium tuberculosis in a lipid-rich dormancy model through RNAseq analysis. *Scientific Reports 2017 7:1* **7**, 1–13 (2017).
62. Garton, N. J. *et al.* Cytological and Transcript Analyses Reveal Fat and Lazy Persister-Like Bacilli in Tuberculous Sputum. *PLoS Med* **5**, 0634–0645 (2008).
63. Landick, R., Krek, A., Glickman, M. S., Socci, N. D. & Stallings, C. L. Genome-wide mapping of the distribution of CarD, RNAP σA, and RNAP β on the Mycobacterium smegmatis chromosome using chromatin immunoprecipitation sequencing. *Genom Data* **2**, 110 (2014).

64. Tuske, S. *et al.* Inhibition of bacterial RNA polymerase by streptolydigin: Stabilization of a straight-bridge-helix active-center conformation. *Cell* **122**, 541–552 (2005).
65. Sekine, S. ichi, Murayama, Y., Svetlov, V., Nudler, E. & Yokoyama, S. The ratcheted and ratchetable structural states of RNA polymerase underlie multiple transcriptional functions. *Mol Cell* **57**, 408–422 (2015).
66. China, A., Mishra, S. & Nagaraja, V. A transcript cleavage factor of mycobacterium tuberculosis important for its survival. *PLoS One* **6**, (2011).
67. Speer, A., Rowland, J. L. & Niederweis, M. Mycobacterium tuberculosis is resistant to streptolydigin. *Tuberculosis (Edinb)* **93**, 401–4 (2013).
68. Maffioli, S. I. *et al.* Antibacterial nucleoside-analog inhibitor of bacterial RNA polymerase. *Cell* **169**, 1240 (2017).
69. WHO. Global Tuberculosis Report 2017. *World Health Organization* 1–262 (2017) doi:WHO/HTM/TB/2017.23.
70. Campbell, E. A. *et al.* Structural mechanism for rifampicin inhibition of bacterial RNA polymerase. *Cell* **104**, 901–912 (2001).
71. Wehrli, W. Rifampin: mechanisms of action and resistance. *Rev Infect Dis* **5 Suppl 3**, S407–S411 (1983).
72. Severinov, K., Soushko, M., Goldfarb, A. & Nikiforov, V. RifR mutations in the beginning of the Escherichia coli rpoB gene. *Molecular and General Genetics MGG 1994 244:2* **244**, 120–126 (1994).
73. Molodtsov, V., Scharf, N. T., Stefan, M. A., Garcia, G. A. & Murakami, K. S. Structural basis for rifamycin resistance of bacterial RNA polymerase by the three most clinically important RpoB mutations found in Mycobacterium tuberculosis. doi:10.1111/mmi.13606.
74. Stefan, M. A., Ugur, F. S. & Garcia, G. A. Source of the fitness defect in rifamycin-resistant mycobacterium tuberculosis RNA polymerase and the mechanism of compensation by mutations in the = subunit. *Antimicrob Agents Chemother* **62**, (2018).
75. Jagielski, T. *et al.* Characterization of Mutations Conferring Resistance to Rifampin in Mycobacterium tuberculosis Clinical Strains. *Antimicrob Agents Chemother* **62**, e01093-18 (2018).
76. Liu, Q. *et al.* Have compensatory mutations facilitated the current epidemic of multidrug-resistant tuberculosis? *Emerg Microbes Infect* **7**, (2018).
77. de Vos, M. *et al.* Putative compensatory mutations in the rpoc gene of rifampin-resistant mycobacterium tuberculosis are associated with ongoing transmission. *Antimicrob Agents Chemother* **57**, 827–832 (2013).
78. Xiao, J. *et al.* Compensatory Mutations of Rifampin Resistance Are Associated with Transmission of Multidrug-Resistant Mycobacterium tuberculosis Beijing Genotype Strains in China. *Antimicrob Agents Chemother* **60**, 2807–2812 (2016).
79. Lin, W. *et al.* Structural Basis of Mycobacterium tuberculosis Transcription and Transcription Inhibition. *Mol Cell* **66**, 169-179.e8 (2017).
80. Ebright, R. H., Ebright, Y. W., MANDAL, S., Wilde, R. & Li, S. Antibacterial agents: n(alpha)-aroyl-n-aryl-phenylalaninamides. (2015).

81. Pronin, S. v. & Kozmin, S. A. Synthesis of streptolydigin, a potent bacterial RNA polymerase inhibitor. *J Am Chem Soc* **132**, 14394–14396 (2010).
82. Maffioli, S. I. *et al.* Antibacterial Nucleoside-Analog Inhibitor of Bacterial RNA Polymerase. *Cell* **169**, 1240-1248.e23 (2017).
83. Maffioli, S. I., Sosio, M., Ebright, R. H. & Donadio, S. Discovery, properties, and biosynthesis of pseudouridimycin, an antibacterial nucleoside analog inhibitor of bacterial RNA polymerase. *J Ind Microbiol Biotechnol* **46**, 335 (2019).
84. Cain, C. F., Scott, A. M., Sarnowski, M. P. & del Valle, J. R. Total synthesis and chemical stability of pseudouridimycin. *Chem. Commun* **58**, 2351–2354 (2022).
85. Chakraborty, A. *et al.* Structural Basis of Transcription Initiation. *Science (1979)* **337**, 591–595 (2012).
86. Lisica, A. & Grill, S. W. Optical tweezers studies of transcription by eukaryotic RNA polymerases. *Biomol Concepts* **8**, 1–11 (2017).
87. Wang, M. D. *et al.* Force and velocity measures for single molecule of RNA polymerase. *Science (1979)* **902**, 902–907 (1998).
88. Adelman, K. *et al.* Single molecule analysis of RNA polymerase elongation reveals uniform kinetic behavior. *Proc Natl Acad Sci U S A* **99**, 13538–13543 (2002).
89. Mejia, Y. X., Mao, H., Forde, N. R. & Bustamante, C. Thermal probing of E. coli RNA polymerase off-pathway mechanisms. *J Mol Biol* **382**, 628–37 (2008).
90. Proshkin, S., Rahmouni, A. R., Mironov, A. & Nudler, E. Cooperation between translating ribosomes and RNA polymerase in transcription elongation. *Science* **328**, 504–8 (2010).
91. Fan, H. *et al.* Transcription–translation coupling: direct interactions of RNA polymerase with ribosomes and ribosomal subunits. *Nucleic Acids Res* **45**, 11043–11055 (2017).
92. Alexander, R. D., Innocente, S. A., Barrass, J. D. & Beggs, J. D. Splicing-dependent RNA polymerase pausing in yeast. *Mol Cell* **40**, 582–93 (2010).
93. Oesterreich, F. C., Bieberstein, N. & Neugebauer, K. M. Pause locally, splice globally. *Trends Cell Biol* **21**, 328–335 (2011).
94. Kamarthapu, V. & Nudler, E. Rethinking transcription coupled DNA repair. *Curr Opin Microbiol* **24**, 15–20 (2015).
95. Epshtein, V. *et al.* UvrD facilitates DNA repair by pulling RNA polymerase backwards. *Nature* **505**, 372–377 (2014).
96. Wang, M. D. Force and velocity measures for single molecule of RNA polymerase. *Science (1979)* **902**, 902–907 (1998).
97. Wang, M. D. *et al.* Force and velocity measures for single molecule of RNA polymerase. *Science (1979)* **902**, 902–907 (1998).
98. Righini, M. *et al.* Full molecular trajectories of RNA polymerase at single base-pair resolution. *Proc Natl Acad Sci U S A* **115**, 1286–1291 (2018).
99. Neuman, K. C., Abbondanzieri, E. A., Landick, R., Gelles, J. & Block, S. M. Ubiquitous Transcriptional Pausing Is Independent of RNA Polymerase Backtracking. *Cell* **115**, 437–447 (2003).

100. Chakraborty, A., Meng, C. A. & Block, S. M. Observing single RNA polymerase molecules down to base-pair resolution. *Methods in Molecular Biology* **1486**, 391–409 (2017).
101. Abbondanzieri, E. A., Greenleaf, W. J., Shaevitz, J. W., Landick, R. & Block, S. M. Direct observation of base-pair stepping by RNA polymerase. (2005) doi:10.1038/nature04268.
102. Meng, C. A., Fazal, F. M. & Block, S. M. Real-time observation of polymerase-promoter contact remodeling during transcription initiation. *Nat Commun* **8**, 1178 (2017).
103. Kouba, T. *et al.* The Core and Holoenzyme forms of RNA Polymerase from Mycobacterium smegmatis. *J Bacteriol* JB.00583-18 (2018) doi:10.1128/JB.00583-18.
104. Comas, I. *et al.* Whole-genome sequenceing of rifampicin-resistant M. tuberculosis strains identifies compensatory mutations in RNA polymerase. *Nat Genet* **44**, 106–110 (2012).
105. Meftahi, N. *et al.* Evidence for the critical role of a secondary site rpoB mutation in the compensatory evolution and successful transmission of an MDR tuberculosis outbreak strain. *Journal of Antimicrobial Chemotherapy* **71**, 324–332 (2016).
106. Dulin, D. *et al.* Signatures of Nucleotide Analog Incorporation by an RNA-Dependent RNA Polymerase Revealed Using High-Throughput Magnetic Tweezers. *Cell Rep* **21**, 1063–1076 (2017).
107. Seifert, M. *et al.* Inhibition of SARS-CoV-2 polymerase by nucleotide analogs from a single-molecule perspective. *Elife* **10**, (2021).
108. Adelman, K. *et al.* Molecular Mechanism of Transcription Inhibition by Peptide Antibiotic Microcin J25 ple, Rifampicin, a drug that specifically blocks RNAP initiation-to-elongation transition, has proven invaluable in probing the molecular mechanism of transcription. *Mol Cell* **14**, 753–762 (2004).
109. Harshey, R. M. & Ramakrishnan, T. Rate of ribonucleic acid chain growth in Mycobacterium tuberculosis H37R(v). *J Bacteriol* **129**, 616–622 (1977).
110. Cox, R. A. Quantitative relationships for specific growth rates and macromolecular compositions of Mycobacterium tuberculosis, Streptomyces coelicolor A3(2) and Escherichia coli B/r: an integrative theoretical approach. *Microbiology (N Y)* **150**, 1413–1426 (2004).
111. Wang, M. D. *et al. Force and Velocity Measured for Single Molecules of RNA Polymerase*. www.sciencemag.org.
112. Forde, N. R., Izhaky, D., Woodcock, G. R., Wuite, G. J. L. & Bustamante, C. Using mechanical force to probe the mechanism of pausing and arrest during continuous elongation by Escherichia coli RNA polymerase. *Proc Natl Acad Sci U S A* **99**, 11682 (2002).
113. Bustamante, C. & Yan, S. The development of single molecule force spectroscopy: from polymer biophysics to molecular machines. *Q Rev Biophys* **55**, e9 (2022).
114. Larson, M. H. *et al.* A pause sequence enriched at translation start sites drives transcription dynamics in vivo. *Science (1979)* **344**, 1042–1047 (2014).

115. Artsimovitch, I., Chu, C., Lynch, A. S. & Landick, R. A New Class of Bacterial RNA Polymerase Inhibitor Affects Nucleotide Addition. *Source: Science, New Series* **302**, 650–654 (2003).
116. Feng, Y. *et al.* Structural Basis of Transcription Inhibition by CBR Hydroxamidines and CBR Pyrazoles. *Structure* **23**, 1470–1481 (2015).
117. Bae, B. *et al.* CBR antimicrobials inhibit RNA polymerase via at least two bridge-helix cap-mediated effects on nucleotide addition. *Proc Natl Acad Sci U S A* **112**, E4178–E4187 (2015).
118. Lu, H. & Tonge, P. J. Drug-Target Residence Time: Critical Information for Lead Optimization. *Curr Opin Chem Biol* **14**, 467 (2010).
119. Rinehart, K. L., Beck, J. R., Epstein, W. W. & Spicer, L. D. Streptolydigin. I. Streptolic Acid. *J Am Chem Soc* **85**, 4035–4037 (1963).
120. Kyzer, S., Zhang, J. & Landick, R. Inhibition of RNA Polymerase by Streptolydigin: No Cycling Allowed. *Cell* **122**, 494–496 (2005).
121. Temiakov, D. *et al.* Structural Basis of Transcription Inhibition by Antibiotic Streptolydigin. *Mol Cell* **19**, 655–666 (2005).
122. China, A., Mishra, S. & Nagaraja, V. A Transcript Cleavage Factor of Mycobacterium tuberculosis Important for Its Survival. *PLoS One* **6**, 21941 (2011).
123. Adelman, K. *et al.* Molecular Mechanism of Transcription Inhibition by Peptide Antibiotic Microcin J25. *Mol Cell* **14**, 753–762 (2004).
124. Kang, J. Y. *et al.* RNA polymerase accommodates a pause RNA hairpin by global conformational rearrangements that prolong pausing. *Mol Cell* **69**, 802 (2018).
125. Guo, X. *et al.* Structural Basis for NusA Stabilized Transcriptional Pausing. *Mol Cell* **69**, 816 (2018).
126. Tare, P., China, A. & Nagaraja, V. Distinct and Contrasting Transcription Initiation Patterns at Mycobacterium tuberculosis Promoters. *PLoS One* **7**, e43900 (2012).
127. Ahmad, E., Hegde, S. R. & Nagaraja, V. Revisiting intrinsic transcription termination in mycobacteria: U-tract downstream of secondary structure is dispensable for termination. *Biochem Biophys Res Commun* **522**, 226–232 (2020).
128. Kumar Jha, R., Tare, P. & Nagaraja, V. Regulation of the gyr operon of Mycobacterium tuberculosis by overlapping promoters, DNA topology, and reiterative transcription. (2018) doi:10.1016/j.bbrc.2018.05.067.
129. Hu, Y., Morichaud, Z., Perumal, A. S., Roquet-Baneres, F. & Brodolin, K. Mycobacterium RbpA cooperates with the stress-response σB subunit of RNA polymerase in promoter DNA unwinding. *Nucleic Acids Res* **42**, 10399–10408 (2014).
130. Shaevitz, J. W., Abbondanzieri, E. A., Landick, R. & Block, S. M. Backtracking by single RNA polymerase molecules observed at near-base-pair resolution. *Nature* **426**, 684–7 (2003).
131. Herbert, K. M. *et al.* E. coli NusG inhibits backtracking and accelerates pause-free transcription by promoting forward translocation of RNA polymerase. *J Mol Biol* **399**, 17–30 (2010).

132. Tolić-Nørrelykke, S. F., Engh, A. M., Landick, R. & Gelles, J. Diversity in the Rates of Transcript Elongation by Single RNA Polymerase Molecules. *Journal of Biological Chemistry* **279**, 3292–3299 (2004).
133. Larson, M. H., Landick, R. & Block, S. M. Single-molecule studies of RNA polymerase: one singular sensation, every little step it takes. *Mol Cell* **41**, 249–62 (2011).
134. Epshtein, V. Nudler, E. Cooperation Between RNA Polymerase Molecules in Transcription Elongation. *Science (1979)* **300**, 801–805 (2003).
135. Forde, N. R., Izhaky, D., Woodcock, G. R., Wuite, G. J. L. & Bustamante, C. Using mechanical force to probe the mechanism of pausing and arrest during continuous elongation by Escherichia coli RNA polymerase. *Proc Natl Acad Sci U S A* **99**, 11682–11687 (2002).
136. Neuman, K. C., Abbondanzieri, E. A., Landick, R., Gelles, J. & Block, S. M. Ubiquitous Transcriptional Pausing Is Independent of RNA Polymerase Backtracking. *Cell* **115**, 437–447 (2003).
137. Yin, H., Landick, R. & Gelles, J. Tethered particle motion method for studying transcript elongation by a single RNA polymerase molecule. *Biophys J* **67**, 2468–2478 (1994).
138. Gotta, S. L., Miller, O. L. & French, S. L. rRNA Transcription Rate in Escherichia coli. *J Bacteriol* **173**, 6647–6649 (1991).
139. Bustamante, C., Chemla, Y. R., Forde, N. R. & Izhaky, D. Mechanical Processes in Biochemistry. *Annu Rev Biochem* **73**, 705–748 (2004).
140. Saba, J. *et al.* The elemental mechanism of transcriptional pausing. *Elife* **8**, (2019).
141. Hein, P. P., Landick, R. & M E N Ta R Y, C. M. The bridge helix coordinates movements of modules in RNA polymerase. **8**, 141 (2010).
142. Weinzierl, R. O. J. The Bridge Helix of RNA polymerase acts as a central nanomechanical switchboard for coordinating catalysis and substrate movement. *Archaea* **2011**, 1–7 (2011).
143. Hassan, H. M., Degen, D., Jang, K. H., Ebright, R. H. & Fenical, W. Salinamide F, new depsipeptide antibiotic and inhibitor of bacterial RNA polymerase from a marine-derived Streptomyces sp. *J Antibiot (Tokyo)* **68**, 206 (2015).
144. Orlova, M. *et al.* Intrinsic transcript cleavage activity of RNA polymerase. *Biochemistry* **92**, 4596–4600 (1995).
145. Epshtein, V., Cardinale, C. J., Ruckenstein, A. E., Borukhov, S. & Nudler, E. An Allosteric Path to Transcription Termination. *Mol Cell* **28**, 991–1001 (2007).
146. Flentie, K., Garner, A. L. & Stallings, C. L. Mycobacterium tuberculosis Transcription Machinery: Ready To Respond to Host Attacks. *J Bacteriol* **198**, 1360–73 (2016).
147. Rammohan, J. Regulation of Mycobacterial Transcription Initiation.
148. Winther, K. S. *et al.* The sigma factors of Mycobacterium tuberculosis: Regulation of the regulators. *Nucleic Acids Res* **43**, 1–10 (2015).
149. Garner, A. L. *et al.* Effects of increasing the affinity of CarD for RNA polymerase on Mycobacterium tuberculosis growth, rRNA transcription, and

virulence"Effects of increasing the affinity of CarD for RNA polymerase on Mycobacterium tuberculosis growth, rRNA transcription. *J Bacteriol* **1994**, 698–16 (2017).
150. Rammohan, J. *et al.* Cooperative stabilization of Mycobacterium tuberculosis rrnAP3 promoter open complexes by RbpA and CarD. *Nucleic Acids Res* **44**, 7304–7313 (2016).
151. Hubin, E. A., Lilic, M., Darst, S. A. & Campbell, E. A. Structural insights into the mycobacteria transcription initiation complex from analysis of X-ray crystal structures. *Nat Commun* **8**, 16072 (2017).
152. Sachdeva, P., Misra, R., Tyagi, A. K. & Singh, Y. The sigma factors of Mycobacterium tuberculosis: Regulation of the regulators. *FEBS Journal* **277**, 605–626 (2010).
153. Stefan, M. A., Velazquez, G. M. & Garcia, G. A. High-throughput screening to discover inhibitors of the CarD·RNA polymerase protein–protein interaction in Mycobacterium tuberculosis. *Sci Rep* **10**, (2020).
154. Stallings, C. L. & Glickman, M. S. CarD: A new RNA polymerase modulator in mycobacteria. *Transcription* **2**, 15–18 (2011).
155. Srivastava, D. B. *et al.* Structure and function of CarD, an essential mycobacterial transcription factor. *Proceedings of the National Academy of Sciences* **110**, 12619–12624 (2013).
156. Kaur, G. *et al.* Mycobacterium tuberculosis CarD, an essential global transcriptional regulator forms amyloid-like fibrils. *Sci Rep* **8**, 10124 (2018).
157. Rammohan, J., Manzano, A. R., Garner, A. L., Stallings, C. L. & Galburt, E. A. CarD stabilizes mycobacterial open complexes via a two-tiered kinetic mechanism. *Nucleic Acids Res* **43**, 3272–3285 (2015).
158. Stallings, C. L. *et al.* CarD Is an Essential Regulator of rRNA Transcription Required for Mycobacterium tuberculosis Persistence. *Cell* **138**, 146–159 (2009).
159. Weiss, L. A. *et al.* Interaction of CarD with RNA polymerase mediates Mycobacterium tuberculosis viability, rifampin resistance, and pathogenesis. *J Bacteriol* **194**, 5621–31 (2012).
160. Gangwar, S. P., Meena, S. R. & Saxena, A. K. Structure of the carboxy-terminal domain of Mycobacterium tuberculosis CarD protein: an essential rRNA transcriptional regulator. *Acta Crystallogr F Struct Biol Commun* **70**, 160–165 (2014).
161. Feng, S. *et al.* Involvement of Transcription Elongation Factor GreA in Mycobacterium Viability, Antibiotic Susceptibility, and Intracellular Fitness. *Front Microbiol* **11**, (2020).
162. Jha, R. K. *et al.* Conditional down-regulation of GreA impacts expression of rRNA and transcription factors, affecting Mycobacterium smegmatis survival. *Sci Rep* **10**, (2020).
163. China, A., Mishra, S., Tare, P. & Nagaraja, V. Inhibition of Mycobacterium tuberculosis RNA Polymerase by Binding of a Gre Factor Homolog to the Secondary Channel. *J Bacteriol* **194**, 1009 (2012).

164. Gulten, G. & Sacchettini, J. C. Structure of the Mtb CarD/RNAP β-lobes complex reveals the molecular basis of interaction, and presents a novel DNA binding domain for Mtb CarD. doi:10.1016/j.str.2013.08.014.
165. Jensen, D., Galburt, A., Manzano, A. R., Rammohan, J. & Stallings, C. L. CarD and RbpA modify the kinetics of initial transcription and slow promoter escape of the Mycobacterium tuberculosis RNA polymerase. *Nucleic Acids Res* 1–14 (2019) doi:10.1093/nar/gkz189.
166. Boyaci, H., Chen, J., Jansen, R., Darst, S. A. & Campbell, E. A. Structures of an RNA polymerase promoter melting intermediate elucidate DNA unwinding. *Nature* **565**, 382–385 (2019).
167. Mejia, Y. X., Nudler, E. & Bustamante, C. Trigger loop folding determines transcription rate of Escherichia coli's RNA polymerase. *Proc Natl Acad Sci U S A* **112**, 743–8 (2015).
168. Vishwakarma, R. K. *et al.* Single-molecule analysis reveals the mechanism of transcription activation in M. tuberculosis *Sci Adv* **4**, eaao5498 (2018).
169. Gourse, R. L., Gaal, T., Bartlett, M. S., Appleman, J. A. & Ross, W. rRNA Transcription and growth rate-dependent regulation of ribosome synthesis in Escherichia coli. *Annu Rev Microbiol* **50**, 645–677 (1996).
170. Zamft, B., Bintu, L., Ishibashi, T. & Bustamante, C. Nascent RNA structure modulates the transcriptional dynamics of RNA polymerases. *Proceedings of the National Academy of Sciences* **109**, 8948–8953 (2012).
171. Stahl ', D. A. & Urbance ', J. W. The Division between Fast-and Slow-Growing Species Corresponds to Natural Relationships among the Mycobacteria. *J Bacteriol* **172**, 116–124 (1990).
172. Zhu, M. & Dai, X. On the intrinsic constraint of bacterial growth rate: *M. tuberculosis* 's view of the protein translation capacity. *Crit Rev Microbiol* 1–10 (2018) doi:10.1080/1040841X.2018.1425672.
173. Tolić-Nørrelykke, S. F., Engh, A. M., Landick, R. & Gelles, J. Diversity in the Rates of Transcript Elongation by Single RNA Polymerase Molecules. *Journal of Biological Chemistry* **279**, 3292–3299 (2004).
174. Perrone, R. *et al.* Mapping and characterization of G-quadruplexes in Mycobacterium tuberculosis gene promoter regions. *Sci Rep* **7**, (2017).
175. Mishra, S. K. *et al.* Characterization of G-Quadruplex Motifs in espB, espK, and cyp51 Genes of Mycobacterium tuberculosis as Potential Drug Targets. *Mol Ther Nucleic Acids* **16**, 698 (2019).
176. Shitikov, E. *et al.* Genome-Wide Transcriptional Response of Mycobacterium smegmatis MC2155 to G-Quadruplex Ligands BRACO-19 and TMPyP4. *Front Microbiol* **13**, 817024 (2022).
177. Beaudoin, J. D., Jodoin, R. & Perreault, J. P. New scoring system to identify RNA G-quadruplex folding. *Nucleic Acids Res* **42**, 1209 (2014).
178. Wanrooij, P. H. *et al.* A hybrid G-quadruplex structure formed between RNA and DNA explains the extraordinary stability of the mitochondrial R-loop. *Nucleic Acids Res* **40**, 10334 (2012).

179. Shrestha, P., Xiao, S., Dhakal, S., Tan, Z. & Mao, H. Nascent RNA transcripts facilitate the formation of G-quadruplexes. *Nucleic Acids Res* **42**, 7236 (2014).
180. Yang, D. G-Quadruplex DNA and RNA. *G-Quadruplex Nucleic Acids* **2035**, 1 (2019).
181. Robinson, J., Raguseo, F., Nuccio, S. P., Liano, D. & di Antonio, M. DNA G-quadruplex structures: more than simple roadblocks to transcription? *Nucleic Acids Res* **49**, 8419 (2021).
182. Stevens, A. J., de Jong, L. & Kennedy, M. A. The Dynamic Regulation of G-Quadruplex DNA Structures by Cytosine Methylation. *Int J Mol Sci* **23**, (2022).
183. Lin, J. *et al.* Stabilization of G-quadruplex DNA by C-5-methyl-cytosine in bcl-2 promoter: Implications for epigenetic regulation. *Bioch emical and Biophysical Resea rch Comm unications* **433**, 368–373 (2013).
184. Oshikawa, D., Inaba, S., Kitagawa, Y., Tsukakoshi, K. & Ikebukuro, K. CpG Methylation Altered the Stability and Structure of the i-Motifs Located in the CpG Islands. *Int J Mol Sci* **23**, (2022).
185. Neuman, K. C. & Block, S. M. Optical trapping. (2004) doi:10.1063/1.1785844.
186. Bustamante, C. J., Chemla, Y. R., Liu, S. & Wang, M. D. Optical tweezers in single-molecule biophysics. *Nature Reviews Methods Primers 2021 1:1* **1**, 1–29 (2021).
187. Smith, S. B., Cui, Y. & Bustamante, C. Optical-trap force transducer that operates by direct measurement of light momentum. *Methods Enzymol* **361**, 134–162 (2003).
188. Comstock, M. J., Ha, T. & Chemla, Y. R. Ultrahigh-resolution optical trap with single-fluorophore sensitivity. *Nat Methods* **8**, 335–340 (2011).
189. Whitley, K. D., Comstock, M. J. & Chemla, Y. R. High-Resolution “Fleezers”: Dual-Trap Optical Tweezers Combined with Single-Molecule Fluorescence Detection. *Methods Mol Biol* **1486**, 183 (2017).
190. Moffitt, J. R., Chemla, Y. R., Izhaky, D. & Bustamante, C. Differential detection of dual traps improves the spatial resolution of optical tweezers. *Proc Natl Acad Sci U S A* **103**, 9006–11 (2006).
191. Malinen, Anssi M.; Turtola, Matti.; Belogurov, G. A. Monitoring translocation of multisubunit RNA polymerase along the DNA with fluorescent base analogues. in *Bacterial Transcriptional Control* (ed. Artsimovitch, Irina, Santangelo, T. J.) 31–51 (Humana Press, New York, NY, 2015). doi:10.1007/978-1-4939-2392-2_3.
192. Nudler, E., Gusarov, I. & Bar-Nahum, G. Methods of Walking with the RNA Polymerase. *Methods Enzymol* **371**, 160–169 (2003).
193. Hodges, C., Bintu, L., Lubkowska, L., Kashlev, M. & Bustamante, C. Nucleosomal Fluctuations Govern the Transcription Dynamics of RNA Polymerase II. *Science (1979)* **325**, 626–628 (2009).
194. Tong, A. MATLAB files for Optical Tweezers. Preprint at https://doi.org/doi.org/10.5281/zenodo.6534021 (2022).
195. Englard, S. & Seifter, S. Precipitation techniques. *Methods Enzymol* **182**, 285–300 (1990).

196. Kim, Y. *et al.* Efficient site-specific labeling of proteins via cysteines. *Bioconjug Chem* **19**, 786–791 (2008).
197. Lee, Y. J. & Chang, G. D. Quantitative display of the redox status of proteins with maleimide-polyethylene glycol tagging. *Electrophoresis* **40**, 491–498 (2019).

Appendix A

Preliminary work recognizes QGs as a possible modulator of MtbRNAP pausing

Around 50% of the MtbRNAP elongation traces produced abnormal RTH. The possible reasons for the abnormal RTH are (i) some enzymes stalled inside and before crossing the repeat region, (ii) some traces are noisier than the average due to multitether events, (iii) a few traces do backtrack along the molecular ruler, and (iv) a few enzymes do not recognize or weakly recognize the elemental pauses. In addition, we questioned whether the DNA template of the Mtb genome's high GC content surrounding the pause *c* in the repeat might facilitate the formation of a G-quadruplex (QG) structure[174–177], including a hybrid QG formed with the nascent RNA during transcription[178–181]. Since neighboring methylated cytosine bases often positively affect QG stability [182–184], we investigated the variation in the RTH of MtbRNAP elongation crossing the demethylated pause repeat. Thus, our results unexpectedly revealed that the unmethylated Mtb *molecular ruler* drops the MtbRNAP residence time by more than 25%. Likewise, using a chemical that stabilized QGs might alter MtbRNAP RTH. Thus, we employed Braco-19[176], a QGs stabilizer and *in vitro* inhibitor of *Mycobacteria* growth [181], on the transcription of methylated DNA. In this manner, we noticed that MtbRNAP RTH has a reduced pause *c* strength indicating that perhaps the surrounding DNA stabilized, compromising the pausing structure stability.

Remain to demonstrate if there are actual GQ structures in Mtb templates that, instead of acting as a roadblock to stop elongation, may modulate transcription pausing via nascent RNA [181].

Appendix B (methods)

Optical tweezers instrumentation

Optical tweezers

Our optical tweezers setup utilizes a high-intensity collimated polarized laser beam to manipulate dielectric particles, i.e., polystyrene microbeads, with a refractive index higher than the medium by conserving the light linear momenta. These microspheres behave as Rayleigh particles because they are smaller than the light wavelength. Thus, the electric field component of the diffraction-limited beam induces a dipole moment on the microbeads to attract to the higher-intensity region of the light. This attractive force is the negative value of the density gradient of the beam intensity-denominated *gradient forces* [185,186]. Moreover, since the upstream force equals the change in the rate of light momentum, the microsphere surface suffers a fractional force pressure proportional to photon absorption events during light diffraction and a fraction of force due to non-absorbed photons during light reflection that pushes them outwardly (*scattering forces*). The rate of change of a microbead's momentum determines the forces that operate on it. In this manner, stable trapping requires balancing these two downstream forces [36,186 187].

Timeshare instrument

The high-resolution optical tweezers (HROT) equipment we employed is an adaptation by a post-doc in our research group from a previous publication [39,98,188,189]. The instrument is a timeshare device that uses a crystal acoustic-optic deflector or modulator (AOM or AOD) of tellurium dioxide with resonating acoustic waves produced by a radio frequency (RF) generator to cause it to diffract the 1064 nm laser beam in a linear frequency-dependent manner to achieve light steering. In contrast to the differential path optical trap instrument (Figure 17A) [190], which splits the laser beam between two polarization paths to utilize all the light, this instrument requires high laser power on the order of 5-10W to achieve high trap intensity, as the AOM cannot steer excessive zero mode light at its exit. In time-sharing, the traps use the same optical path, which reduces low-frequency noise and improves trap-distance estimations. In addition, a Field-Programable Gate Array (FPGA) controls and switches the RF signal at a frequency near the local sound speed (5 µsec) between two sets of frequency and amplitude generated in the RF board to change the laser beam angle and intensity to have two interlacing optical traps. Since the instrument does not collect fluorescent signals[39,188], interlacing always has one trap enabled, resulting in a sampling frequency of 100 kHz. The beam deflection angle determines the instrument trap distance.

For a maximum trap separation of 4-6 m at 30 MHZ, the angle is a function of the light order, material refractive index, laser wavelength, RF board frequency, and optical density employed in the fluidic chamber. Therefore, only one trap is displaced by 150 nm to the other for every megahertz shift. The trap's intensity, however, changes with its position and requires applying intensity feedback. Specifically, the FPGA receives data from the trap avalanche photodiodes (APDs) to obtain the trap intensity difference and correct it, then sends the frequency and amplitude data separately to the direct digital RF

synthesizer (RFS) that generates a new RF signal via buffering. A clock chip generates the RF signal called a frequency shift key (FSK) that records and swiftly shifts between two operating frequencies. Finally, to send enough voltages to the AOD (100-200mV0, an amplifier increases the signal.

Optics

The beginning of the optics setup consists of a collimated laser beam with a diameter of 0.8-1 mm that passes through an optical isolator composed of a tandem of two ½ wave plates to prevent reflections from downstream components that damages the laser cavity by rotating twice the optical polarization of the light 45 degrees (Figure 17a). Immediately close, a beam splitter reflects light to a dump to limit the amount of polarized laser input and prevent laser profile change during light expansion. To reach the AOM aperture, a set of telescoping lenses with pinholes immediately collimates and extends the beam by around 1.5-2 mm. Closed to the AOM outlet, a mirror deflects only the zero mode to a laser dump. A second telescope then enlarges the diffracted guide beams to 8 mm to overfill the far objective aperture to avoid an extended confocal point and Z-axis weak trapping in the chamber. Therefore, trapping occurs in the microfluidic chamber immediately adjacent to the back focal plane conjugating the AOM plane, where the objective body is. In addition, APDs receive a portion of the incoming laser beam before reaching the chamber for feedback trap intensity purposes. The bright light field reaches the objective and chamber through the second telescope.

Downstream of the objective, a second condenser on the other side of the chamber collects the light from the bright field and the laser trap and allows them to travel to a beamsplitter to take two paths. One path at the end of the optics records the bright field with a video camera for monitoring the fluidics and trapping, while the other records the laser beam with position-sensitive detectors (PSDs). Thus, we measured the position of beams using these QPDs, which had a maximum response time of 1 µsec.

Fluidics:

A serial connection exists between the syringe pumps, stage motors, and fluidic positioner valves with the computer. We modified the microfluidics chamber to have multiple shunts from previous works. It consists of a nescofilm sandwiched between two 0.2mm glass coverslips (Figure 17b). Glass chamber dispensers connect the main channel, where the experiment takes place, to two secondary channels. These additional channels are for the sample injection from syringes pumps. Additionally, we introduced three glass shunts to connect the main channel to the gravity columns for buffer exchange purposes (Figure 17c).

Methodology

Plasmid preparation.

To make the expressing vectors for RNAP biotinylation, we did round-the-horn site mutagenesis of plasmid pET-DUET-BC by long PCR to introduce at the c-term of the rpoC gene the avitag or the sortase tag (sortag) sequence. The names of the new

plasmids were pET-DUET-BC-avitag and pET-DUET-BC-sortag, respectively. Concerning the vectors for expression of Mtb transcription factors, we amplified the corresponding gene from the Mtb genome and inserted it into plasmid pET-his6-Lic1 Kan by ligation-independent-Cloning (LIC).

To make plasmids coding the DNA template for SM assays, we cloned in pUC19 the promoter AC50, the 10nt stalling cassette, and the transcribable region, which derived from a ~ 2.7kb region of genes rpoB and C from *M. tuberculosis* str Erdman genome (a gift from Professor Sara Stanley). We named this plasmid pUC19-AC50-MtbrpoBC.

To make the plasmid for the molecular ruler, we replaced the stalling cassette with a 20nt CU-less cassette and inserted a chemically synthesized dsDNA sequence of the pause *c* repeats (Genscript) on the gene rpoB and other minor modifications. We named the plasmid pSGUML1T1. The molecular ladder consists of eight repeats of 63bp coding a derivative of elementary pause c.

DNA template preparation.

PCR or restriction reactions, we prepared the DNA templates for our single-molecule transcription assays. In the first case, we simultaneously amplified and labeled with digoxigenin the DNA product from the plasmid pUC19-AC50-MtbrpoBC using a dig-labeled primer. Depending on the direction of primer annealing, we made ~4.2kb assisting or ~2.8kb opposing force templates. In the other case, we linearized the plasmid pSGUML1T1 having the Mtb pause repeat with BsaI and selected for a specific sticky end by using DNA polymerase Klenow-Exo in the presence of either ddATP or ddCTP to produce the opposing or assisting force template, respectively. We made two types of DNA handle based on the end modification by PCR and oligonucleotides. The oligo could have a double dig- modification or a sequence coding a restriction enzyme site to fabricate a single-strand overhang.

To make a DNA template for the smFRET TIRF assay, we similarly used PCR to amplify a DNA fragment of 290 bp that includes the AC50 promoter from plasmid pUC19-AC50-MtbrpoBC.

Production of biotinylated and non-biotinylated MtbRNAP

As previously published, we made the holoenzyme sigma A of MtbRNAP by co-expressing its subunits in *E. coli* [13]. We used two different methods to produce the biotinylated MtbRNAP. We added an avitag at the c-terminal of the β' subunit in the first method. We used the enzyme BirA to transfer the biotinoyl group to the epsilon amine group of the amino acid lysine in the tag. We found that *in vitro* biotinylation reduced the yield due to increased purification steps. Therefore, we did *in vivo* biotinylation by co-expressing three plasmids in *E. coli*, including pCDF-BirA (gift of prof Nicola Burgess-Brown), without changes in protein activity. In the second method, we added a small tag -LPETG to the same end and utilized the enzyme sortase A to catalyze the biotinylated peptidyl (GGGL-biotin) transfer reaction[98].

To produce a flag-tagged MtbRNAP σ^A holoenzyme, we replaced the avitag sequence with a flag-tag one and added a TEV cleavage site on the histidine tags of α subunits, and followed the co-expression in *E. coli,* as mentioned before. Before the MonoQ chromatography, we did the TEV proteolysis and the reverse nickel column purification. The enzyme was pure and highly active for smFRET assays.

Production of transcription factors

We purified the transcription factor MtbCarD as before[13]. To obtain the MtbGreA, we expressed it in *E. coli* BL21(DE) with a pET vector and purified the protein with a nickel column. Then, we did TEV protease cleavage to remove the histidine tag, reverse nickel column purification to remove the free tags, and later anion exchange chromatography (HiTraPQ) in Tris-saline Buffer to improve purification.

In vitro transcription bulk assay

We follow a previous publication[13] to perform the promoter-initiated transcription to evaluate the MtbCarD effect using radiative rNTPs and artificial bubble-based transcription to evaluate the elemental pause sequences using a FAM-label RNA.

*In bulk r*eal-time fluorescent assay for post-translocation formation detection

We prepared per condition to assay ~ 145 µL of reaction (TEC mix), which contains 0.5 mg/mL BSA, 1mM DTT 1.5 µM MtbRNAPσ^A, and 1µM pre-annealed 2-aminopurine-labeled DNA-RNA hybrid[191] in 1x transcription buffer (40 mM HEPES-K pH 7.5, 0.1 mM Na_2EDTA, 5% Glycerol, 80 mM KCl, and 10 mM $MgCl_2$) incubated at 22° C for 10 min, before the addition of the complementary non-template DNA and incubation for another 20 min. In parallel, we made a reaction of ~145 µL (nucleotide-factor mix) containing 200 µM rATP supplemented with either 200 µM rATP, 0.5 µM MtbGreA, 15 µM STL or 0.5 µM MtbGreA plus 15 µM STL in 1x transcription buffer. We measured the formation of the post-translocated state in real-time from position *i*+2 to *i*+1 in the transcription bubble upon fast mixing the TEC and nucleotide-factor mixes while recording the enhancement in fluorescent at 375 nm of the nitrogen base analog (2-aminopurine) excited at 330 nm using a stop-flow instrument (*Kin Tek corporation*)[18,28,191].

Ternary elongation complex formation

To study elongation, we stalled the biotinylated MtbRNAP on a cassette lacking one nucleotide to form the ternary elongation complex (TEC) as previous research[12,192].

Sample preparation for *in-singulo* transcription elongation assay

To prepare the promoter-initiated stall elongation complexes, we made two strategies related to using MtbCarD. In the case of MtbCarD in initiation [193], we pre-incubated ~ 1 µM biotinylated-MtbRNAP with ~ 10 µM MtbCarD at 37° C for 5 min in a final volume of 2 µL. After that, we diluted the biotinylated MtbRNAP in buffer TB40 (20 mM Tris-HCL pH 7.9, 40 mM KCl, 5 mM $MgCl_2$, 0.5 mM TCEP) to 10 nM. Then, we stalled 5 nM of polymerases by incubation with 150 µM GpG, 2 nM Mtb DNA template in stall Buffer (20 mM Tris-HCl pH 7.9, 3 µM rATP, 3 µM rGTP, and 3 µM rCTP) at 37° C for 20 min. If we used the Eco DNA repeat, we would replace GpG for ApU.

To do the beads depositions, we made two strategies relating to the attachment of the beads to the microbeads surfaces. In the first case, for a DNA template labeled with double-dig, we incubated 0.1nM stall complex with 0.1-0.05 % passivated anti-dig beads

in TB40 buffer for 10 min at 22° C and added 0.05 µg /µL heparin at 22° C for 5 min to get rid of non-competent polymerases. Likewise, we incubated in another tube 0.5-0.2 nM digoxygenin-labeled DNA handle with 300 nM Neutravidin and the mentioned amount of anti-dig beads at 22° C for 10 min and later with the corresponding heparin. Here we could preserve the beads depositions by flash freezing and storage at -80° C or use them the same, keeping them in Ice.

We did ligation-based deposition by incubating 0.1 nM stall complex with 0.1-0.05 % passivated oligo beads, 0.1 mM rATP, 4 U/ µL T4 DNA ligase in TB40 buffer at 22° C for 45 min to promote the ligation reaction followed by addition of heparin for 5 min at 22° C.

Correspondingly, the deposition of 0.5–0.2 nM DNA handle was achieved by incubation with the passivated complementary oligo beads, 300 nM Neutravidin, 0.1 mM rATP, and 4 U/ µL of T4 DNA ligase in TB40 buffer for an identical prolonged incubation followed by the heparin treatment. Again here, we could do preservation of deposition.

For every 10 µL of deposition, we used, before injecting into the fluidics chamber, 1 000- 1 500 of degassed TB130 Buffer.

In the experiments with MtbCarD and MtbGreA, the final amount of initiating CarD contributed to the amount free in solution in elongation was as low as ~13 picomolar (diluted from 100-120 nM MtbCarD) and neither causes any effects on pausing nor velocity.

High-Resolution Optical Tweezer transcription elongation assay

In the supplementary Figure 18, there is a representation of our DNA-pulling-based setup under an opposing and assisting mode. The SM assay to measure transcription elongation involves attaching a single MtbRNAP via a biotin-neutravidin interaction to a ~1.5 kb dsDNA handle that isolates the polymerase from the laser beam to reduce any possible photodamage. We also used an oxygen-scavenger system based on sodium azide to increase the robustness of collecting processive activities. The other end of the handle and template of the stalled complex form an attachment with the surface of 1-micron beads via digoxygenin/anti-digoxygenin (dig/anti-dig) interactions. In this manner, we deposited the DNA handle and the stalled complex separately on different microbead surfaces. As an alternative to utilizing two dioxygen molecules at the DNA ends and microbeads anti-dig, we made a single-strand overhang in the handles and template ends complementary to the sequence of an oligo attached to the microbeads to perform DNA ligation via T4 DNA ligase.

To form the single molecule tether, we injected the microbeads into a microfluidics chamber through different channels to diffuse them to a central main channel, trapped them by optical tweezers, and brought them closer to each other to allow the neutravidin molecule -already linked on the DNA handle- bind the biotin group of the MtbRNAP.

To resume the elongation activity, we flow the solution of rNTPs or derivates, including transcription factors or antibiotics, using valve positioners connected to different gravity columns (multi-shunt) under remote control (Supplementary Figure 18 B). To compare the residence time between EcoRNAP and MtbRNAP transcribing the Eco elementary pauses sequence, we injected a nucleotide cocktail of 1 mM rUTP, 1mM rGTP, 0.5mM rATP, 0.25mM rCTP[39].

Simultaneously with the shunt opening, the instrument tracks the displacement in the bead-bead distance, holds the traps in passive mode, or moves the traps according to

the enzyme movement in *constant* mode [98]. Finally, we obtained trap calibration and offset data before or after the data acquisition of *in-singulo* trajectories for each pair of beads.

Analysis of Single-Molecule (SM) elongation traces

The MATLAB tools to extract RNA polymerase dwells, pause chances, and residence time are a contribution of another graduate student in the lab and are in a repository[194]. To get the dwells of the polymerase, we fit the traces as a base-pair staircase. The dwells distribute following a complementary cumulative distribution function (CCDF). We represent the CCDF as the summation of multiexponential functions $\sum_{i=1}^{n} a_i e^{-k_i t}$, where i represents the *i-th* mode of action of the RNA polymerase, a_i is the mode probability with the total sum equals one ($\sum_i a_i = 1$), and k_i is the kinetic rate such that $k_1 > k_2 > \ldots k_n$. Our model can attribute the first exponential *average parameters k* and *p* to the pause-free velocity or effective elongation rate (k_{el}) above 4 nt/sec. Between 0.5-4 nt/s average rate corresponds to the kinetics of elemental pause escape rate (k_{-p}) and pause probability (P_{total}), and slower rates of higher-order exponentials correspond to long pauses or backtracking events, k_{-n} and P_n, respectively (Figure 18c of the Supplementary).

To get the pause chances distributions, we binned the trace data in regions of 100bp and counted how many pauses were using a threshold based on the distribution k_{el} followed by a normalization process relative to the total amount of pauses [41]. We calculated the residence time histogram (RTH) of the polymerase transcribing the pauses repeat according to a previous publication [39]. Briefly, the procedure implies discretizing the distance axis in small bins to get the time expended per bin or residence time per trace, followed by the periodization to maximize the probability of finding higher similarity scores of folded residence histogram with itself under specific periods using cross-correlation and acceptable bp/nm conversation values. To align the traces, the second maximization of cross-correlation of RTHs renders the inter-trace offset.

Production of fluorescent and non-fluorescent labeled MtbCarD and MtbGreA

We mutated the amino acids E30 and T26 to cysteines in proteins MtbCarD and MtbGreA. We purify the proteins using excess DTT in the nickel and anion exchange chromatography. To prepare the proteins for maleimide-thiol chemistry, we removed any possible oxidizing agent of the thiol-reactive group of the soluble-accessible cysteines by precipitating the proteins with 70% ammonium sulfate[195] before the incorporation of the maleimide-linked Cy3 and Cy5 as previously determined[196,197]. Proteins are entirely active after resuspension from their precipitated state. After the conjugation reaction, we diluted the resuspended pellet of MtbGreA in low salt tris buffer and did an additional anion exchange chromatography to remove the free dye, misfolded, and aggregated proteins. For MtbCarD, we did ammonium sulfate precipitation at a lower concentration to remove the aggregated byproducts and a second precipitation before resuspension of the soluble fraction protein in a tris-saline buffer. The yield and labeling efficiencies for Cy5-MtbCarD and Cy3-MtbGreA were ~107 µM and 76%; and 5.2 µM and 88%, respectively.

smFRET assay sample preparation.

We prepared the Mtb initiation complex (MtbIC) by combining 200 nM of 290 bp DNA template containing AC50 promoter with 20 nM of Flag-tagged MtbRNAP holoenzyme σ^A and 200 nM of Cy5-MtbCarD in buffer TB40 for 10 min at 22 °C. Then, we added 70 nM of mouse biotinylated antibody anti-DYKDDDDDK flag tag (FG4R, Invitrogen) and let it incubate for an additional 10 min at the same temperature. Before imaging, we diluted the MtbIC ~ 20 times with buffer TB130 (TB40).

The oxygen scavenging system for imaging consisted of 2 mM Trolox, 50mM D-Glucose, 12.5 mM ascorbic acid, 1 mg/mL beta-casein, 0.9 U/mL pyranose oxidase, 0.25mg/mL catalase, and 0.2 U/µL RNaseOUT in TB40 buffer.

smFRET surface preparation and data acquisition.

We used glass coverslips and quartz slides to make microfluidic chambers for the smFRET experiments subjected to quality control of the number of fluorescent dust spots. The biotin/PEG coverslips were from MicroSurfaces, Inc. Our cleaning procedure of the coverslips and slides consists of sonication with acetone, methanol, and piranha solutions. We performed all the smFRET experiments on an objective-based TIRF microscopy at 22 ° C and aligned the two signal channels for Cy3 and Cy5 dyes using beads mapping through a three-point algorithm.

We prepared the chambers with successive steps of 10 min incubation at 22 ° C in the following order: equilibration with TB40 buffer, passivation with 30 mg/mL beta-casein, coating, and functionalization with 3 µM neutravidin. Between steps, we applied a procedure of three times washes with buffer TB40 to remove free molecules, and the last step to equilibrate the surface was incubation in the oxygen-scavenging buffer.

Once functionalized and equilibrated, we added to the glass surface ~ 2.7 nM of pre-assembled initiation complex Cy5-CarD-MtbRNAPσ^A and antibody anti-Flag and incubate for 10 min to allow the binding on the surface via flag -anti-flag interactions. Through Cy5 excitation by a red laser, we checked the immobilization density of Cy5-CarD-MtbRNAPσA complexes. Next, we flowed ~10 nM Cy3-MtbGreA into the chamber to promote binding and formation of complex Cy5-CarD-MtbRNAPσ^A-Cy3-GreA in the presence of the imaging buffer (oxygen-scavenging buffer) and recorded fluorescent signals at 100 ms exposure time. We excited Cy3 at 550 nm on a Felix fluorometer (Horiba, Kyoto, Japan). To calculate the FRET efficiency, we used the formula $E = \frac{I_A}{(I_D+I_A)}$, where I_A and I_B correspond to donor and acceptor fluorescence intensities, respectively. We use Origin (Pro) 2022 to open and analyze the data.

Additional Supplementary figures

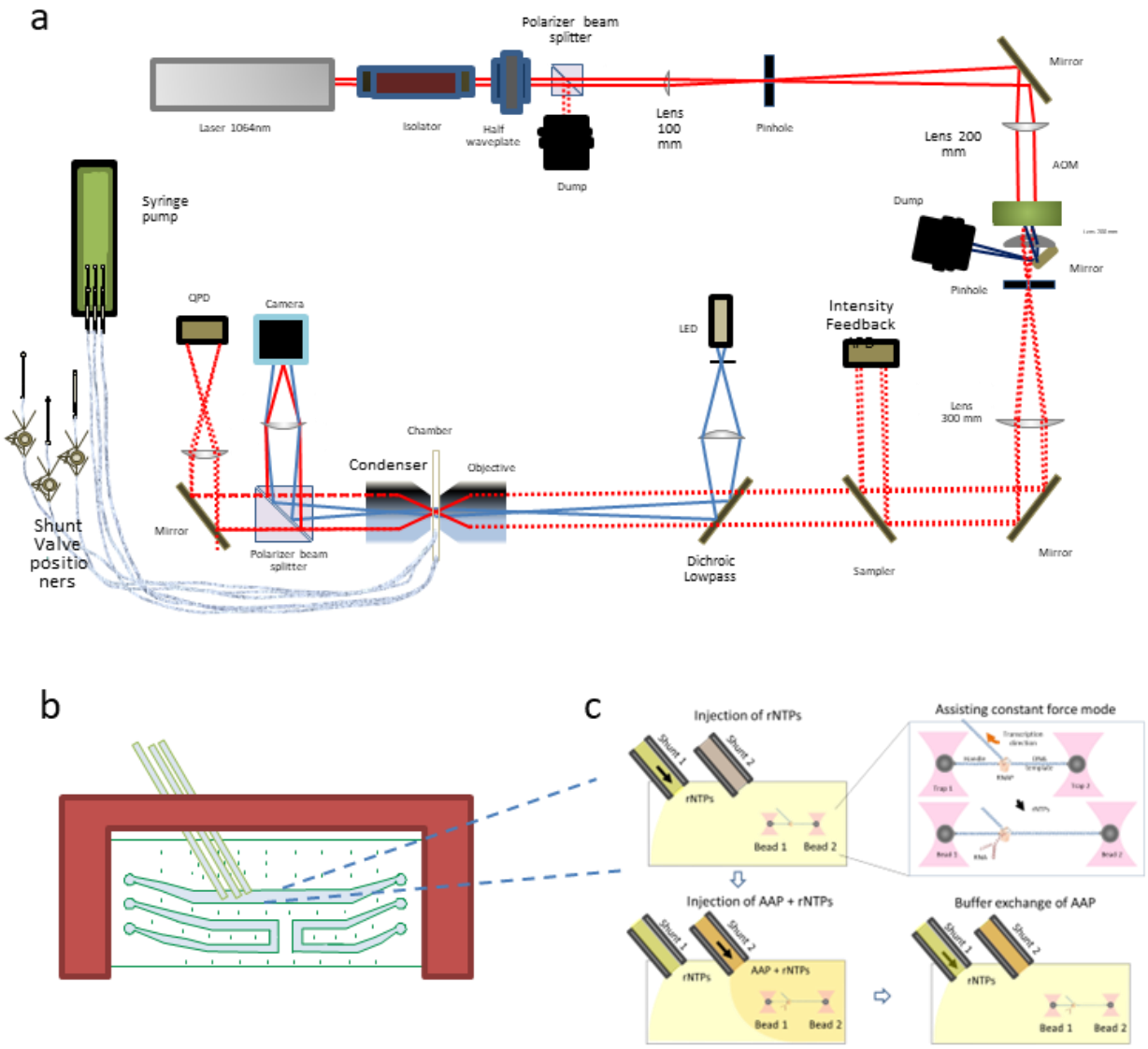

Figure 17. High-resolution optical tweezers instrumentation

a. Representation of the time-share instrument, the microfluidics chamber, syringe pumps, and valve positioners.
b. Representation of a microfluidics chamber.
c. Example of the buffer exchange procedure

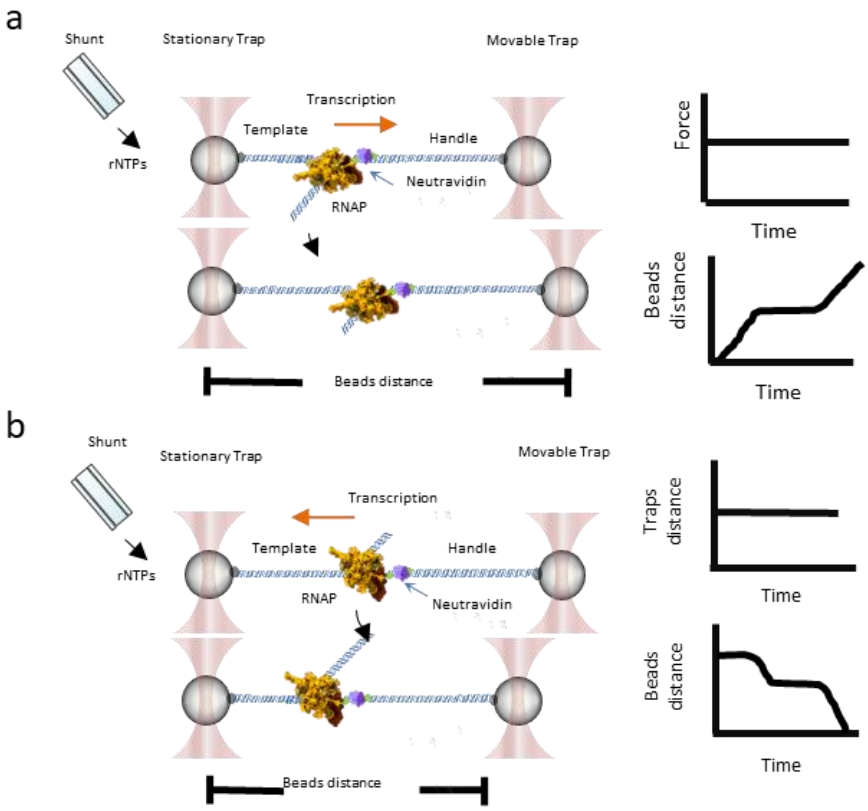

Figure 18. Single-molecule setup for elongation studies

a. Representation of the assisting force geometry. The small plots on the right represent the change of force *vs*. time and bead-bead distance over time.
b. Representation of the opposing force geometry. Similarly, the small plots on the right represent the change of force *vs*. time and bead-bead distance *vs*. time.